A STUDY OF SWIRLING FLOW IN HYDRAULIC MODELS

by

J.A. McCORQUODALE

UNIVERSITY OF GLASGOW

DEPARTMENT OF AERONAUTICS AND FLUID MECHANICS

APRIL 1964

A STUDY OF SWIRLING FLOW IN HYDRAULIC MODELS

SUMMARY

In this paper a study is made of vortex behaviour in axially asymmetrical hydraulic models. A brief review of the existing research on vortex models is given. Some of the existing theories have been extended to obtain theoretical descriptions of the vortices studied.

The effects of model scale and geometry on vortices with well-developed air cores were investigated experimentally. Three model sizes having 2", 4" and 6" diameter sharp-edged orifices were tested and for each two reservoir configurations (rectangular and 'horseshoe' shaped) were used. An eccentric inflow produced a reasonably stable swirl.

Similarity of swirl production, discharges and air cores has been considered.

It was found that vortex behaviour was sensitive to the irregularity of the model geometry. The vortices in the rectangular models were weaker and less stable than those in the 'horseshoe' shaped models.

A general dissimilarity was found between the swirls produced in the smallest model and those in the larger models. The highest swirl numbers were observed in the smallest model.

Apart from the above effect, a local scale effect was observed in the region of the air core; the swirl reduction in the region of the air core was greatest in the smallest model. A theoretical explanation is given for this effect.

Most of the experimental work was confined to steady flow at low submergence ratios ((flow depth)/(orifice diameter) < 3) in order to obtain reasonably stable well-devloped air cores.

J. A. McCORQUODALE

23 APRIL 1964.

ACKNOWLEDGEMENTS

This thesis has been submitted on application for the degree of Master of Science at the University of Glasgow.

The author appreciates the help and encouragement that he has received from Professor T.R.F. Nonweiler, Dr. A.S. Thom and Mr. P.H. Tanner of the Department of Aeronautics and Fluid Mechanics and from Dr. R.A. Robb of the Mathematics Department. He also wishes to thank the workshop staff for fabricating and setting up the apparatus.

TABLE OF CONTENTS

LIST OF ILLUSTRATIONS

Figure No.

Drawing No.

LIST OF SYMBOLS

r, θ, z	Cylindrical co-ordinates. (θ positive clockwise, z positive downwards).
u, v, w	Velocities in the direction of increasing r, θ and z respectively.
t	Time.
ρ	Density.
σ	Surface Tension.
ν	Kinematic Viscosity.
ξ	Eddy Viscosity.
H	Stagnation depth measured above the plan of the orifice.
h	Depth of flow in the models.
V	A characteristic velocity.
D	Diameter of the orifice.
r_o	Radius of the orifice.
A_o	Area of the orifice.
a_o	Observed air core radius.
a_t	Theoretical (ideal) air core radius.
b	Radius of the vena contracta.
Δz	Distance of the vena contracta below the plane of the orifice.
r_x	Radius of annular discharge jet.
c	Swirl constant (= vr).

m	Strength of source.
λ_b	Vena contracta swirl number $(= \frac{c}{b} \cdot \frac{1}{\sqrt{2gh}})$.
S	Specific swirl number $(= \frac{c}{\sqrt{2g \times r_o \, r_a}})$.
C_λ	(Discharge) swirl coefficient based on an inviscid fluid.
C'_λ	Discharge swirl coefficient based on a constant 'w' at the critical section.
a_{max}	Air core radius corresponding to C'_λ.
C_c	(Discharge) coefficient of contraction.
C_D	Discharge coefficient.
H/D	Submergence ratio.
R	Reynolds number.
W_1	Width of inlet.
X	A characteristic plan length of a model.

1. INTRODUCTION

It is common practice to assume that dynamic similarity of open channel models is adequately described by Froude's Law [1] i.e., for dynamic similarity to exist between two models the ratio between the inertial and the gravitational forces should be the same in each. In general any deviation from this law is called scale effect. If scale effect is present it is because the Froude Law assumption has neglected some significant force or forces such as the viscous and turbulent shear forces. In this thesis scale effects on swirling flow in axially asymmetrical models will be studied.

1.1 SIMILITUDE IN VORTEX MODELS

Several criteria have been suggested for operating vortex models. In 1962 Young [2], in a review of the existing work on vortex models, gave instances where three different criteria were used to describe three different aspects of similarity. Denny [3] investigated the behaviour of vortices in model sumps and found that vortices collapsed at similar submergence ratios when the intake velocities in the model and prototype were the same. Haindl [4] showed that

1. p.225.

commencement of vortex air entrainment, in a slowly drained symmetrical resevoir, depended on Reynolds' Law. Quick [5], also using symmetrical resevoirs, found that, except very near the air core, similarly shaped vortices were produced when Froude's Law was used.

Hattersley [6] investigated vortex similarity in pump sumps and concluded that a certain augmentation of velocity in the model, over that required by the Froude criterion, was necessary to produce similar swirls at the intakes. This exaggeration, he reasoned, was required because of the dissimilar velocity distributions in the approach channels.

Some exploratory tests, carried out in connection with the hydraulic investigations for the Culligran Tunnel Intake [7], indicated that similarity of vortex collapse could be obtained in Froude models if the intake area exceeded a certain minimum. A minimum area of 10 sq.in., was suggested. It is noted that exact geometric similarity did not exist in the models tested.

Similar results to those of Denny [3], were found by Iversen [8] and Fraser [9]. This suggests [5] that vortex collapse may be influenced by the surface

5. p.85.

The Froude Law criterion, suggested by Quick[5], for producting similarly shaped vortices with well-developed air cores, is not in conflict with the other criteria, provided the models are operated in the turbulent range.

As yet very little has been discovered about the influence of turbulence and eddies on swirling flow in hydraulic models. Turbulent losses depend on viscosity, boundary roughness, velocity and model size. Eddy losses depend on all of these but also on the model geometry. Thus in the axially symmetrical models tested by Haindl[4], Quick[5] and Binnie[12,13] the problem of eddy formation was largely avoided.

In our investigations geometrically similar axially asymmetrical models were tested to study the effects of model scale and geometry on the behaviour of a drained vortex. Discharge and air core similarities were considered for steady flow with a stable well-developed air core. Similarity of swirl production was also investigated. It was because of the air core stability requirement that the major part of this work was confined to $H/D < 3$.

tension forces in the air core. Similarity of collapse would then show a dependence on the Weber number,

$$\frac{V}{\sqrt{\sigma/\rho\, L}}$$

where V is velocity

ρ is density

σ is surface tension

and L is a length.

Now if L refers to the air core diameter just before collapse which, it is assumed, would be of the same order of magnitude in the model and prototype then the velocity would have to be of the same order of magnitude in the model and prototype to satisfy the Weber Law [10].

The Reynolds Law criterion for vortex formation in small models is reasonable since viscous forces would be significant in the region of the orifice prior to the development of the air core [11]. However, as the size of the model is increased turbulent forces will start to predominate and these will tend to be proportional to the model scale [20]. Also after the air core has developed the influence of the viscous forces should diminish according to a theory presented in section 2.5.

10. p.143.

1.2 OTHER RESEARCH ON VORTICES

Much of the early theoretical investigation of vortex motion in a perfect fluid was done by H. Helmholtz and Lord Kelvin. A resume of their work is given by Lamb [14].

The use of vorticities to specify rotational flow is due to Helmholtz and Stokes. The components of vorticity are defined by

$$\xi = \frac{\partial w}{\partial y} - \frac{\partial v}{\partial z} \quad , \quad \eta = \frac{\partial u}{\partial z} - \frac{\partial w}{\partial x} \quad , \quad \zeta = \frac{\partial v}{\partial x} - \frac{\partial u}{\partial y} \qquad (1.2.1).$$

If all of these are zero, the flow is irrotational.

The strength of a vortex is given by its circulation [14] which is

$$\Gamma = \oint (u\,dx + v\,dy + w\,dz) \qquad (1.2.2).$$

$$= \iint_S (l\xi + m\eta + n\zeta)\,dS$$

where l, m, n are the directional cosines and dS is an element of area on the integration surface. For regions of irrotational flow the circulation will be zero for any circuit not enclosing a singularity. However a circulation can exist for a circuit enclosing a singularity in an otherwise irrotational system.

14. Chap. 3 and 7.

Binnie and Hookings [12] and Binnie and Davidson [13], assuming an inviscid fluid, made a theoretical study of swirling flow through rounded and sharp-edged circular orifices. Using water as the working fluid they compared theoretical and experimental values of discharge and found that these differed significantly.

Numerous approximate solutions have been suggested for the Navier-Stokes equations for vortex flow in a viscous fluid. Some of the most recent of these are by Long[15], Lewellen[16], Einstein and Li[11] and Donaldson and Sullivan[17].

Einstein and Li made the following assumptions in order to solve the Navier-Stokes equations

1) All derivatives with respect to t, θ and z are negligible.

2) No friction on planes normal to the z axis.

3) $Q = Qo\ (r/r_o)^2$ for $r < r_o$, and
$w = 0$ for $r > r_o$,

4) $u^2 \ll v^2$,

Their solution for the tangential velocity distribution is

$$v_* r_* = \frac{\left[A-2\left(1-e^{-\frac{A}{2}}\right)\right]\left(1-r_*^{-(A-2)}\right)}{A\left(1-e^{-A/2}r_{o*}^{(A-2)}\right)-2\left(1-e^{-A/2}\right)} + r_*^{-(A-2)}$$

$$A \neq 2 \qquad (1.2.3)$$

where $r_* = \frac{r}{R}$,

$v_* = \frac{v}{V}$

$A = \frac{Q_o}{2\pi l_o \nu}$ (1.2.4)

and l_o is taken as the stagnation depth. They modified equation 1.2.4 by introducing an eddy viscosity ξ, to

$$A_e = \frac{Q_o}{2\pi l_o(\nu + \xi)}$$

which they found gave a better approximation to experimentally determined velocity distributions.

2. SOME THEORETICAL CONSIDERATIONS

In this chapter a theoretical model is proposed which, although it is a great oversimplification of the real models, provides a basis for comparing the real models. A very simple model is considered first and modifications are introduced later to show the influences of viscosity and turbulence.

2.1 A THEORETICAL MODEL

It is assumed in the theoretical model that it has a horizontal floor coinciding with the plane of the sharp-edged circular orifice; its boundaries are axially symmetrical about the orifice; in plan its dimensions are large with respect to the orifice diameter; the working fluid is inviscid; a constant tangential velocity is supplied by an axially symmetrical inflow; the flow is steady; the discharge tends to its maximum for a given head; and surface tension is negligible.

These assumptions lead to the relation

$$vr = \text{constant}, \ (= c) \qquad (1.1.1)$$

for the fluid above the plane of the orifice.

2.2 THE THEORETICAL DISCHARGE

For the model proposed in section 2.1 Binnie and Davidson [13] gave,

$$Q = \frac{\pi c^2}{\sqrt{2gH}} \left[\left(\frac{r_o}{a_t}\right) \left\{ \left(\frac{r_c}{a_t}\right)^2 - 1 \right\}^{1/2} - \cosh^{-1}\left(\frac{r_o}{a_t}\right) \right]$$

which they found over-estimated the discharge. The following development differs slightly from the above in that the critical flow is assumed to occur at the vena contracta VC instead of at the plane of the orifice.

Figure 2.2.1

Defining Diagram

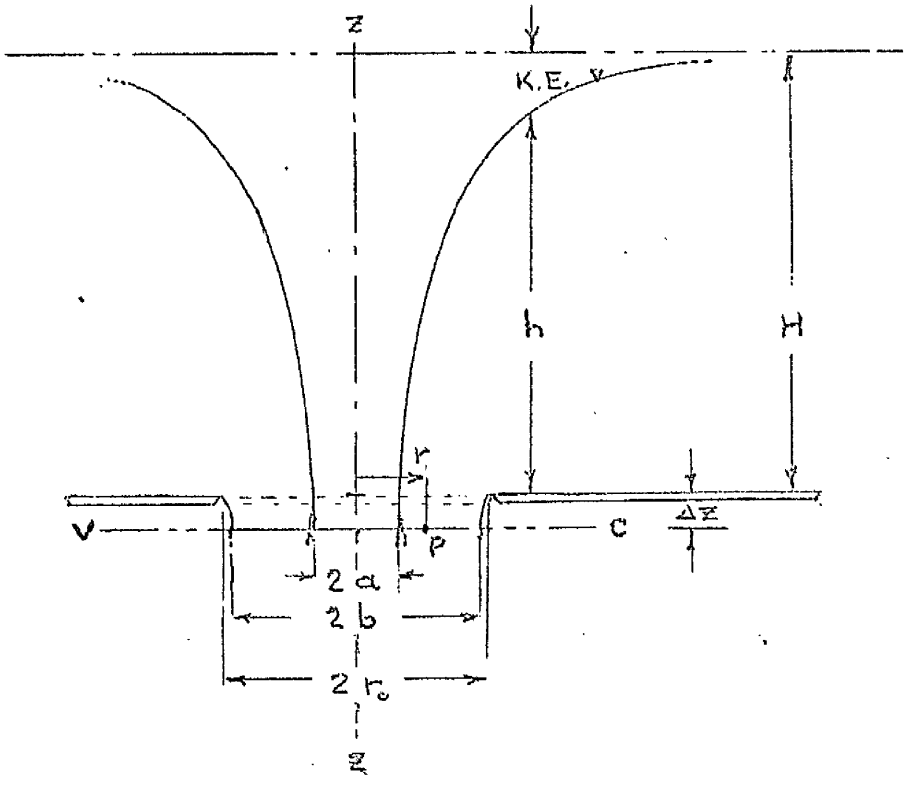

It is assumed that radial flow is negligible at the vena contracta and the air core diameter here is nearly equal to that at the plane of the orifice.

Applying Bernoulli's equation to point P in the plane V - C gives,

$$H + \Delta z = \frac{v^2}{2g} + \frac{u^2}{2g} + \frac{w^2}{2g} \qquad (2.2.1)$$

$$= H' .$$

From $vr = c$, and $u \ll v$

$$w = \sqrt{2gH' - \left(\frac{c}{r}\right)^2} \qquad (2.2.2)$$

and $$Q = 2\pi \int_a^b \sqrt{2gH' - \left(\frac{c}{r}\right)^2}\, r\,dr \qquad (2.2.3).$$

For the condition of maximum Q, it can be shown that

$$\frac{dQ}{da} = 0 \qquad \text{(b not a function of a.)}$$

for $$a = \frac{c}{\sqrt{2gH'}} \qquad (2.2.4).$$

The integration of equation 2.2.3 gives,

$$Q = \pi \sqrt{2gH} \left\{ b \sqrt{b^2 - a^2} - a^2 \ln \left| \frac{b + \sqrt{b^2 - a^2}}{a} \right| \right\}$$

(2.2.5a).

Putting $\frac{a}{b} = \lambda_b$ (2.2.6)

and $b = r_o\sqrt{C_c}$ and neglecting Δz

we have

$$Q = A_o\sqrt{2gH}\ C_c\left(\sqrt{1-\lambda_b^2} - \lambda_b^2 \ln\left|\frac{1+\sqrt{1-\lambda_b^2}}{\lambda_b}\right|\right) \quad (2.2.5b).$$

For λ_b small ($<.5$ say) the discharge is given approximately by

$$Q = A_o\sqrt{2gH}\ C_c\left(1 - \lambda_b^2 \ln\left|\frac{3.80}{\lambda_b}\right|\right) \quad (2.2.7).$$

The factor involving λ_b in equations 2.2.5 and 2.2.7 is denoted by the swirl coefficient C_λ .

Whence $C_D = C_c C_\lambda$ (2.2.8).

It is noted that λ_b is similar to a Froude number. It is dimensionless and independent of scale. If we write,

$$\lambda_b = \frac{c}{b} \cdot \frac{1}{\sqrt{2gH}} \quad (2.2.9).$$

it is seen that λ_b represents the ratio of the swirling velocity at b to the maximum possible velocity through the orifice. λ_b is proportional to the strength of swirl and is called the vena contracta swirl number.

If two models operate exactly by Froude's Law then their λ's will be the same. The concept of

C_λ will be useful in determining a local scale effect in the region of the orifice in the presence of a general scale effect in the region outside the orifice.

2.3 ESTIMATION OF SWIRL STRENGTHS FROM THE DIMENSIONS OF THE ANNULAR JET

Measurement of swirl by the divergence of the discharge jet was suggested by Kolf and Zielinski [19]. It was decided to develop the 'annular jet' method when difficulties arose in the measurement of swirl by the 'surface float' method.

Figure 2.3.1

Defining Diagram

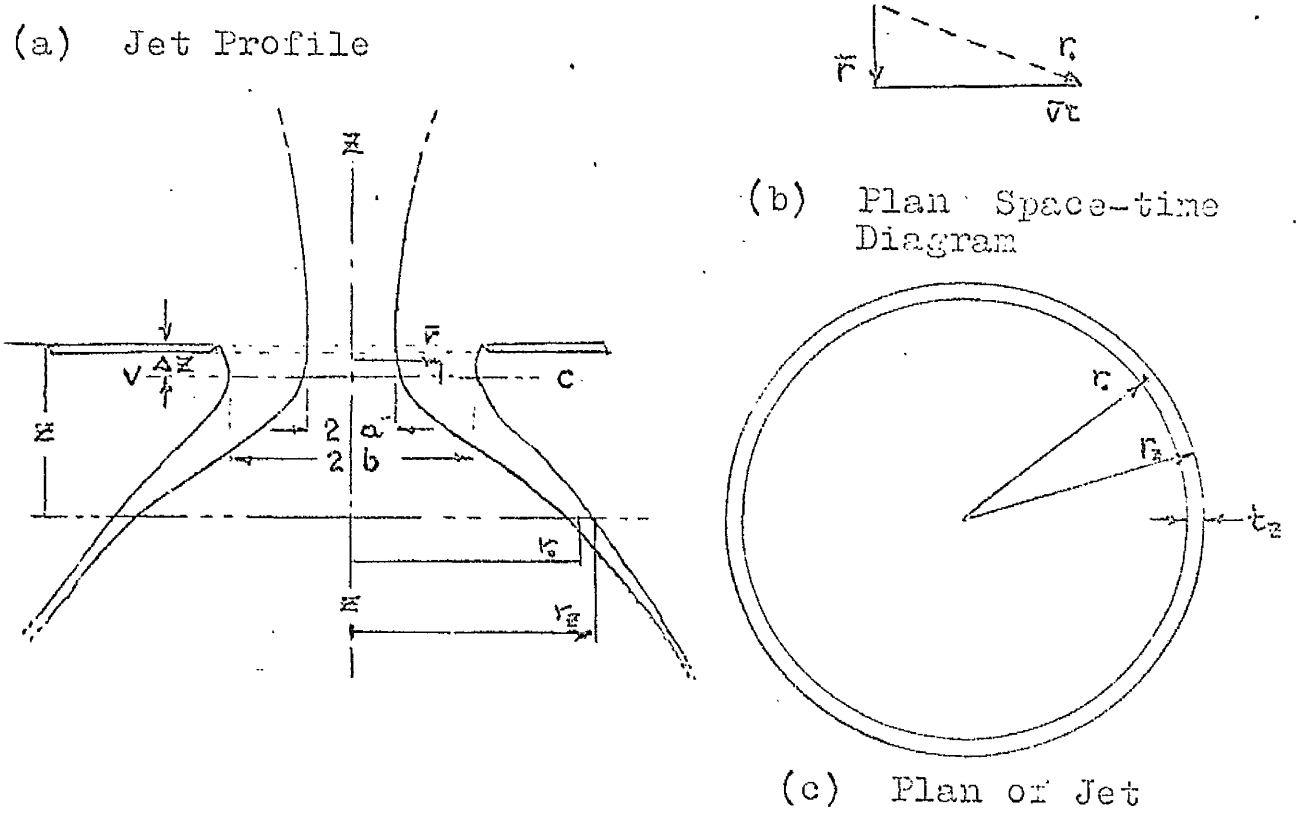

The following assumptions are added to those of the theoretical model:

1) tangential momentum is conserved in the annular jet;

2) the jet originates from the vena contracta;

3) the jet remains intact, its thickness decreases and the horizontal velocity will tend to become independent of the jet thickness as z increases;

4) Air friction is negligible.

Below the vena contracta the swirling particles are not constrained to move in circular paths. Considering the annular jet in plan, we choose an average velocity to represent the tangential movement. Basing this on momentum we have

$$\bar{v} = \frac{2\int_a^b vrdr}{b^2 - a^2}$$

$$= \frac{c}{\frac{1}{2}(b + a)} \qquad \text{or}$$

$\bar{v}$ is the velocity at $\bar{r} = \frac{1}{2}(b + a)$ which is the mean radius of the ring.

From figure 2.3.1c the mean radius of the ring r_o, after a time t, is

$$r_o = \sqrt{(\bar{r})^2 + (\bar{v}t)^2}$$

from which

$$\overline{vr} = \bar{r}\frac{\sqrt{r_o^2 - \bar{r}^2}}{t} \qquad (2.3.1).$$

Now $$t = \sqrt{\frac{2}{g}}\left(\sqrt{z + \bar{h}} - \sqrt{\bar{h}}\right) \qquad (2.3.2)$$

where $\bar{h}$ is the average velocity head at V - C.

From equations 2.3.1 and 2.3.2,

$$\overline{vr} = \frac{\bar{r}^2\sqrt{\frac{g}{2}}\sqrt{\left(\frac{r_o}{\bar{r}}\right)^2 - 1}}{\sqrt{\bar{h} + z} - \sqrt{\bar{h}}} \qquad (2.3.3a)$$

Very little error will be introduced if $\bar{h}$ is equated to H and Δz neglected; this gives

$$\overline{vr}_{jet} = \frac{\bar{r}^2\sqrt{\frac{g}{2}}\sqrt{\left(\frac{r_o}{\bar{r}}\right)^2 - 1}}{\sqrt{H + z} - \sqrt{H}} \qquad (2.3.3b).$$

2.4 A SEMI-EMPERICAL APPROACH TO THE DETERMINATION OF C_c FOR SWIRLING DISCHARGE

The diameter of the vena contracta is increased by the presence of swirl in the discharge [13]. The following discussion is intended as an aid to the empirical investigation of this effect.

Let us assume that the diameter of the discharge jet can be found by combining its displacement components due to radial and tangential momentum. The former will tend to give the normal coefficient of contraction; it is with the latter that we are now concerned.

It is reasoned that

$$b^2 \propto (r_o^2 + v_o^2 t^2) \qquad (2.4.1)$$

by virtue of the conservation of tangential momentum. Equation 2.4.1. reduces to,

$$C = K\left(1 + \left(\frac{v_o}{r_o}\right)^2 t^2\right) \qquad (2.4.2a)$$

where $v_o = \frac{c}{r_o}$;

$C_c = \left(\frac{b}{r_o}\right)^2$;

$t \simeq \sqrt{\frac{2}{g}}\left(\sqrt{h + \Delta z} - \sqrt{h}\right)$, being the descent time from the plane of the orifice to the vena contracta; and K is the constant of proportionality which, it is assumed, will be approximately equal to

the ideal non-vortex coefficient of contraction

i.e. $\frac{\pi}{\pi + 2}$.

Now assuming $\Delta z = \phi(H/D)$, equation 2.4.2 can be written

$$C_c = K\left\{1 + \left(\frac{c}{\sqrt{2gr_c \cdot r_o}}\right)^2 F\left(\frac{H}{D}\right)\right\} \qquad (2.4.2b)$$

For the purposes of an empirical development this is written more generally as

$$C = K\left(1 + (S)^{\alpha} F(H/D)\right) \qquad (2.4.2c)$$

where S is a swirl number,

$K \simeq 0.62$ say,

and α and $F(H/D)$ will be found empirically.

2.5 THE INFLUENCE OF VISCOSITY AND TURBULENCE ON THE DRAINED VORTEX

The following is an extension of Einstein and Li's [11] theory (see section 1.2) to the case of a well-developed air core. Proceeding with their assumptions, except that in the range $a \leqslant r \leqslant r_o$ it is assumed that,

$$u = \frac{-Q_o}{2\pi r_o l_o}\left(\frac{r - a}{r_o - a}\right) \qquad (2.5.1)$$

the solution of the general equations of motion and continuity follows: The Navier - Stokes equations in

cylindrical coordinates are

$$\frac{D'u}{Dt} - \frac{v^2}{r} = \frac{-1}{\rho}\frac{\partial}{\partial r}(p + \gamma h) + \nu\left(\nabla^2 u - \frac{u}{r^2} - \frac{2}{r^2}\frac{\partial v}{\partial \theta}\right) \qquad (2.5.2)$$

$$\frac{D'v}{Dt} + \frac{uv}{r} = \frac{-1}{\rho r}\frac{\partial}{\partial \theta}(p + \gamma h) + \nu\left(\nabla^2 v + \frac{2}{r^2}\frac{\partial u}{\partial \theta} - \frac{v}{r^2}\right) \qquad (2.5.3)$$

$$\frac{D'w}{Dt} = \frac{-1}{\rho}\frac{\partial}{\partial z}(p + \gamma h) + \nu(\nabla^2 w) \qquad (2.5.4)$$

and the continuity equation is

$$\frac{1}{r}\frac{\partial(ru)}{\partial r} + \frac{1}{r}\frac{\partial v}{\partial \theta} + \frac{\partial w}{\partial z} = 0 \qquad (2.5.5).$$

Now neglecting derivatives with respect to t, θ and z, equation 2.5.3 yields,

$$u\frac{\partial v}{\partial r} + \frac{uv}{r} = \nu\left(\frac{\partial^2 v}{\partial r^2} + \frac{1}{r}\frac{\partial v}{\partial r} - \frac{v}{r^2}\right) \qquad (2.5.6)$$

Putting [11] $A = \frac{Q_o}{2\pi l_o \nu}$, equation 2.5.1 gives

$$u = -\frac{A(r - a)\nu}{r_o(r_c - a)} \qquad (2.5.1b).$$

Substituting for 'u' in equation 2.5.6 and rearranging one obtains

$$r^2 \frac{\partial^2 v}{\partial r^2} + r\left[A \cdot \frac{r^2 - ar}{r_i(r_i - a)} + 1\right]\frac{\partial v}{\partial r} + \left[\frac{A(r^2 - ar)}{r_i(r_i - a)} - 1\right] v = 0$$

$$a \leqslant r \leqslant r_o \qquad (2.5.7).$$

The solution of this is

$$v = \frac{C_o}{r} + \frac{C_1}{r}\left\{ e^{-\frac{A(r-a)^2}{2r_o(r_o-a)}} - \frac{a\sqrt{2A\pi}}{\sqrt{r_o(r_o-a)}} \operatorname{erf} \frac{\sqrt{A}(r-a)}{\sqrt{r_o(r_o-a)}} \right\}$$

$$(2.5.8).$$

Applying the boundary conditions that

1) at $r = r_o$ $v = v_o$, and

2) at $r = a$, $\frac{\partial (v/r)}{\partial r} = 0$,

the final solution is

$$vr = v_o r_o \left\{ \frac{1 + \frac{Aa^2}{2r(r_o-a)} - e^{-\frac{A(r-a)^2}{2r_o(r_o-a)}} + \frac{a\sqrt{2A\pi}}{\sqrt{r_o(r_o-a)}} \operatorname{erf} \frac{\sqrt{A}(r-a)}{\sqrt{r_o(r_o-a)}}}{1 + \frac{Aa^2}{2r_i(r_i-a)} - e^{-\frac{A(r_o-a)^2}{2r_i(r_i-a)}} + \frac{a\sqrt{2A\pi}}{\sqrt{r_o(r_i-a)}} \operatorname{erf} \frac{\sqrt{A}(r_o-a)}{\sqrt{r_o(r_i-a)}}} \right\}$$

$$\text{for } a \leqslant r \leqslant r_o \qquad (2.5.9).$$

For turbulent flow A is written

$$A = \frac{Q_o}{2\pi l_o(\nu + \xi)} \qquad (2.5.10).$$

2.6 FLOOR FRICTION

The following is not intended to be a rigourous treatment of the floor friction problem; it is meant to show the order of magnitude of the floor friction losses and consequently their possible influence on similitude.

The system is assumed to be composed of a converging stream channel as shown in figure 2.6.2.

Figure 2.6.2

Defining Diagram

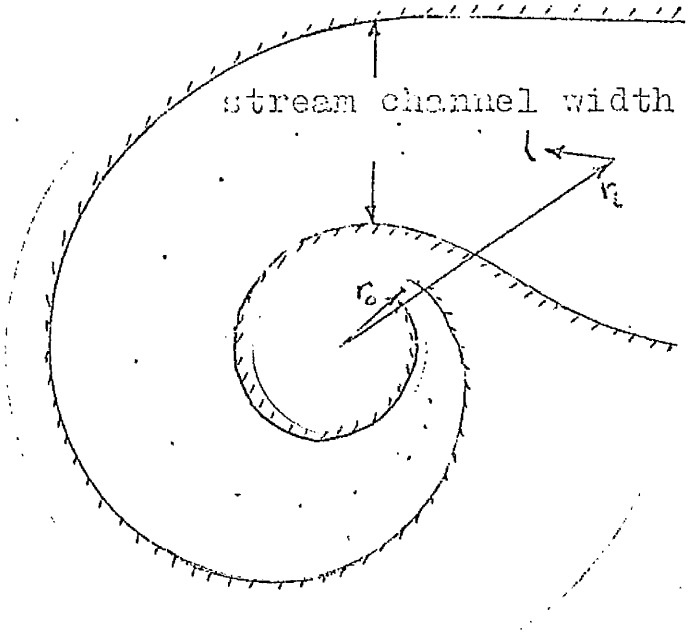

(a) Stream Channel (Plan)

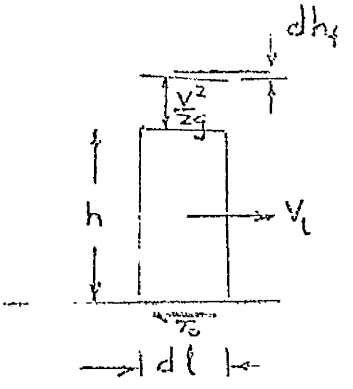

(b) Stream Channel Element of Length

The following approximations and assumptions are made:

1) h is constant for $r_o \leqslant r \leqslant r_i$;

2) the hydraulic radius may be equated to h;

3) for hydraulically smooth surfaces

$$f = .316\, R^{-1/4} \qquad \text{where} \quad R = \frac{4hV}{\nu} \ ;$$

4) centrifugal effects on the floor boundary layer can be neglected;

5) shear on vertical planes is neglected.

Now $v = c/r$ and $u = m/r$ whence for convenience

$$k \equiv \sqrt{c^2 + m^2} \ .$$

The friction loss over a short length of the stream-channel, dl, is

$$dh_f = \frac{lfV^2}{4h2g} \left[\frac{dl}{l} + \frac{df}{f} + 2\frac{dV}{V} \right] \qquad (2.6.1)$$

Now $V = k/r$,

$dl = \frac{k}{m} \cdot dr$, and taking

$f = q\left(\frac{4hk}{\nu r}\right)^p$ for generality,

$df = -\frac{pq}{r}\left(\frac{4hk}{\nu r}\right)^p dr$; using these relations equation 2.6.1 can be integrated to give the friction loss between r_i and r_o . The solution is

$$h_f = \frac{V_o^2}{2g} \cdot \frac{k}{m} \cdot \frac{f_o}{4h} (r_i - r_o) \qquad (2.6.2)$$

where f_o is the friction factor at the orifice.

Thus the similarity of friction losses will depend on the ratio of the friction factors in the model and prototype. Using Blasius' equation for the friction factor it is noted that h_f/h is very small even for the smallest model considered in this investigation (h_f/h being about 0.7%).

2.7 TREATMENT OF SWIRL IN AN AXIALLY ASYMMETRIC RESERVOIR

It was noted in section 2.1 that vr is constant for the theoretical model; however for the more general case of irrotational flow in an axially asymmetric reservoir, the circulation

$$\Gamma = \oint (v_i \, dl) \qquad (2.7.1)$$

$$= \text{a constant for a circuit enclosing the singularity.}$$

Taking the integration path to be

$$r = \text{(a constant)},$$

we have, $$\Gamma = r \int_0^{2\pi} v \, d\theta \qquad (2.7.2)$$

$$= 2\pi c \qquad \text{say.}$$

Considering n finite intervals of θ, ($\Delta\theta_i$ with an associated v_i), equation 2.7.2 can be written,

$$r \sum_{\lambda=1}^{n} v_i \, \Delta\theta_i = 2\pi c$$

or $$c = r \frac{\sum_1^n v_i}{n} \qquad (2.7.3).$$

i.e. the angular average of vr is constant.

3. A DESCRIPTION OF THE EXPERIMENTAL INVESTIGATION

Four series of tests dealing mainly with steady flow model behaviour are described in this chapter. A fifth series of tests concerned with the formation of a vortex during reservoir drawdown is described in chapter 7.

3.1 THE APPARATUS

The basic apparatus is shown in drawing numbers 1 and 2 and consists of:

1) an open-top welded steel tank (5' x 8' x 5' deep) having a coating of bituminous paint on the inside, a perspex viewing window, and a flow straightener fitted so as to leave a 5' x 5' test section,

2) 5 sharp edged orifices (2"D, 4"D, 6"D, 8"D and a square orifice with an area equivalent to the 6"D orifice) which can be fitted into any of the four positions provided in the large tank,

3) a pump with a maximum delivery of about 2.5 c.f.s.

Figure 3.1.1 illustrates how plywood partitions were used to make the medium and small models within

the large tank. The eccentricity of the inflow was produced by a plywood barrier fixed across part of the flow straightener. All hydraulic surfaces of the partitions and barriers were planed and varnished. In the small model all the hydraulic surfaces were waxed and polished.

Plasticene was used to seal the orifices and make the models water tight.

Staff gauges with 1/8" and 1/10" divisions were used to measure the depths of flow in the models.

Discharges were measured by one or a combination of the following methods:

1) A weigh tank,

2) A V - notch weir calibrated by the weigh tank,

3) the venturi meter gauge on the pump delivery line.

A stroboscope-stroboflood and a 35mm camera were used in the measurement of swirl, air core diameter, and the dimensions of the annular jet.

3.2 EXPERIMENTAL PROCEDURE

(a) Series I - The purpose of this series of tests was to study the effect of model scale on a fairly stable vortex. Three models (D = 2", 4" and 6") were set up as shown in Figure 3.2.1 i.e. with a half-rounding in the test section.

The following test procedure was used for each model.

A stage/discharge curve was developed from several measurements of depth and discharge in the range $0 < H/D < 5$. Figure 3.2.1 shows the staff gauge position. In the large and medium models the staff gauge divisions were 1/8" and the readings were estimated to 1/32". In the small model a gauge with 1/10" divisions was used and the readings were estimated to 0.02". Readings of meniscus were taken and corrections applied to gauge readings. The staff gauge datums were related to the orifice lips by a water level transfer to the centres of discs replacing the respective orifices but having the same thicknesses.

The discharge of the small model was measured by the V - notch weir and/or the weigh tank. In the other models the V - notch weir was used to measure the lower discharges and the venturi meter,

the higher discharges. Long waiting periods were required for steady flow to become established in the models. This was particularly true of the small model which took up to an hour to come to equilibrium. Since it was thought that $\frac{dH}{dt}$ might influence the strength of the vortex, readings were only taken for steady or very nearly steady conditions.

Surface swirl was estimated from time exposed photographs (35mm, 400 and 800 ASA, f = 2.8, B = 3 seconds) of small 'polyzote' floats illuminated by flashes from 3 floods triggered by a stroboscope. Frequencies between 400 and 600 r.p.m. were used. It was assumed that surface tension would keep the small floats moving with the flow. These photographs also showed the air cores.

Photographs were taken of the annular jets in order to measure the vena contracta and jet diameters. The jet thickness was estimated by probing it with a scale.

3.2. (b) Series II - The purpose of this series of tests was to study the effects of rectangular geometry on discharge similarity.

Stage/discharge curves were developed for the model configuration shown in figure 3.2.2 by the

methods of section 3.2.(a). The range of H/D was extended to about 10 and observations of vortex behaviour were noted. Three models (D = 2", 4" and 6") were tested.

3.2 (c) Series III - The purpose of these tests was to study the effects of the X/D ratio (model size) on vortex behaviour.

All the tests in this series were performed with orifices centrally placed in the 5 x 5 test section. Half of the inflow was blocked as shown in figure 3.2.2 so that the model boundary shape was the same as in series II but the plan size was different. Four orifices (D = 2", 4", (6") and 8") were tested for heads up to 48 inches.

3.2. (d) Series IV - Special Tests

To study the effect of the orifice shape on vortex behaviour, a square sharp-edged orifice with an area equivalent to the 6" diameter orifice was tested in place of the 6" diameter orifice of series II. Stage/discharge curves were developed and observations made for comparison with the series II tests.

The 6" diameter orifice was tested in the

configuration shown in figure 3.2.3 to show the influence on the discharge of an increase in the eccentricity of the inflow.

4. THE EXPERIMENTAL DATA

4.1 Series I - Observations

The discharge observations for this series of tests are summarized in figures 4.1.1 to 4.1.3. No vortex collapse occurred in the range $0 < h/D < 4$ but a slight instability of the vortex was noticed at $h/D > 2$.

The photographs shown in figures 4.1.4 to 4.1.9 are typical of the records used to determine surface swirl, air core diameters, vena contracta and annular jet diameters. The negatives were projected on to drawing paper where pertinent distances were marked for measurement. The scales for the measurements were obtained from photographs of objects placed either in the plane of measurement or at a measured distance from the camera and in the neighbourhood of the plane of measurement. For example using the latter, the water surface scale could be found from,

$$\frac{\text{datum scale} \times \text{water surface distance}}{\text{datum distance}}$$

A small correction was applied to the measured values of the vena contracta and jet diameters because the photographs were not orthogonal projections.

The correction is given by

$$r_{actual} = \frac{r_{measured}}{\sqrt{1 + \left(\frac{r_{measured}}{\text{datum distance}}\right)^2}}$$

Air core, vena contracta, and certain annular jet measurements are presented in figures 4.1.10, 4.1.11 and 4.1.12 respectively.

The tangential velocity of the surface floats about the air core centre was calculated by,

$$v = \frac{(\text{tangential path distance})f}{(N - 1)}$$

where f is the stroboscope frequency and N is the number of float images. Values of $v_t . r$ are plotted in figures 4.1.13 to 4.1.15 with the approximate angular positions of the measurements indicated.

4.2 (a) Series I - Description of Flow in the Region Outside the Orifice.

Figures 4.2.1 to 4.2.3 show the surface patterns indicated by the floats and the floor boundary layer flow patterns as determined by cotton tufts and dye traces. The locations of large eddies are also shown.

The velocity of swirl was observed to vary inversely with the distance from the air core. The floats followed inward spiralling paths in quadrants A and B and in all quadrants in the region near the orifice. Otherwise the surface flow in quadrants C and D tended to move away from the centre. This is caused by the divergence of the streamlines as the flow approaches the corner D and is in accord with the irrotational flow pattern shown in figure 4.2.4.

Very weak counter rotating eddies were sometimes observed in the corner of quadrant D; this seemed to be a more prominent feature of the large and medium models than of the small model. Such eddies result from the instability of diverging flow and are often encountered at transitions in open channels.[10,21]

Separation eddies formed at the inside of the inlet I in all models. Their direction of rotation was the same as the main circulation. They seemed to separate at a nearly constant time intervals in each model. After separation they followed the stream channel separation path IS and decayed beyond visual recognition at about the third quadrant (C) of revolution.

Apart from the eddies mentioned above there

10. p.626,
21. p.267.

was a tendency for a roller to develope immediately downstream of the inlet in the large and medium models. This was most noticable at $H/D < 2$ which corresponded with the maximum losses through the flow straightener. The influence of the roller on the depth/velocity distribution was not appreciable at distances greater than D from the inlet.

The model swirls were observed to vary in the following ways:

1) with time at a given point,

2) with r at a given θ,

3) with θ at a given r,

4) with depth at a given point.

The latter is referred to as the floor boundary layer effect.

Dye traces were used to investigate the behaviour of swirl with depth. Although reliable magnitude comparisons could not be made, it was possible to determine the directional variation of velocity with depth. The results of these investigations are shown by the dotted arrows in figures 4.2.1 and 4.2.3; they show the direction of the floor boundary layer flow. In both the large and small models this directional effect was confined to a layer near the tank floor, which in

the large models had a maximum value between 1/2 and 1 inch and in the small models about 0.2". The boundary layer effect increased with increasing distance along the stream channel until it reached its maximum in quadrant D near the boundary of quadrant A.

4.2 (b) Series I - A Note on the Flow in the Region of the Orifice.

It was observed in all models that as H/D increased the air core centre moved away from the centre of the orifice in the downstream direction as shown in figures 4.2.1 to 4.2.3. It is noted that the relative deviation is least in the smallest model.

Figure 4.2.5 illustrates the distortion of the air core axis which accompanied the effect of paragraph 1 (above). Again this effect was least in the smallest models.

Figure 4.2.5
Distortion of the Air Core Axis

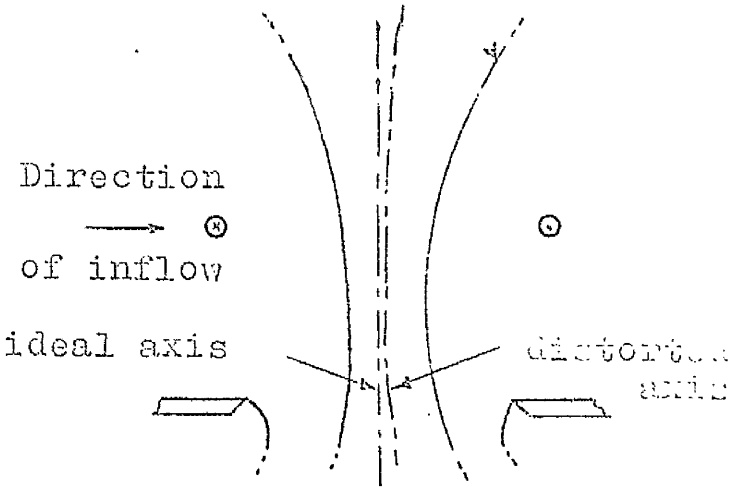

Figure 4.2.5 also indicates the downstream shift of the vena contracta. It was assumed that the air core at the vena contracta would be the same as at the plane of the orifice; however this was not so. The air core, in fact, expanded below the orifice. Attempts to photograph its expansion were unsuccessful but it was great enough to be noticable.

In the development of the ideal discharge coefficient, it was inferred that w = 0 at the vena contracta air core surface. In the real models a downwards velocity existed over the whole of the air core surface.

4.3 Series II, III, IV - Observations

The stage/discharge curves for series II, III and IV are shown in figures 4.3.1, 4.3.2 and 4.3.3 respectively. It was observed that the vortices were generally less stable in these tests than in series I and this is the reason for the more scattered stage/discharge readings.

5. ANALYSIS OF THE EXPERIMENTAL DATA

5.1 THE DISCHARGE COEFFICIENTS

The normal discharge coefficient C_D provides a convenient dimensionless means of comparing observed discharges in scale models. Defining the discharge coefficient as

$$C_D = \frac{Q}{\sqrt{2gH}\, A_o}$$

where H = depth at r = 4D and A_o = area of the orifice, values of C_D have been calculated from the mean discharge curves for the first series of tests; these are shown in figure 5.1.1. For the second, third and fourth series of tests the upper and lower limits of C_D were found and these are given in figures 5.1.2, 5.1.3 and 5.1.4 respectively.

5.2 SURFACE SWIRL

The surface swirl strength as given by $C = v.r$ was observed to vary with y, H, r, θ and t for a given model. With H and y fixed (i.e. the surface y = 0) and considering the mean of the temporal variations, use was made of the theory of section 2.7, namely

$$\overline{vr}_\theta = \frac{r\sum_1^n (v)i}{n}$$

to obtain an indication of the variation of the swirl strength with r. Figures 4.1.13 to 4.1.15 show the curves of $\overline{vr}_\theta$ vs r obtained from the above equation with n = 8. Values of $r(\bar{v})_i$ were obtained by interpolation from topographical plots of vr. A plot of vr vs θ (taken along the centreline of the stream channel) as shown in figure 5.2.1 was sometimes used to aid in the interpolation.

For comparison purposes the $(\overline{vr})_\theta$ curves have been made dimensionless by dividing them by the scale dependant datum,

$$\sqrt{2gr_o}\ r_o$$

The $\dfrac{(\overline{vr})_\theta}{\sqrt{2gr_o}\ r_o}$ vs r curves for the series I models are compared in figure 5.2.2.

Reliable estimates of surface $(\overline{vr})_\theta$ could not be obtained for $r < .8D$ because of the lack of accurate observations. The observations obtained were quite random but generally indicated a sharp decrease in the surface circulation for $r < D$. It was not clear whether this marked decrease was real - perhaps resulting from an air core surface boundary layer such

as equation 2.5.9 would seem to suggest - or not, being the result of a difference between the float velocity and the flow velocity. Certainly the floats move rotationally near the air core i.e. they do not maintain their orientation. The floats moving in towards the air core would thus have to be accelerated by the surrounding flow and if a slip occurred in the tangential direction a tangential velocity lag would result.

5.3 ESTIMATION OF THE AVERAGE SWIRL AT THE VENA CONTRACTA

For the purpose of finding relative swirl strengths at the vena contracta sections the approximate formula 2.3.3.b

$$\overline{vr}_{jet} = \frac{\bar{r}^2 \sqrt{\frac{g}{2}} \sqrt{\left(\frac{r_*}{\bar{r}}\right)^2 - 1}}{\sqrt{H + z} - \sqrt{H}}$$ was used,

where z is the distance below the orifice at which r_* is measured,

H is the depth of flow at $r \doteq 4D$,

$$\bar{r} = \frac{a + b}{2},$$

$$r_* = r_x - \frac{t_z}{2}$$

and t_z is the jet thickness at z.

Values of $\overline{vr}_{jet}$ were calculated from the data of figures 4.1.10, 4.1.11 and 4.1.12, and plotted in figures 4.1.12 (a) to (c). For the comparison of discharge swirls, dimensionless values of $\overline{vr}_{jet}$ were obtained as in section 5.2 by, $\overline{vr}_{jet} / (\sqrt{2gr_o}\ r_o)$ and these were plotted in figure 5.3.1 with H/D for the models of series I. To confirm that the estimation of relative swirl strength by equation 2.3.3(b) is reasonable, its maximum value was compared with the average surface swirl at r = D for corresponding H/D's. The differences were found to be small (about 3%, 0.2% and 2.1% for the small, medium and large models respectively) with the surface swirl being larger in each case.

Factors tending to cause such a difference are:

1) The neglect of the depth-wise distribution of swirl at r = D;

2) The decrease in the discharge swirl by rotational flow near the air core.

In view of the rather large standard deviations for both estimates of swirl, even larger differences could have resulted from chance alone. The reason for choosing r/D = 1 in the above comparison is implied in section 5.2.

5.4 THE COEFFICIENT OF CONTRACTION

An attempt to correlate the contraction coefficient with the swirl number using the theory presented in section 2.4 was not very successful mostly because of insufficient information about the vena contracta and the swirl. Nevertheless the following analysis indicates that equation 2.4.2(b) is a valid description of the influence of swirl on the vena contracta.

From equation 2.4.2(c) we have,

$$C_c = 0.62(1 + (S)^{\alpha} F(H/D)).$$

Now considering two coefficients of contraction C_{c1} and C_{c2} with swirl numbers S_1 and S_2 respectively, at a given H/D, equation 2.4.2(c) gives

$$\alpha = \frac{\log(C_{c1} - 0.62) - \log(C_{c2} - 0.62)}{\log(S_1) - \log(S_2)} \qquad (5.4.1).$$

Further if scale effects are neglected we can use the information of figures 4.1.11 and 4.1.12 to estimate an average α for the three models. The average value of α was found to be 1.93. The function F(H/D) was found to be approximately constant (value of 0.50) in the range

$1 < H/D < 3$. Therefore the approximate formula for C_c is

$$C_c = 0.62(1 + 0.50(S)^{1.93}) \qquad (5.4.2)$$

which has a possible error of about $\pm$ 2%.

5.5 SWIRL AND VELOCITY COEFFICIENTS

Series I

It was found in section 2.2 that the ideal discharge coefficient was,

$$C_D = C_c C_A \qquad (2.2.8).$$

However in the case of a real fluid it is necessary to include a coefficient C_v to account for head losses and a non-ideal velocity distribution; the discharge coefficient is then written

$$C_D = C_v C_c C_A \qquad (5.5.1).$$

The velocity coefficient

$$C_v = \frac{C_D}{C_c C_A}$$ is used to compare the model flows in the region of the orifice. It is reasoned that if the values of C_v are equal in two models then for practical purposes the models exhibit local discharge similarity.

The dimensionless parameter $\lambda_b = \frac{C}{\sqrt{2gh}\, b}$ calculated from the data of figures 4.1.11 and 4.1.12 and values of λ_b are plotted in figure 5.5.1.

$$C_\lambda = \left(\sqrt{1-\lambda^2} - \lambda^2 \left|\ln \left|\frac{1-\sqrt{1-\lambda^2}}{\lambda}\right|\right|\right)$$

was found from figure 2.2.2.

Finally C_v is plotted with H/D in figure 5.5.2 for the three models of series I.

5.6 COMPARISON OF AIR CORE RADII

If exact Froude similarity exists throughout the models then the ratio of the air core radius to the orifice radius should be the same for all the models. Accordingly, a_o/r_o was plotted in figure 5.6.1. A general dissimilarity was noted and attributed to the difference in the relative swirl levels of the models.

The ratio a_o/r_o alone does not give much information about a local scale effect in the region of the orifice. To investigate this effect we note that local Froude similarity would exist if the ratios, of the actual air core radius to the theoretical air core radius based on the existing swirl levels, are equal in the models.

The theoretical air core radii were estimated

from

$$a_t = \frac{C_{jet}}{\sqrt{2gH}} \qquad (5.6.1)$$

where C_{jet} represents the average swirl in the discharge as given by equation 2.3.3(b).

The ratios of a_o / a_t are plotted in figure 5.6.1 for the models of series I.

5.7 REYNOLDS NUMBER

An inlet Reynolds number, defined by,

$$R_i = \frac{Q}{W_i \nu} \qquad (5.7.1)$$

was chosen as a convenient parameter for model comparisons. It is difficult to say what value of Reynolds number should be used in the region of the air core; the Reynolds number there would involve the three components of velocity, the air core size and the depth of flow.

It is noted that R_i for the small model at $H/D = 0.5$ is 1450 and it is considered to be just in the turbulent range.[23]

The water temperature was $15 \pm 1°$ C for all the experiments.

23. p.24.

5.8 STATISTICAL TREATMENT OF THE EXPERIMENTAL DATA

(a) Treatment of Observations.

The general approach used on fitting a curve to the observed data was:

1) The data (x_i, y_i) was plotted either arithmetically or logarithmically in order to obtain the best linear fits;

2) The points were grouped into ranges which could be represented by straight lines;

3) These lines were fitted by a trial and error least squares method;

4) The ranges were then joined by smooth curves to give a continuous curve.

The standard deviation of the mean curve for a given range was taken to be

$$\sigma_m = \sqrt{\frac{\sum^n (\delta_i)^2}{n(n-2)}}$$

where δ_i is the deviation of an observation from the mean curve, and n is the number of observations considered to be in the range.

The above procedure was used to fit and find the standard deviations of the curves: a_o , r_z , b/r_o , and Q (H/D as the ordinate).

The random errors in H and z were found to be relatively small and representative standard deviations were assigned to them.

For the purpose of finding the standard deviations of derived functions it was assumed that the deviations of the experimental observations could be treated as normally distributed. The standard deviations for derived functions were found by

$$\sigma_{f(x,\ y,\ z,\ \ldots)} = \sqrt{\left(\frac{\partial f}{\partial x}\ \sigma_x\right)^2 + \left(\frac{\partial f}{\partial y}\ \sigma_y\right)^2 + \left(\frac{\partial f}{\partial z}\ \sigma_z\right)^2 + \ldots}$$

Typical values of standard deviations for the observed and derived functions are given in table 5.8.1. The statistical treatment of the discharge observations for series II, III and IV was abandoned when the deviations of the observations were found to be considerably greater than the standard deviation inferred by the discharge calibration curves. Also these discharges were extremely sensitive and seemed to take on preferred upper or lower values. The upper and lower limits rather than standard deviations are considered for these tests.

(b) The Significance of the Scale Effects.

The main purpose of the following statistical analysis is to provide a basis for judging the significance of an observed 'scale effect'. Since the scale effects were expected to be relatively small it was important to know something about the probability of an indicated 'scale effect' being due only to chance deviations of the mean curves.

The problem is: to determine the probability of the difference between two curves m_1 and m_2, with respective standard deviations σ_{m_1} and σ_{m_2} being due to chance alone.

The deviations of the derived data ~~is~~ are assumed to be normally distributed, and so the standard deviation in $(m_1 - m_2)$ is

$$\sigma_{m_1 - m_2} = \sqrt{\sigma_{m_1}^2 + \sigma_{m_2}^2} \quad .$$

Now from probability tables[22] we can find the probability of

$$k \geq \frac{m_1 - m_2}{\sigma_{m_1 - m_2}}$$ i.e. the probability of $(m_1 - m_2)$ being due to chance alone.

A convention is introduced here to define a positive scale effect as one that exists when a

relative swirl reduction can be attributed to the smaller model. Accordingly the p figures in table 5.8.1 refer to the probability of a positive scale effect being due to chance. The significance level of p is taken to be 5% so that for $p<0.05$ a positive scale effect is said to be probable. On the other hand $p>0.95$ suggests a negative scale effect.

The above procedure was applied to the dimensionless air core curves (a_o/a_c see figure 5.6.1) and to the velocity coefficients (C_v). The results are summarized in table 5.8.1.

6. DISCUSSION OF THE EXPERIMENTAL RESULTS

The experimental results of this investigation indicate the existence of a general and a local scale effect between the small and large models and between the small and medium models. The term 'general scale effect' is used to denote overall dissimilarities in the behaviour of the models. The local scale effect refers to a dissimilarity which predominates in a certain region of the models (e.g. the air core region).

6.1 THE OVERALL DISSIMILARITY OR GENERAL SCALE EFFECT

Series I

The general scale effect between the small and large and the small and medium models was found to be negative according to the convention of section 5.8(b) i.e. the swirl levels in the small model were relatively greater than in the larger models.

The indications of this effect are:

1) For $H/D < 3$ the discharge coefficients C_D of the small model (series I) were consistently less than those of the larger models, (see figure 5.1.1). Figure 5.1.2 shows that this

was generally true of the second series of models as well.

2) The average surface swirl number at $r \simeq D$ is greater in the small model than in the larger models; this is shown in figure 5.2.2.

3) The average swirl in the discharge as calculated by equation 2.3.3(b) is relatively greater in the small model than in the larger models, as figure 5.3.1 shows.

4) The a_o/r_o of the small model is greater than the a_o/r_o of the larger models for $H/D < 2.50$ as shown in figure 5.6.1.

A possible explanation for this effect is, that the relative differences in the overall swirl levels resulted from differences in the inlet conditions. An attempt was made to check this experimentally by observing the effects of certain inlet alterations.

It was thought that the inlet surface velocity in the small model may have been exaggerated by the strip at the base of the flow straightener; however no change was noticed in the model performance when this strip was planed to 1/3 of its original thickness. Also the surface velocity of the largest

model was artificially exaggerated by an obstruction placed across the inlet; this produced very little change in the vortex (a slightly stronger swirl was found in some cases).

Dye traces showed that certain cross-currents were peculiar to the inlet of the small model and when these were eliminated by plasticene packing (as shown in figure 6.1.1) the swirl level was reduced considerably.

Figure 6.1.1

(Plan)

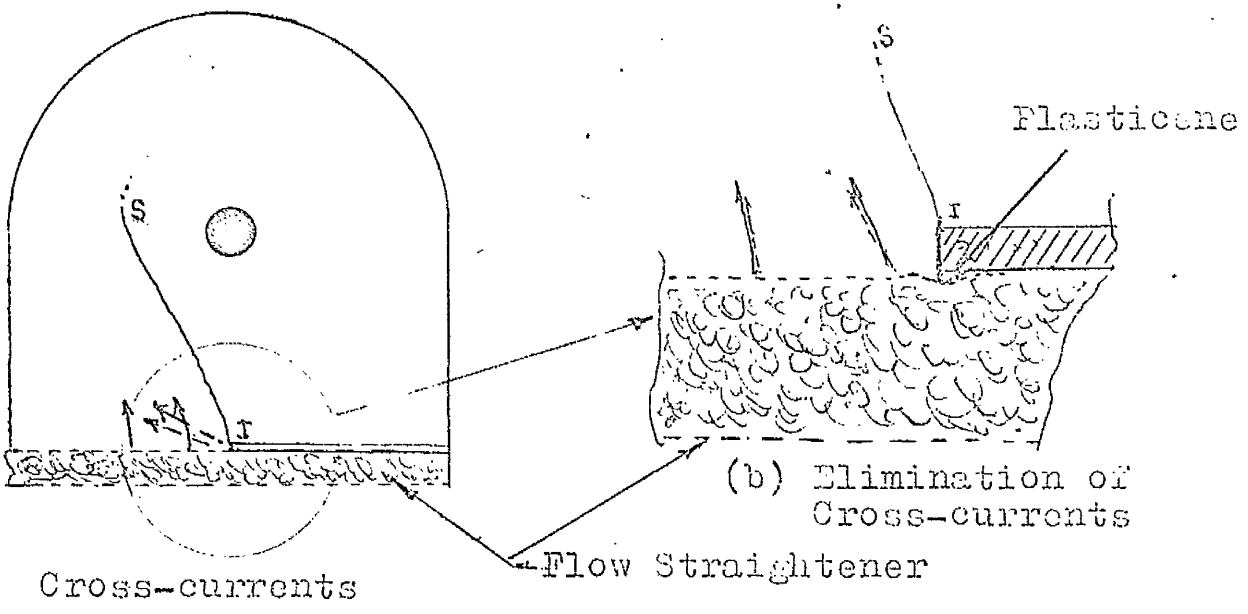

Curves in A and B in figure 4.1.12 represent the swirl strength before and after the elimination of the cross currents. Curve B was used thereafter for all model comparisons but the negative scale effect was still not

completely explained.

Since the same flow straightener was common to all models and the scales of the 'turbulence' eddies would be influenced by the properties of the screens,[10] a negative scale effect on the turbulent losses might result in the neighbourhood of the inlet. These losses were assumed to be of the same order of magnitude as the friction losses discussed in section 2.6 and were neglected. Lack of time prevented us from fully investigating the influences of the flow straightener.

It is now thought that large eddies had a greater influence on the swirl in the larger models than in the small model. This was suggested by figures 5.2.1 and 5.2.2 which show that the entrance values of $\frac{vr}{\sqrt{2gr}\, r_0}$ for the large and small models differed by much less than the values in the region of the corner D and in the region of and inside the stream channel separation line. Since both these are regions of large eddy activity it is concluded that some of the main circulation was lost in the rotational flow of these eddies. This loss was greater in the larger models because they were more prone to eddy formation.

10. pp. 91-92.

6.2 LOCAL SCALE EFFECTS

Series I

The statistical analysis of section 5.8(b) indicated that a positive local scale effect existed in the region of the air core between the small and either larger models. Using a significance level of 5% and comparing the a_s/a_l curves (figure 5.6.1) this effect is probable for $H/D > 1$. A possible exception to this is in the immediate neighbourhood of $H/D = 2$ where there is some doubt ($p = 8.6\%$) about the significance of the scale effect between the small and large model. No certainty could be attached to the apparent 'scale effects' that are shown in figure 5.6.1 between the medium and large models for $H/D < 3$.

The only significant scale effect ($p < 5\%$) on the discharge similarity between the small and either of the larger models was in the neighbourhood of $H/D = 2$ where the C_v of the small model was considerably larger than the C_v for the others (see figure 5.5.2 and table 5.8.1). This would seem to suggest that the exception to the air core scale effect noted in the previous paragraph, can be disregarded.

It was therefore concluded that in the range $1 < H/D < 3$ there is a positive scale effect in the region

of the air core but this is not so great as to have much influence on the discharge similarity. The air core scale effect starts to be significant in models of the same order of size as the small model (2"D).

The reduction in all the air core radii with increasing H/D, as indicated by the a_o/a_t curves in figure 5.6.1, is attributed to rotational flow in the region of the vortex air core surface and because of the relative importance of viscous forces in the small model its rotation flow was the most extensive.

The following is an attempt to explain the local scale effect by the theory of section 2.5. Although numerical values are used, the argument is only qualitative. From section 2.5 we have

$$\frac{vr}{v_o r_o} = \frac{1+\frac{Aa^2}{2r_c(r-a)} - e^{-\frac{A(r-a)^2}{2r_c(r-a)}} + \frac{a\sqrt{2A\pi}}{\sqrt{r_c(r-a)}}\operatorname{erf}\frac{A(r-a)}{\sqrt{2r_c(r-a)}}}{1+\frac{Aa}{2r_c(r_c-a)} - e^{-\frac{A(r_c-a)}{2r_c}} + \frac{a\sqrt{2A\pi}}{\sqrt{r_c(r_c-a)}}\operatorname{erf}\frac{A(r_c-a)}{\sqrt{r_c(r_c-a)}}}$$

for $a \leqslant r \leqslant r_o$ (2.5.9)

and $A = \dfrac{Q_o}{2\pi l_o(\nu + \xi)}$ (2.5.10).

Let us consider the limit of equation 2.5.9 as $r \to a$, for a large A (say $A > 1000$)

$$\frac{vr_a}{v_o r_o} = \frac{1}{1 + \sqrt{2}\pi \frac{\sqrt{r_o (r_o - a)}}{a\sqrt{A}} + \frac{2r_o (r_o - a)}{a^2 A}} \qquad (6.2.1).$$

Let $\psi = \sqrt{\frac{2\frac{r_o}{a}\left(\frac{r_o}{a} - 1\right)}{A}}$

then $$\frac{vr_a}{v_o r_o} = \frac{1}{1 + \pi\psi + \psi^2} \qquad (6.2.1a).$$

It is seen from equation 6.2.1 that vr decreases as 'a' decreases and becomes zero at a = 0, this explains the reduction in the a_o / a_t values with increasing H/D.

Equation 2.5.10 and 6.2.1 will now be used to give an explanation for the observed local scale effect. For illustrative purposes we assume that $\xi \sim O(\nu)$ at H/D = 3 in the small model, and $\xi \propto R_{INLET}$[20,10].

$$\text{Now,} \quad A \simeq \frac{Q}{2\pi l_o \nu} \frac{1}{1 + \frac{R_{1p}}{R_{1mB}}} \qquad (6.2.2)$$

where the subscripts p and m refer to the prototype and model, and B denotes a base Reynolds number (say the R_{INLET} at H/D = 3 in the small model).

20. pp. 385-394,
10. p. 91.

Table 6.2.1

A THEORETICAL EXPLANATION OF

MODEL BEHAVIOUR AT THE AIR CORE

	D	SMALL 2"	MEDIUM 4"	LARGE 6"	∞
	$\nu = 1.0 \times 10^{-5}$ FT²/SEC.				
H/D = 3	a_o/a_t	.567	.714	.771	
	a_o/r_o	.136	.143	.143	
	A	1040	1600	1970	
	$\frac{va}{v_o r_c}$	0.493	0.565	0.590	
	.....				
	$\frac{va}{v_o r_o}$ at $\frac{a_o}{r_o} = 1/10$	0.403	0.464	0.490	A = 2080 0.503

The comparison of a_o / a_t and $\frac{va}{v_o r_c}$ in table 6.2.1 shows that these quantities vary in a similar way for the models considered. It is noted that for a given a_o/r_o the swirl reduction is greatest in the small model; as a result of this the air core diameter

in the small model is reduced more than in the larger models; this is the 'local scale effect.

Since the small model was operated at a greater swirl number than the larger models, its Froude velocities in the region of the orifice would also be greater, which would give rise to a relatively greater 'eddy viscosity' effect in the small model.

Further reference is made to the behaviour of the air core in section 6.3.

6.3 PECULIARITIES IN THE AIR CORE BEHAVIOUR

Series I

The author has not found satisfactory explanations for some aspects of the air core behaviour. For example we have not been able to explain completely the observed instability in the air core which started at $H/D \simeq 1.6$. It was not clear whether this was a local effect or the result of an overall change in the model behaviour.

The more rapid decrease in the air core at $H/D > 1.6$ can be partly attributed to the decrease in the inlet velocity as the discharge begins to vary as the square root rather than directly as the depth. Also it was seen in section 6.2 that the local (air core)

swirl reduction becomes greater as the air core decreases i.e. as the depth increases. It is thought that the instability may have been due to presence of large eddies in the models. This was suggested by the intermittent 'gulping' phenomenon noticed in the region of the air core.

The existence of an air core larger than the ideal as shown in figure 5.6.1 at $H/D < 1.6$ can be accounted for by the existence of a significant downward velocity 'w' on the air core surface at the critical section; thus the air core must expand in order to satisfy Bernoulli's equation. In the limit if 'w' is constant throughout the critical section then a theory due to Binnie [12] gives

$$a_{max} = \frac{a_t\sqrt{1 + \sqrt{1 + 8\left(\frac{r_o}{a_t}\right)^2}}}{2} \qquad (6.3.1)$$

where $a_t = \frac{c}{\sqrt{2gH}}$.

In equation 6.3.1, since $r_o/a_t < 1$,

$$a_{max} > a_t.$$

However as the air core decreases the ideal velocity distribution is more closely approached.

6.4 THE VELOCITY COEFFICIENT

The coefficient of velocity increases rapidly as H/D decreases below 0.4. This is due to the predominence of sill control at low heads. For $0.5 < H/D < 3$, C_v has maximum values of 0.950, 0.955, and 0.991 at H/D's of 1.5, 1.4, and 1.8 for the large, medium and small models respectively.

Some reasons for C_v being < 1 are:

1) The head loss between the position where H was measured and the orifice;
2) The expansion of the air core due to a non-ideal Z velocity distribution; and
3) Expansion of the air core at the vena contracta.

Factors which would tend to increase C_v are:

1) The vena contracta occurring at a significant distance below the plane of the orifice;
2) The decrease in the air core radius due to viscous and turbulent shear.

6.5 THE DETERMINATION OF SWIRL

Equation 2.3.3(b) was used to obtain an estimate of swirl for comparison purposes and although it is not claimed to be a precise expression, it should give an approximation to the absolute average swirl in the discharge. Resort was made to this indirect method of determining swirl when the surface float method proved unreliable in the region of the orifice. One would expect equation 2.3.3(b) to become less reliable at higher H/D's (>2.5 say) because of the increasing asymmetry of the vortex with respect to the orifice.

6.6 REGIME SIMILARITY OF MODEL BEHAVIOUR

Series I

By regime similarity we mean similarity of events with respect to stage (H/D).

Air core instability commenced at H/D values of 1.6, 1.6, and 1.8 for the large medium and small models respectively. In all models sill effects existed for $H/D < 0.4$. Other regime similarities and dissimilarities are mentioned in sections 6.4, 4.2(a) and 4.2(b).

In general for the series I tests similar

events occurred in all three models but complete regime similarity only existed between the two large models.

6.7 INFLUENCES OF MODEL GEOMETRY

(a) The Boundary Shape - Series II

It was found that vortex flow in the models of series II (i.e. of rectangular shape) was less stable and weaker than in series I models (i.e. models of more symmetrical shape). This difference in behaviour was attributed to the existence of stronger eddies in the rectangular shaped models. Comparing the discharge coefficients from figures 5.1.1 and 5.1.2, it is seen that the C_D for series II is larger and more random. The random behaviour of the series II models made similarity difficult to infer; however the order of magnitude of the 'shape' effects was relatively the same for the three models; this is shown by the $\frac{C_{DM}}{C_{DP}}$ curves in figure 6.7.1. The regime behaviour was quite random and generally dissimilar. The large model vortex became unstable at a much lower H/D (2.1) than did the vortex in the medium (2.5) or small model (2.7).

(b) Model Exaggeration - Series III

Figure 5.1.3 suggests that floor friction influences on model swirl are predominant for $H/D < 0.8$ and thereafter the vortex formation is increasingly determined by other factors such as wall effects, large eddies, and turbulent shear. The 8", 6" and 4" diameter models had unstable vortices at H/D greater than (1.3 to 2.0), (1.4 to 1.8), and (2.0) respectively whereas the 2" diameter model had a stable vortex for $H/D < 4.2$. The 8", 6" and 4" models showed reasonably similar behaviour but the 2" diameter model showed dissimilar behaviour for $H/D > 0.8$.

(c) Orifice Shape - Series IV

The square orifice gave discharge coefficients (figure 5.1.4a) which were slightly less than those of the equivalent circular orifice. This, it is thought, was because the vena contracta of the square orifice was less effected by swirl.

(d) Eccentricity of Inflow - Series IV

Increasing the eccentricity of the inflow (as shown in figure 3.2.3) caused an increase in swirl for $H/D < 2$ (see figures 4.3.3 and 5.1.4b). However,

vortex instability started at about H/D of 1.4 and a considerable reduction in swirl resulted in the range $1.4 < H/D < 4$. The swirl recovered and a violent vortex formed for $H/D > 4.5$. Final collapse was not observed for $H/D < 7.5$.

7. THE FORMATION OF A VORTEX DURING DRAINAGE OF AN AXIALLY ASYMMETRICAL RESERVOIR

Several observations were made of vortex behaviour during free drainage from an axially asymmetrical reservoir in order to demonstrate the formation of a swirl greater than that which would arise from the earth's rotation alone.

7.1 PROCEDURE

The 4 inch diameter orifice was placed in the central position of the tank and all the partitions and roundings were removed. In each test the orifice was plugged and the tank filled to a depth of about 1 foot. Periods of 2 hours to 6 days were allowed for random currents to decay.

Two methods were used to block the orifice. A rubber diaphram glued to the underside of the orifice was punctured to initiate flow. A flat hard rubber stopper, placed over the orifice, was carefully slid off to start the flow. Both methods gave similar drainage behaviour and since the second method was the more convenient it was used in most of the tests.

Small 'polyzote' floats (approximately 1/4" cubes) were scattered on the water surface to indicate

velocities and flow patterns; accurately timed exposures were taken with a 35mm camera to determine the velocities of the floats. Cotton tufts and dye traces were used to determine the flow patterns throughout the tank.

7.2 OBSERVATIONS AND COMMENTS

Visual observations of the cotton tufts showed that the flow near the floor was not greatly affected by swirl. However the surface flow was quite haphazard; sometimes a strong general swirl developed and at other times only a weak swirl in the region of the orifice was noticed. Dye traces showed that the violent swirl activity started at the water surface.

A record of one of the most violent vortices is given by the sequence of photographs in figure 7.2.1. Measurements are given in table 7.1. Figure 7.2.2 shows surface velocities determined from this record. The strength of the surface vortex reached a maximum of about 0.1 Ft^2/sec in the anticlockwise direction at a depth of about 1.1/2 inches. The swirl due to the earth's rotation alone would be about 3.8×10^{-4} ft^2/sec. It was noted that an anticlockwise vortex appeared over the orifice at a depth of about 4 inches.

The water surface became covered with a film of dust during the stilling periods before some of the tests. In these tests the surface layer remained almost stagnant while a very weak anticlockwise vortex developed over the orifice when the depth fell to about 2 inches. This effect was attributed to surface tension and when liquid soap was sprinkled on the surface, a more general surface swirl developed.

In all tests anticlockwise rotation was observed. The foregoing observations indicate that, in the arrangement tested,

1) the formation of violent vortices was primarily a surface phenomenon;

2) the surface swirl can greatly exceed that due to the earth's rotation;

3) the earth's rotation seems to initiate the vortex motion in the anticlockwise direction.

Diesel[18] has explained the growth of a drained vortex in an axially asymmetrical reservoir as follows: In a perfect fluid the vortex flow is maintained by a pressure difference between A and B (figure 7.2.3) but in a real fluid the flow near the floor, as it moves more slowly, will be subject to a greater deviation than surface flow. This it is

claimed would cause the vortex to increase in strength.

Figure 7.2.3

Vortex Formation in an Axially Asymmetrical Reservoir.

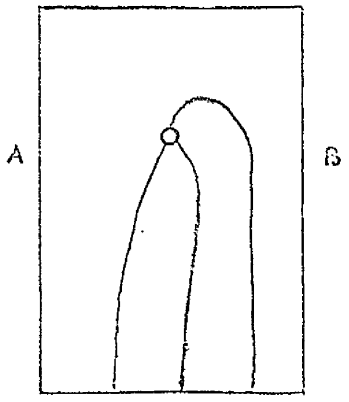

This explanation, however is not entirely in agreement with our observations; in particular the strong vortices appeared to originate at the surface and not in the region of the floor. It is suggested that the pressure difference between A and B has its greatest influence on the surface layer since its resistance to movement would be least. This would cause the surface layer to have a greater circulation than the original circulation due to the earth's rotation.

8. CONCLUDING REMARKS

The effects of model scale and geometry on vortex flow in axially asymmetrical reservoirs were studied for low submergence ratios ($H/D < 4$). It was found that the vortex behaviour was quite sensitive to the abruptness of the model geometry. The 'horseshoe' shaped models (i.e. those with the half-rounding) produced stronger and more stable vortices than did the rectangular models. It was concluded that the instability and loss of swirl in the rectangular models was largely due to the formation of eddies in the rapidly diverging flow approaching the corners.

Similarity of model behaviour was examined closely in the 'horseshoe' shaped models. General and local dissimilarities existed between the smallest model (2" diameter orifice) and either of the larger models (4" diameter and 6" diameter orifice). The two larger models showed reasonably similar behaviour as regards swirl production and local (air core) scale effects.

The general scale effect refers to the relatively stronger swirls produced in the smallest

model. It is thought that large eddies had a greater influence on the vortex formation in the larger models.

The local scale effect refers to the swirl reduction in the neighbourhood of the air core which was greatest in the smallest model. This scale effect became more significant as H/D increased above 2 i.e. as the air core became smaller. At H/D = 3 the a_o/a_t of the smallest model was 0.73 of the a_o/a_t of the largest model.

The scale effects mentioned above were confirmed by the discharge and velocity coefficients, (C_D and C_v). The local scale effect on the velocity coefficient C_v was less significant than the effect on the air core diameter.

It would appear that the scale effect on the air core diameter depends on both a_o/r_o and Reynolds number. It is suggested that models of absolute size not smaller than the smallest model used in this investigation (2" diameter orifice) would exhibit small local scale effects (i.e. less than 15% relative reduction in a_o/a_c) if $a_o/r_o > 0.25$ and $R_I > 1500$.

9. REFERENCES

1. Streeter, V.L. — Fluid Mechanics. McGraw-Hill, Toronto, 1958.

2. Young, G.A.J. — Swirl and Vortices at Intakes. British Hydromechanics Research Association Report SP726, April, 1962.

3. Denny, D.F. — An Experimental Study of Air-entraining Vortices at Pump Sumps. Proc. I. Mech. E., 170, 2, pp. 106-16, 1956.

4. Haindl, K. — Contribution to Air-entrainment by a Vortex. Proc. 8th Congress I.A.H.R., Montreal, Paper 16-D, 1959.

5. Quick, M.C. — A Study of the Free Spiral Vortex. Ph.D. Thesis University of Bristol, 1961.

6. Hattersley, R.T. — Factors of Inlet Channel Flow Affecting the Performance of Pumping Plant. Univ. of N.S.W., Water Research Lab. Report No. 23, Sept., 1960.

7. North of Scotland Hydro-Electric Board. — Report on a Hydraulic Investigation of the Proposed Culligran Tunnel Intake. George Wimpey and Company, Nov., 1959.

8. Iversen, H.W. — Studies of Submergence Requirements of High-Specific-Speed Pumps. Trans. A.S.M.E., 75, 4, pp. 635-641, May, 1953.

9. Fraser, W.H. — Hydraulic Problems Encountered in Intake Structures of Vertical Wet-pit Pumps and Methods Leading to Their Solution. Trans. A.S.M.E., 75, 4, pp, 643-652, May, 1953.

10. Rouse, H. — Engineering Hydraulics. Wiley, New York, 1958.

11. Einstein, H.A., Li, H. — Steady Vortex Flow in a Real Fluid. La Houille Blanche, 10, 4, pp. 483-496, Aug.-Sept., 1955.

12. Binnie, A.M. Hookings, G.A. — Laboratory Experiments on Whirlpools. Proc. Roy. Soc. A., 194, pp.398-415, Sept., 1948.

13. Binnie, A.M. Davidson, J.F. — The Flow Under Gravity of a Swirling Liquid Through an Orifice Plate. Proc. Roy. Soc. A., 199, pp. 443-457, 1949.

14. Lamb, H. — Hydrodynamics, Cambridge Univ. Press, 1953.

15. Long, R.R. — A Vortex in an Infinite Viscous Fluid. J. Fluid Mech. 11, part 4, pp. 611-624, 1961.

16. Lewellen, W.S. — Three-dimensional Vortex Flows with Strong Circulation. J. Fluid Mech. 14, part 3, pp. 420-432, 1963.

17. Donaldson, C.du P., Sullivan, R.D.
Examination of the Solutions of the Navier-Stokes Equations for a Class of Three-dimensional Vortices. Part I. Velocity Distribution for Steady Motion. Proc. Heat Transfer and Fluid Mech. Inst., Stanford Univ. Press, pp. 16-30, 1960.

18. Biesel, L.F.
Reflection sur les Vortex de Vidange. La Houille Blanche, 10, 4, pp. 497-505, Aug. - Sept., 1955.

19. Kolf, R.C., Zielinski, P.B.
The Vortex Chamber as an Automatic Flow-Control Device. Proc. A.S.C.E., 85, (Hydraulic 12), pp. 1-8, Dec., 1959.

20. Dryden, H.L., Murnaghan, F.P., Bateman, H.
Hydrodynamics. Dover Publications, N.Y., 1956.

21. Chow, V.T.
Open-Channel Hydraulics. McGraw-Hill, Toronto, 1959.

22. Pearson, K.
Tables for Statisticians and Biometricians. Cambridge Univ. Press, N.Y., 1930.

23. Allen, J.
Scale Models in Hydraulic Engineering. Longmans, Green and Co., London, 1952.

TABLES

H/D	1/2			1			2			3		
D in.	6	4	2	6	4	2	6	4	2	6	4	2
σ_{ao}"	.0197	.0106	.0042	.0197	.0106	.0043	.0324	.0113	.0082	.0324	.0113	.0082
σ_{b}/r_{o}	.205	.114	.122	.072	.0114	.024	.083	.068	.022	.083	.094	.034
σ_{r_z}"	.0082	.0082	.0026	.0056	.0050	.0030	.0032	.0050	.0043	.0032	.0032	.0037
σ_{a}/Q	.017	.039	.029	.0066	.010	.012	.0052	.0057	.0058	.0071	.0047	.0055
σ_{a}/σ_{p}	.019	.039	.030	.0079	.0102	.013	.0057	.0058	.0062	.0071	.0047	.0055
σ_{a}/σ_{c}	.020	.020	.0066	.013	.012	.0095	.0076	.012	.010	.0077	.0077	.0085
σ_{h} "	.041	.0171	.061	.041	.0171	.016	.041	.017	.016	.041	.017	.016
σ_{z} "	.029	.029	.029									
q/c	.042	.035	.064	.019	.034	.015	.024	.032	.016	.027	.040	.025
σ_{x}/λ	.044	.037	.064	.020	.034	.017	.025	.032	.017	.027	.040	.025
σ_{c_x}/σ_{n}	.087	.063	.195	.022	.036	.026	.011	.012	.0013	.0069	.010	.0096
σ_{c}/σ_{v}	.091	.077	.197	.021	.039	.030	.018	.019	.017	.012	.014	.014
$\sigma_{\cdot}/a_{b}/\sigma_{c}$	.054	.044	.072	.027	.041	.019	.047	.039	.027	.062	.039	.037

Table 5.8.1a

STANDARD DEVIATIONS OF END LOADS - Series I

H/D	1/2	1	2	3
D	6" and 2"			
$k_a=\frac{\sigma_h-\sigma_z}{\sigma_{z-z}}$	1.39	2.53	1.38	2.82
p_a	.081	.005	.086	.003
$k_c=\frac{\sigma_{z_1}-\sigma_{z_2}}{\sigma_{z-c}}$	.157	.180	2.60	1.31
p_c	.44	.42	.005	.095
D	4" and 2"			
k_a	1.10	2.66	2.44	2.66
p_a	.136	.004	.007	.004
k_c	.166	- .22	2.90	1.43
p_c	.43	.59	.002	.076
D	6" and 4"			
k_a	.035	- .035	- .84	.84
p_a	.23	.76	.80	.20
k_c	- .009	.39	- .42	- .12
p_c	.50	.35	.66	.55

Table 5.6.1b

Table 7.1

Reservoir Drainage - Test No. 7

Stilling Period 6 Days. Water temperature 15°C.

H feet	t sec.	t sec.	frequency r.p.m.	Photo no.	Remarks
1.000	0	15	600	0	Datum distance 62"
.803	15				
.750	25	10		1	
.661	35				
.618	40	10		2	
.535	50				
.500	55	10		3	
.425	65				
.390	70	10		4	Anticlock-wise vortex over orifice.
.327	80				
.297	85	10		5	
.242	95				
.236	96	15		6	
.165	111				
.148	115	10		7	
.109	125				
.093	130	10	600	8	
.063	140				

FIGURES

FIGURE 2.2.2

DISCHARGE SWIRL COEFFICIENTS

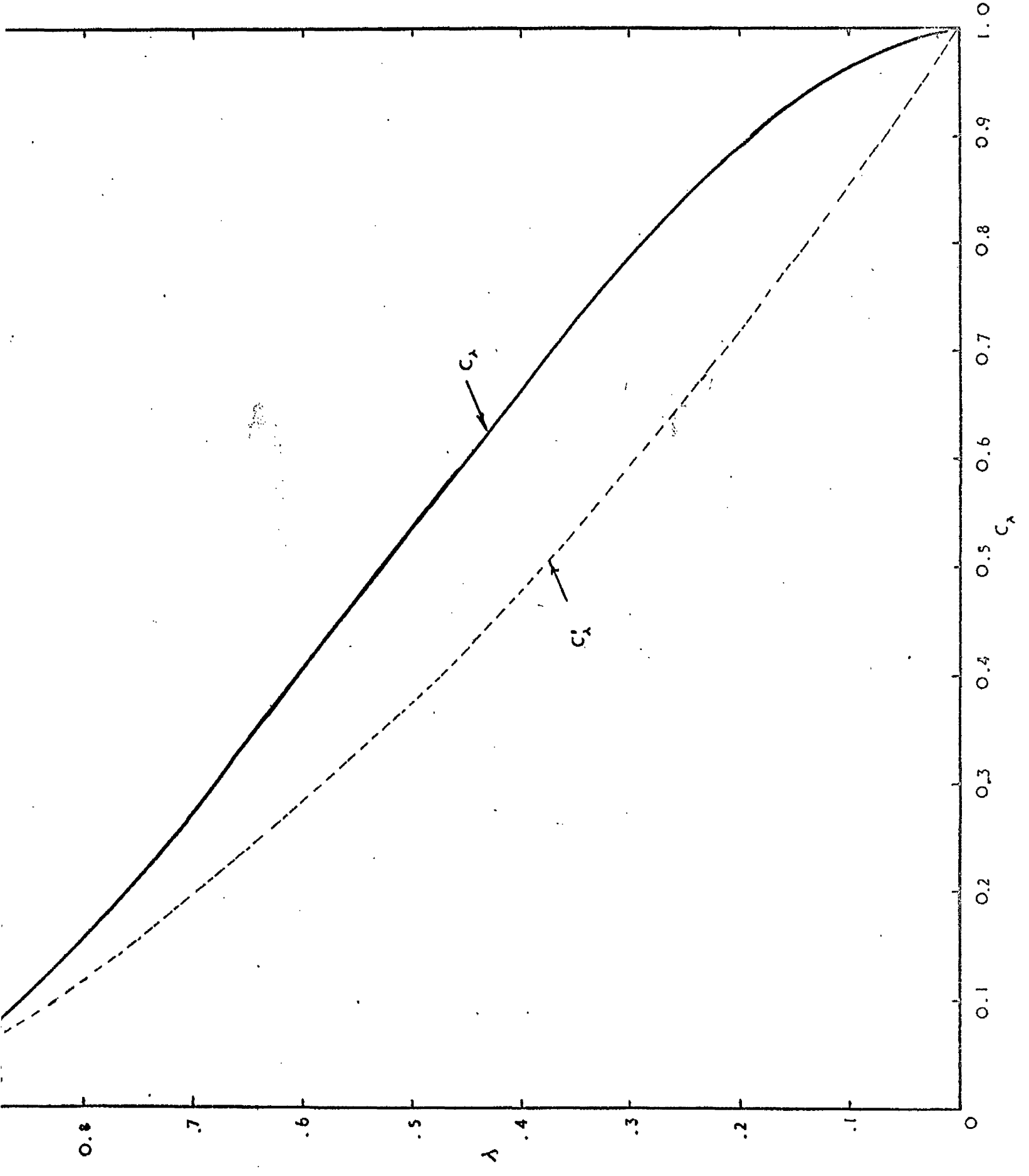

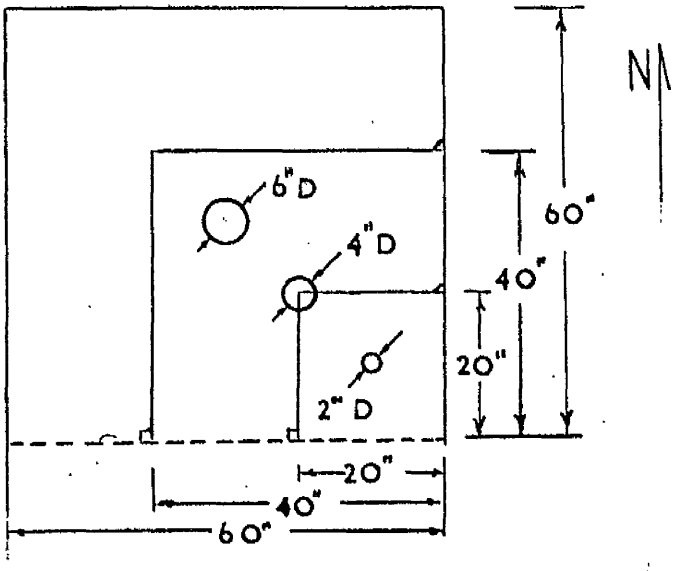

RESERVOIR PLANS

FIGURE 3.1.1
PARTITIONS

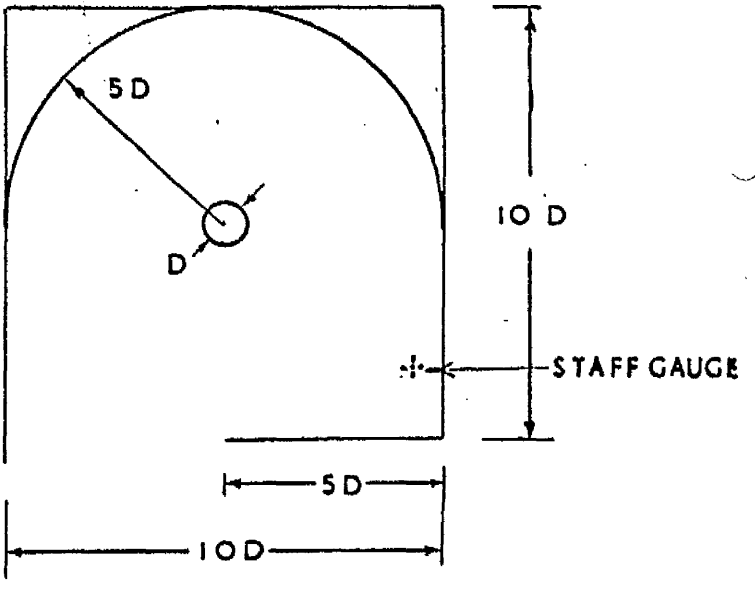

FIGURE 3.2.1
SERIES I MODEL
(HORSESHOE)

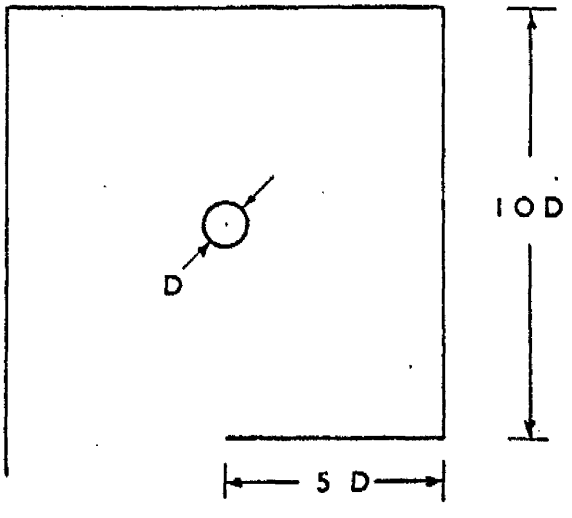

FIGURE 3.2.2
SERIES II MODEL

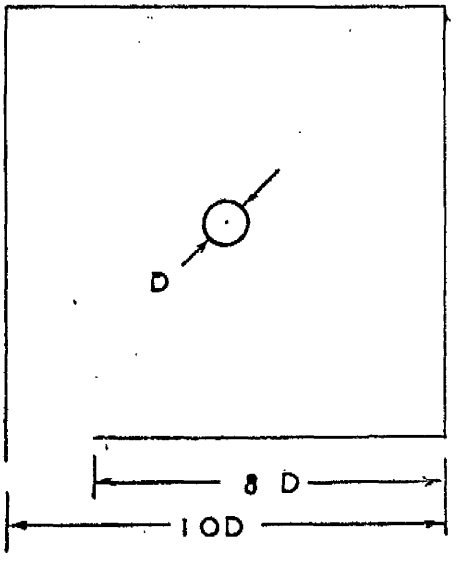

FIGURE 3.2.3
SERIES IV

FIGURE 4.1.1
STAGE/DISCHARGE CURVE
SERIES I
D=6" SHARP-EDGED ORIFICE
TEMPERATURE 15°C.

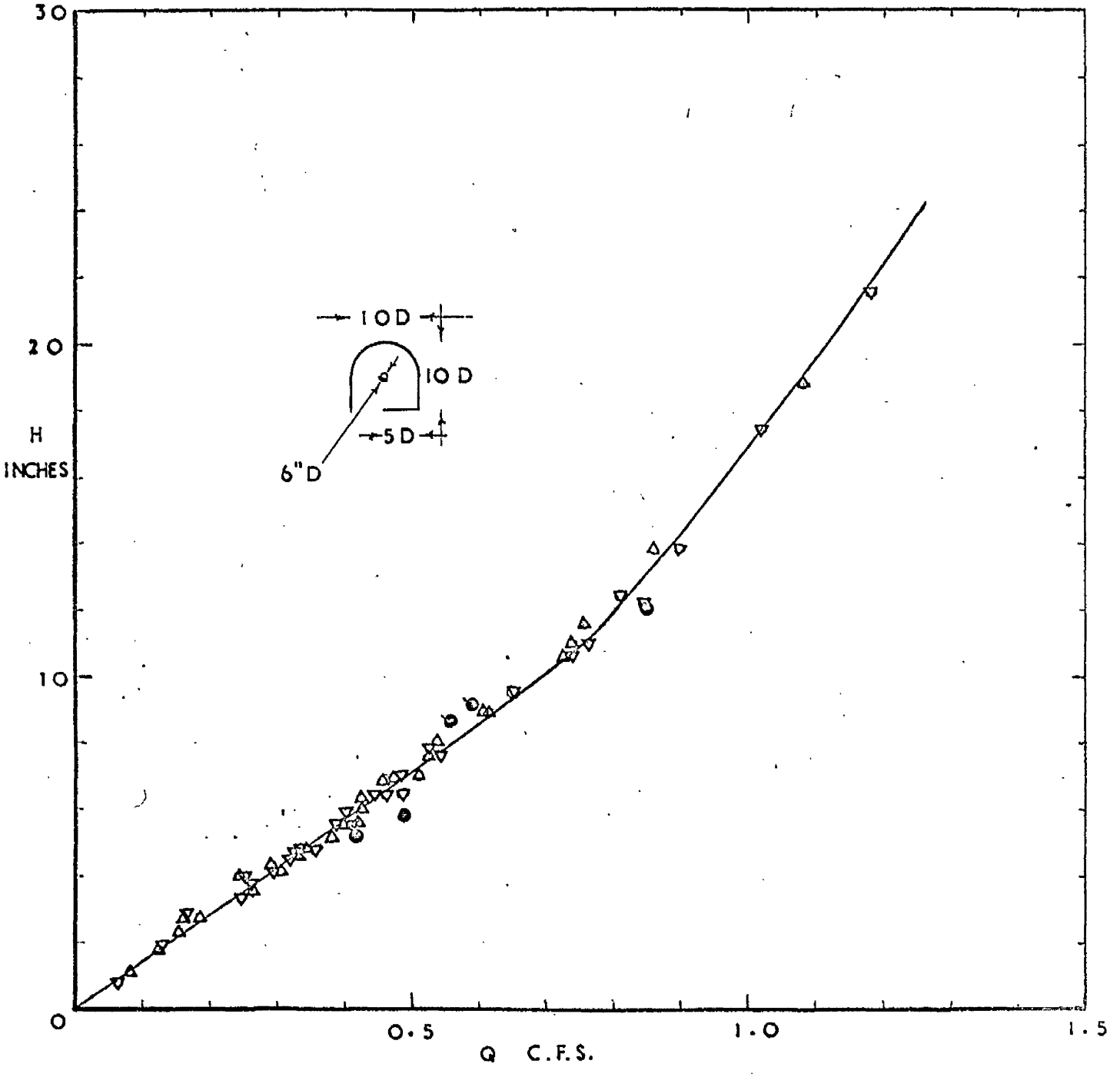

FIGURE 4.1.2
STAGE/DISCHARGE CURVE
SERIES I D=4"

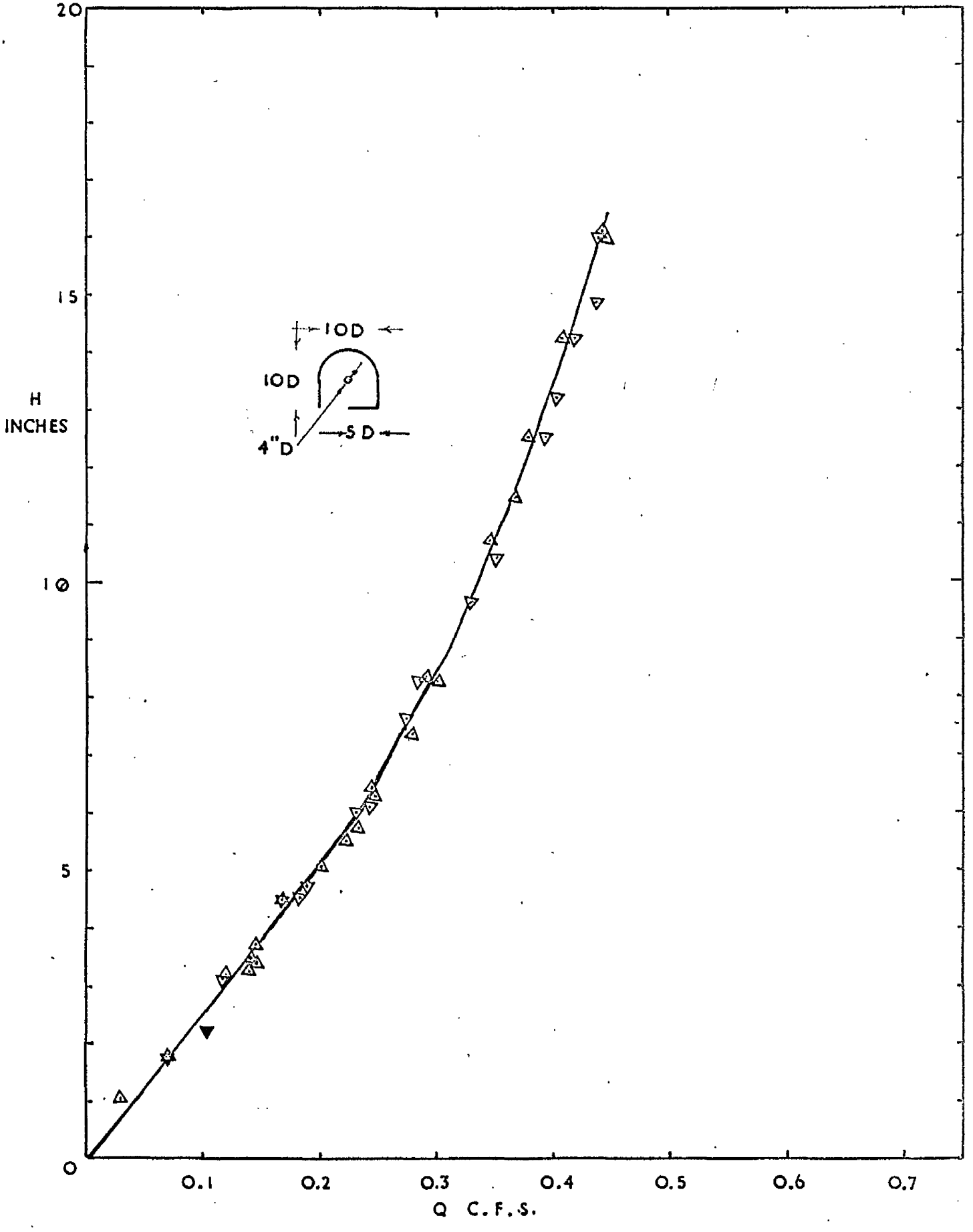

STAGE/DISCHARGE CURVE

SERIES I D=2"

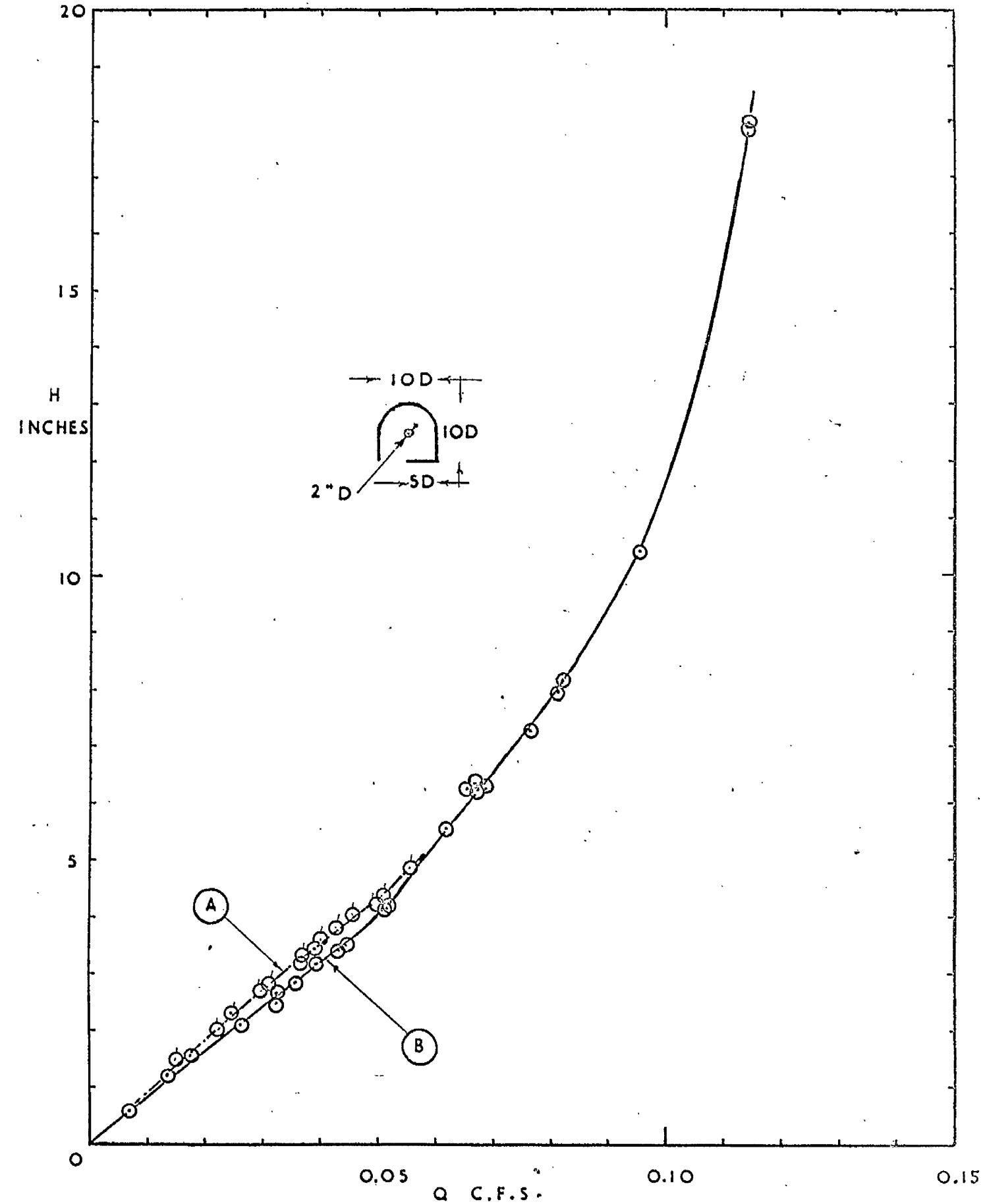

FIGURE 4.1.4
SURFACE FLOATS AND AIR CORE
SERIES I D=6"
H/D 1.5.

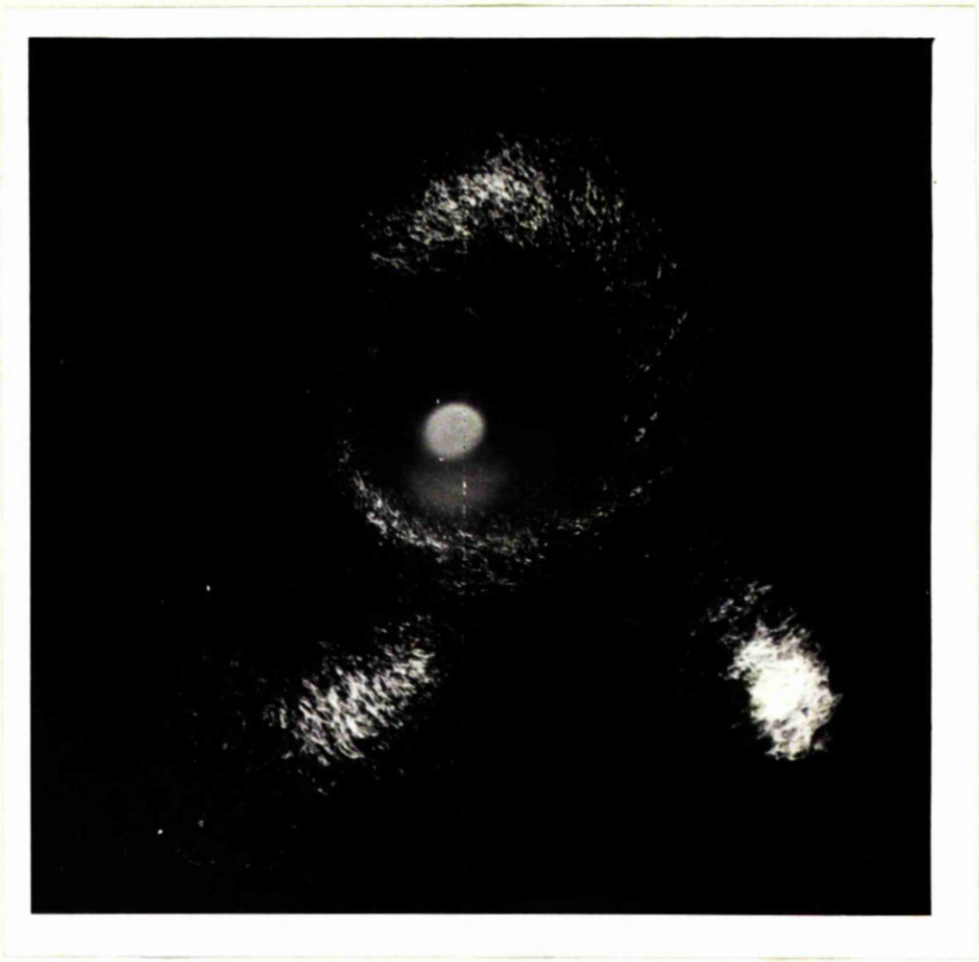

FIGURE 4.1.5
SURFACE FLOATS AND AIR CORE
SERIES I D=4"
H/D 1.5.

FIGURE 4.1.6
SURFACE FLOATS AND AIR CORE
SERIES I D=2"
H/D 1.5.

FIGURE 4.1.7
ANNULAR JET
SERIES I D=6"
H/D 1.5.

FIGURE 4.1.8
ANNULAR JET
SERIES I D=4"
H/D 1.5.

FIGURE 4.1.9
ANNULAR JET
SERIES I D=2"
H/D 1.5.

AIR CORE RADII MEASURED FROM PHOTOGRAPHS
SERIES I

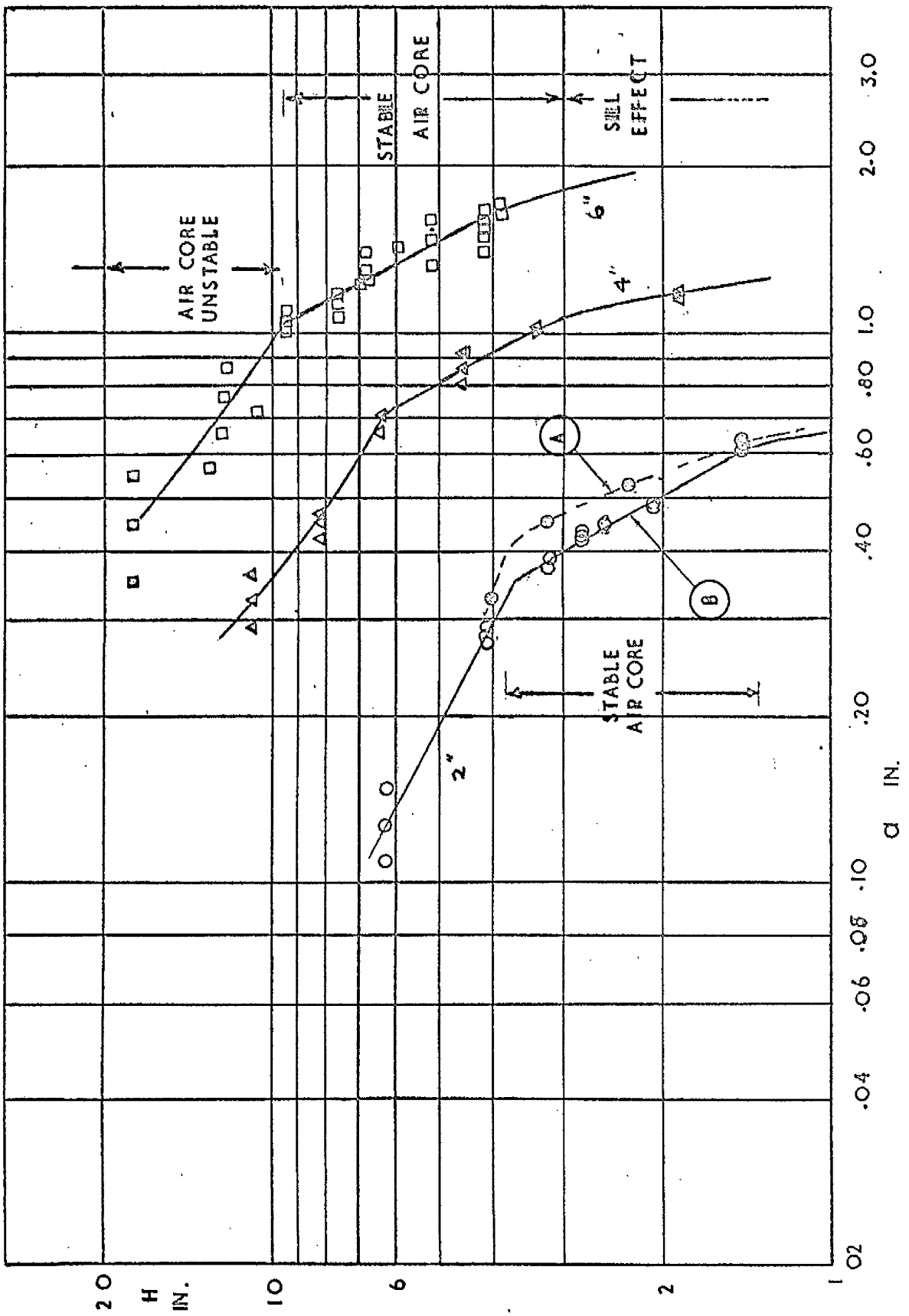

JET RADII AT THE VENA CONTRACTA
SERIES I

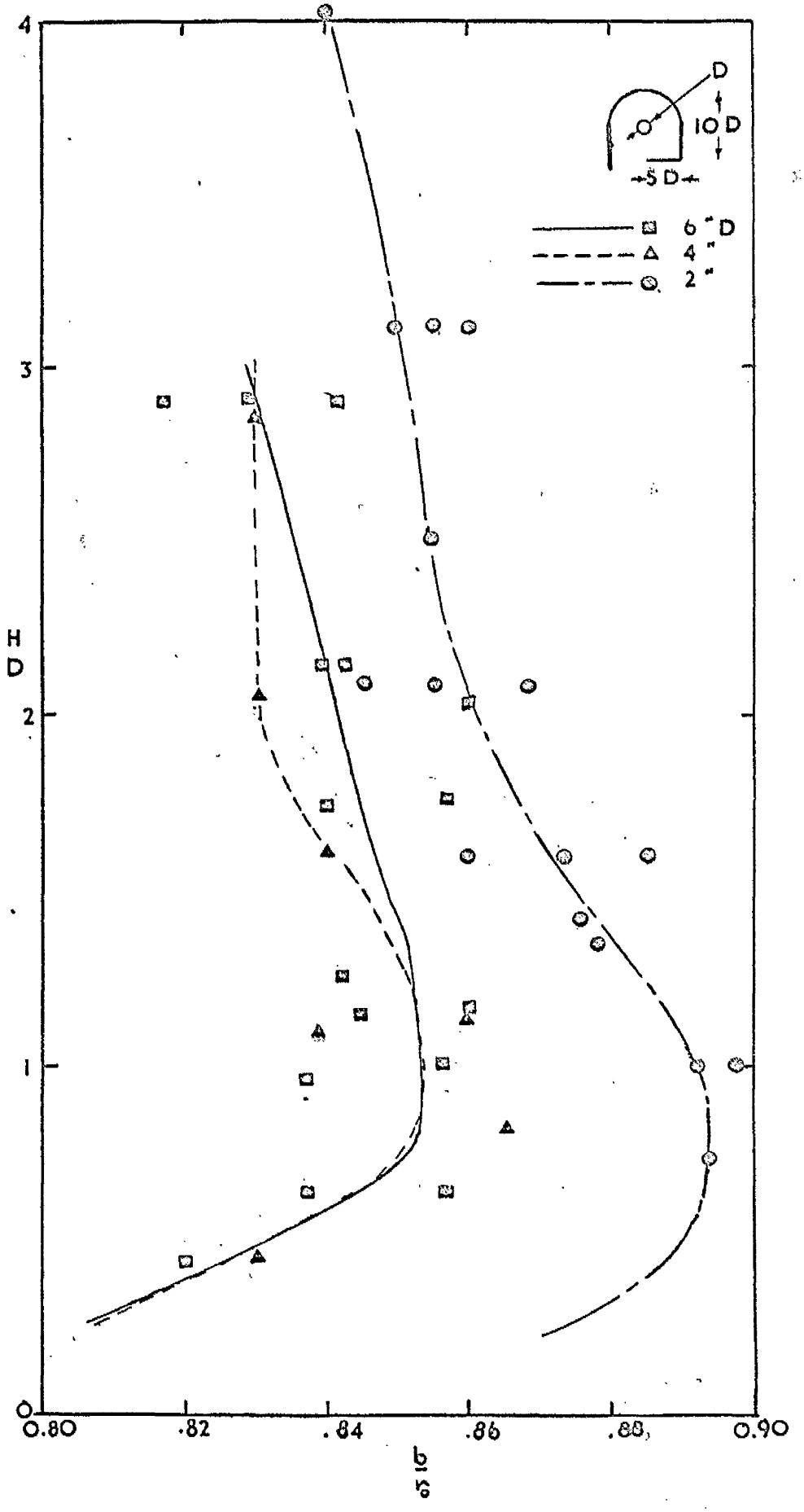

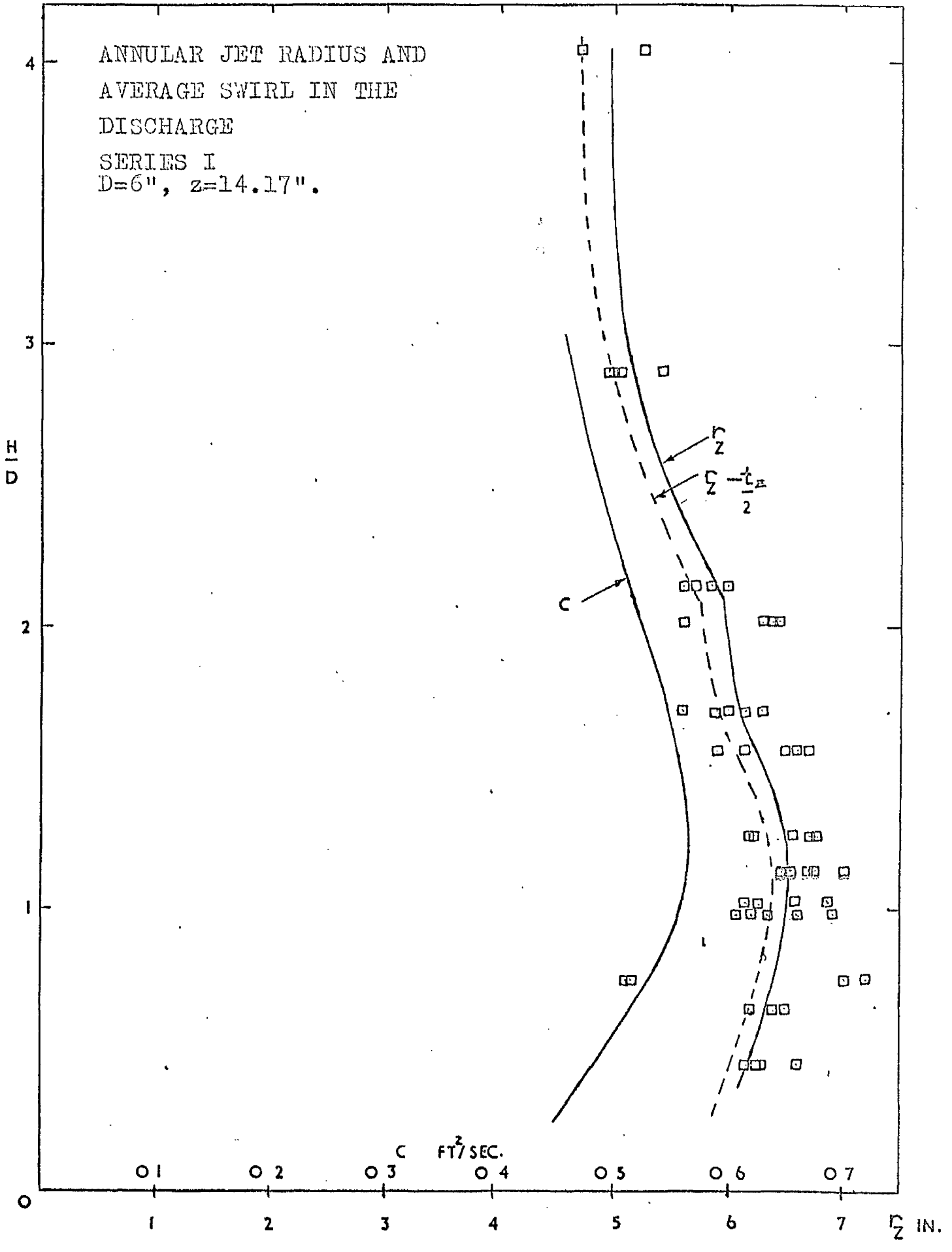
ANNULAR JET RADIUS AND
AVERAGE SWIRL IN THE
DISCHARGE
SERIES I
D=6", z=14.17".
H/D
0
1
2
3
4
C
r_z
$r_z - \frac{t_m}{2}$
C FT²/SEC.
0 1
0 2
0 3
0 4
0 5
0 6
0 7
1
2
3
4
5
6
7
r_z IN.

FIGURE 4.1.12 (b)

JET RADIUS AND AVERAGE SWIRL IN THE DISCHARGE

SERIES I D=4", z=9.21"

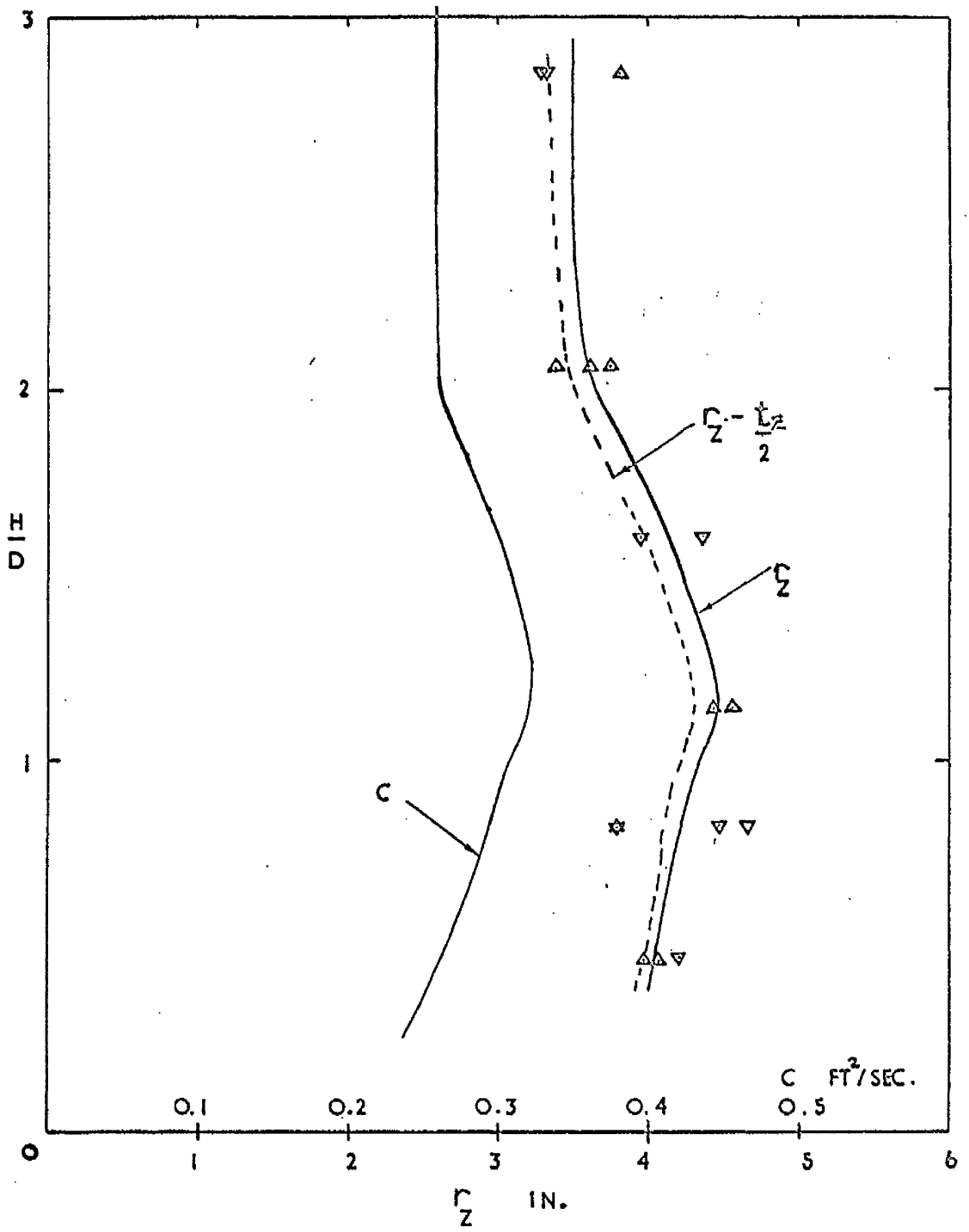

JET RADIUS AND AVERAGE SWIRL IN DISCHARGE

SERIES I D=2", z=4.57".

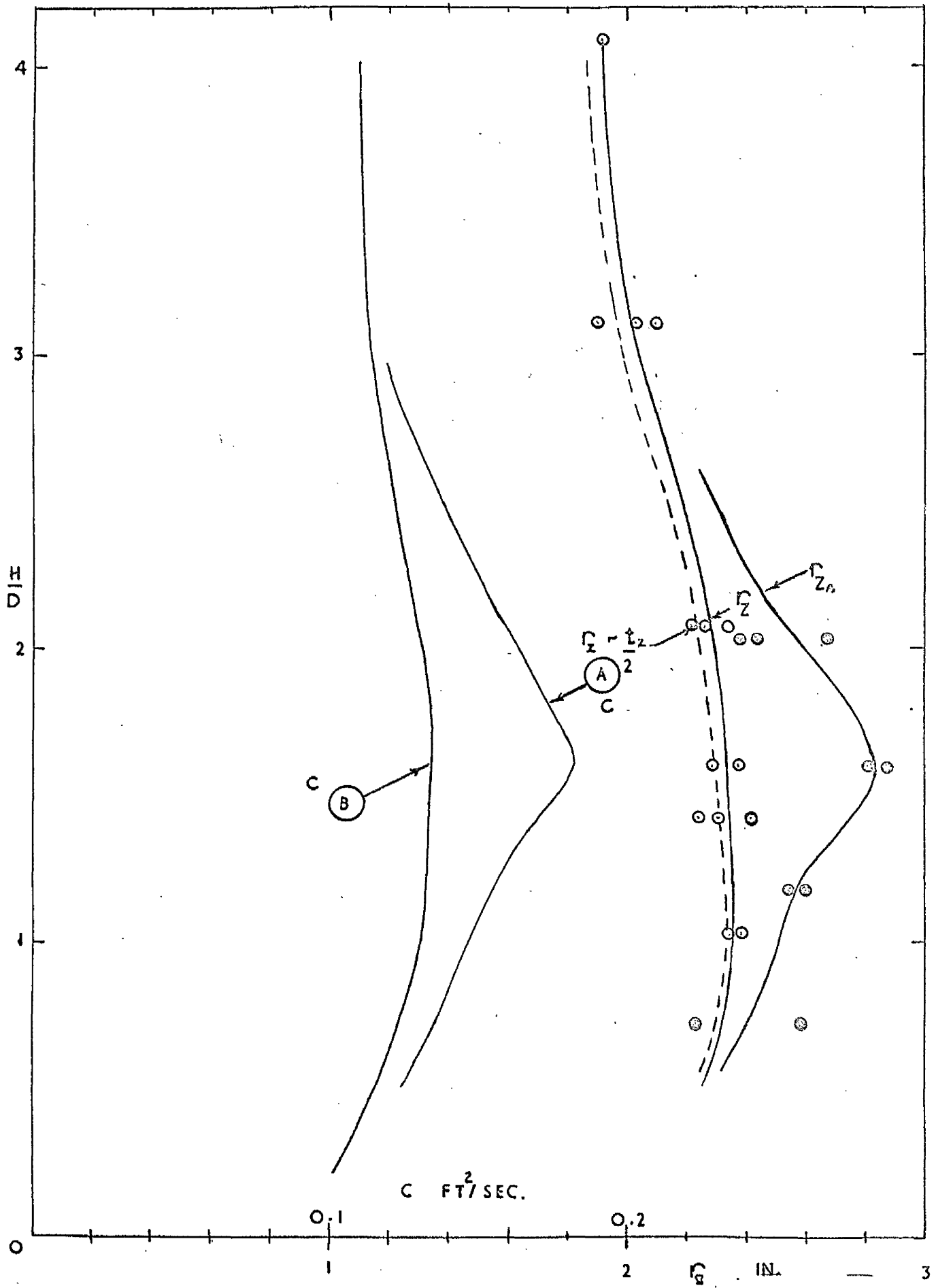

SURFACE SWIRL STRENGTHS

SERIES I D=6",.

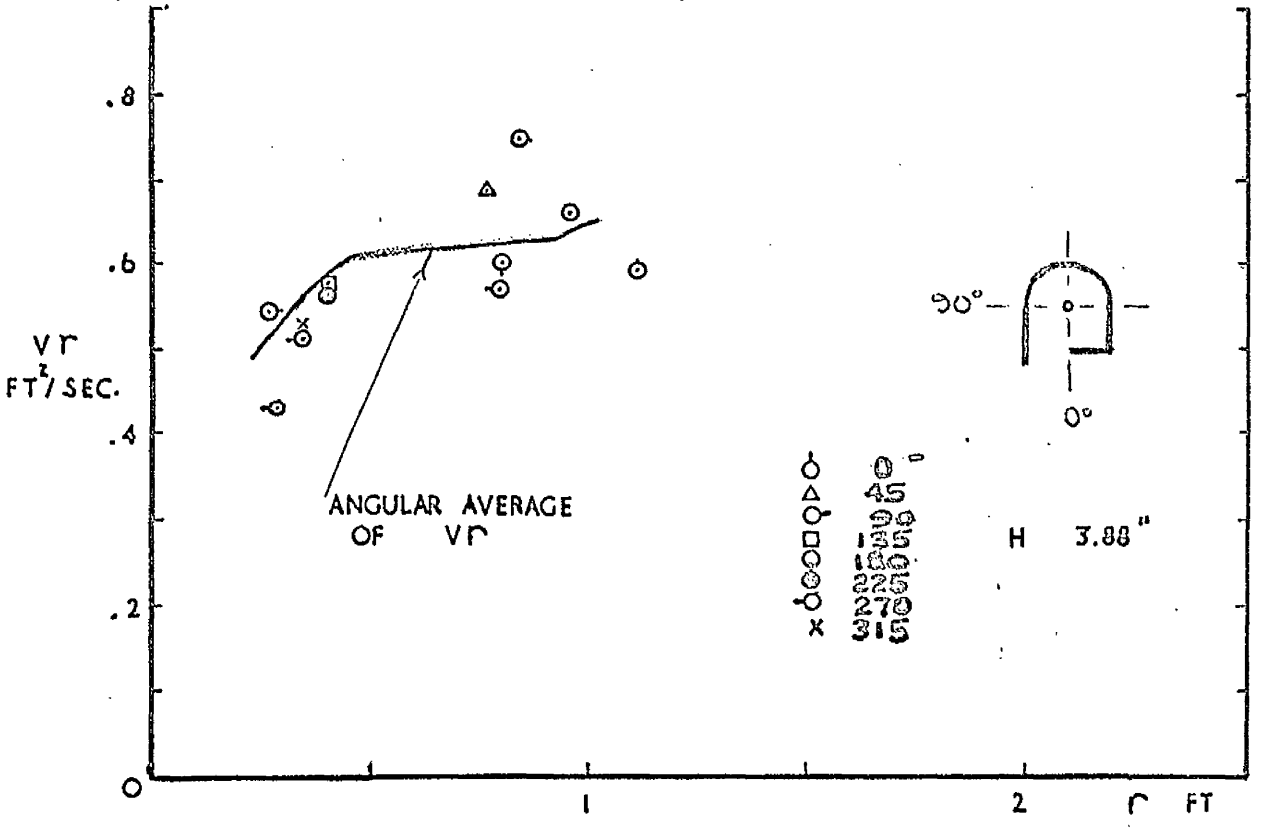

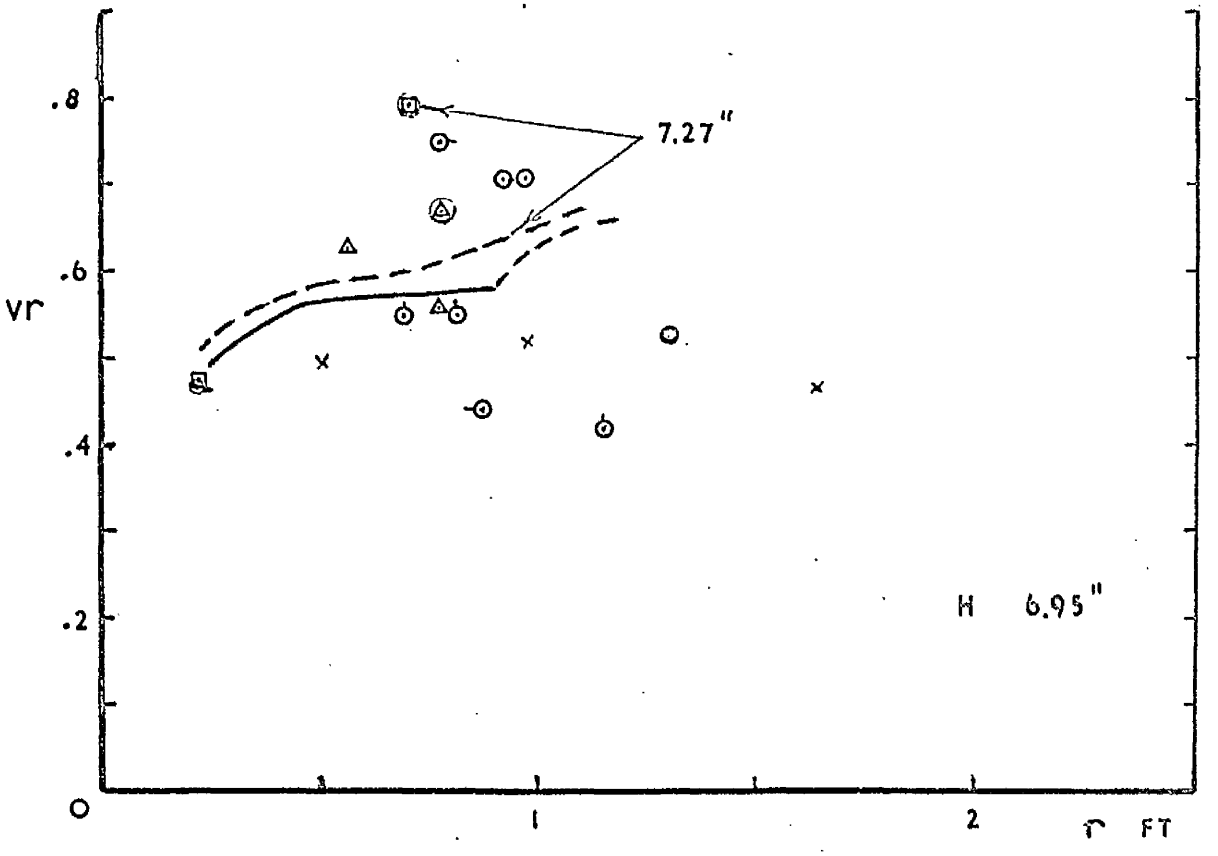

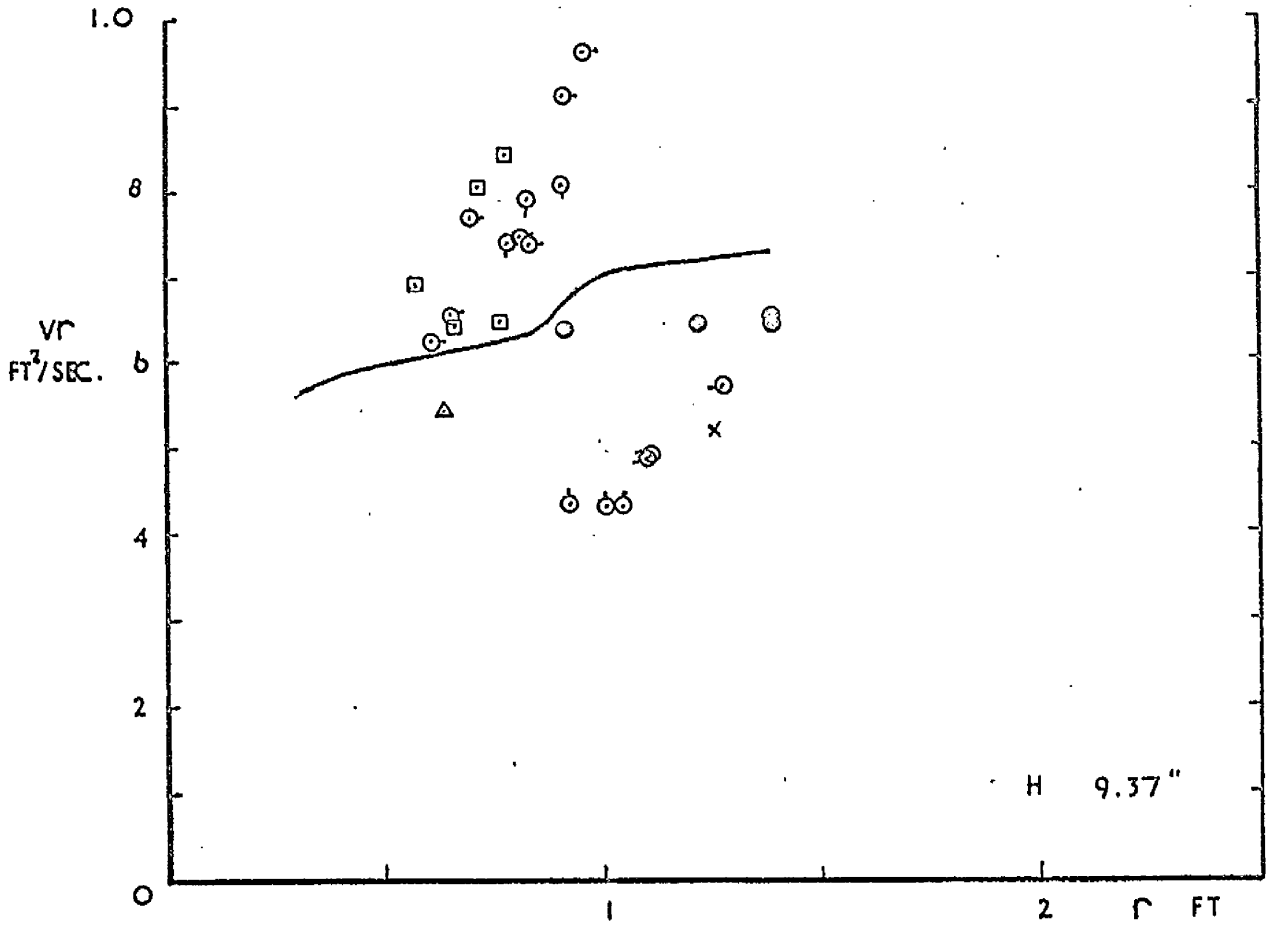
1.0
8
6
4
2
0
Vr
FT³/SEC.
1
2
r FT
H 9.37"

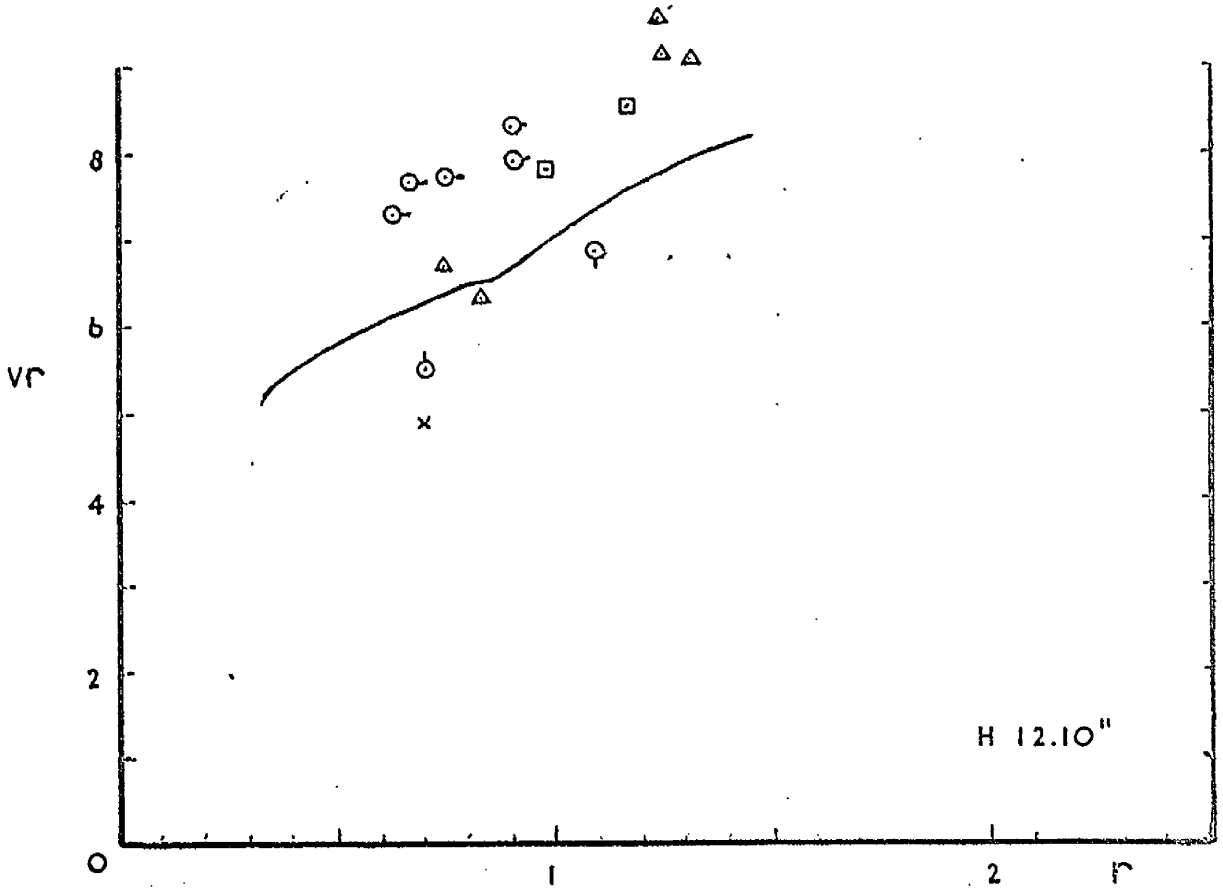
8
6
4
2
0
Vr
1
2
r
H 12.10"

SURFACE SWIRL STRENGTHS
SERIES I D=4".

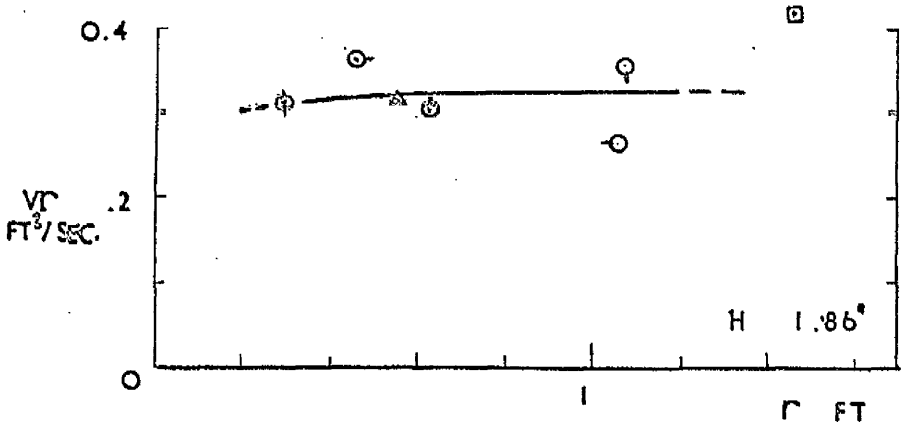

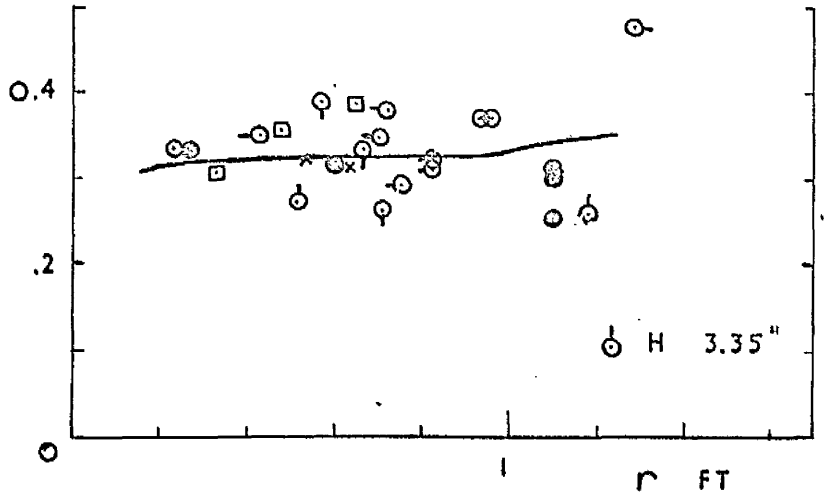

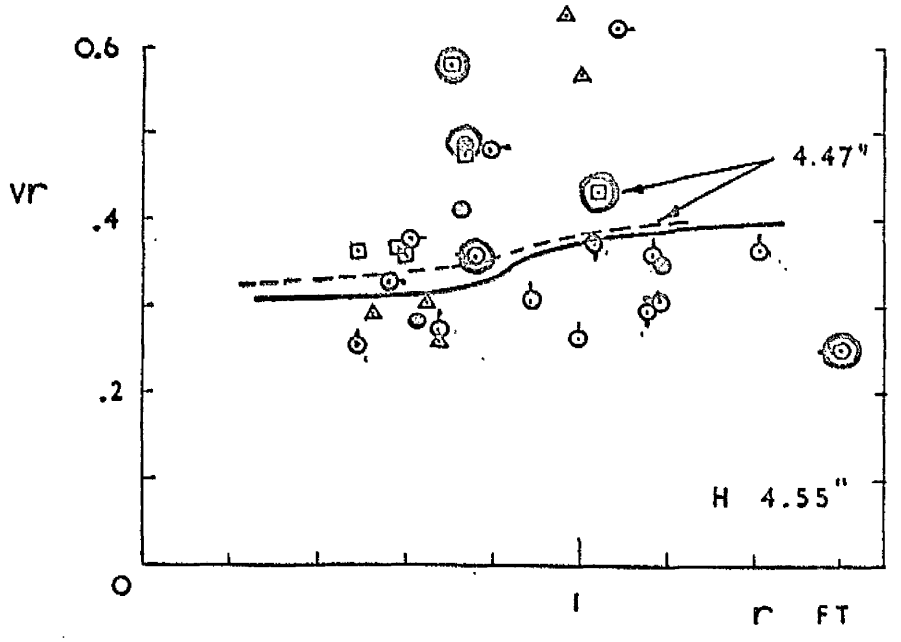

FIGURE 4.1.14 (Continued)

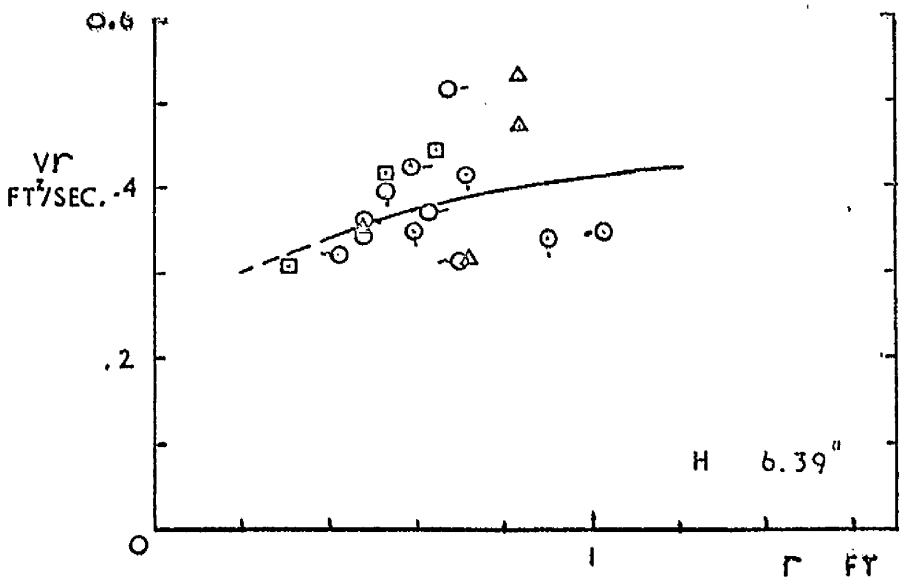

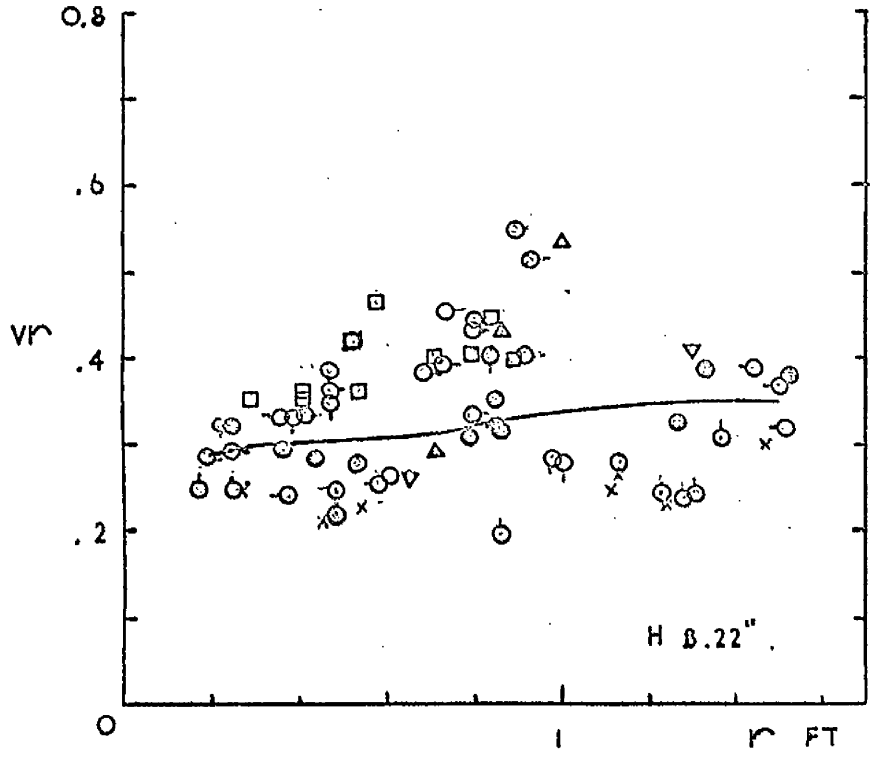

FIGURE 4.1.19
SURFACE SWIRL STRENGTHS
SERIES I D=2".

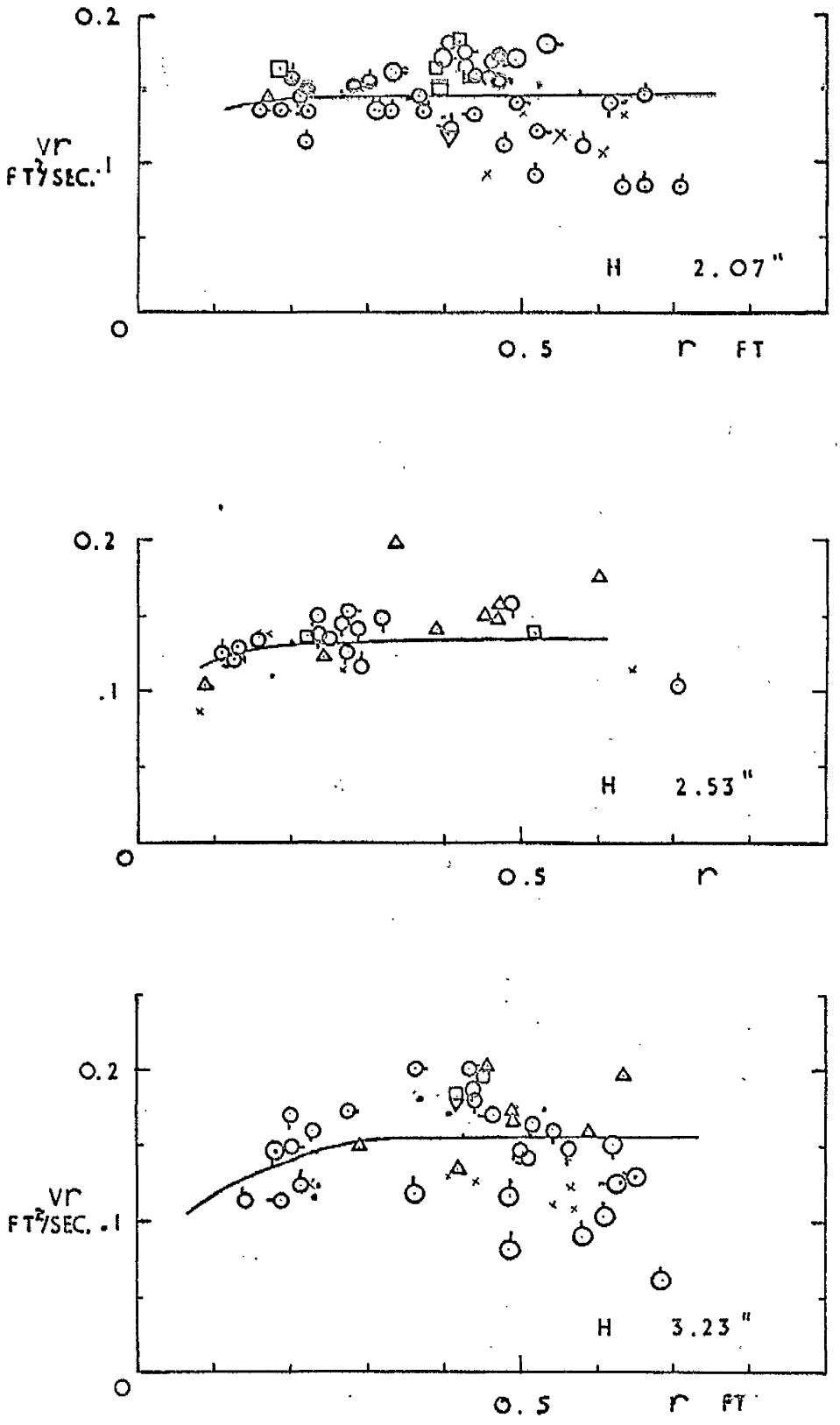

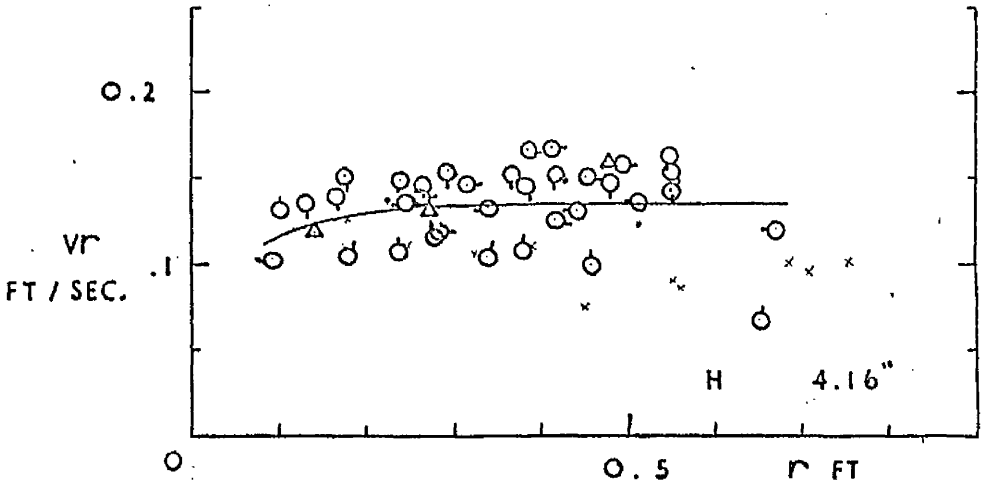
0.2
Vr
FT / SEC.
.1
H 4.16"
0
0.5
r FT

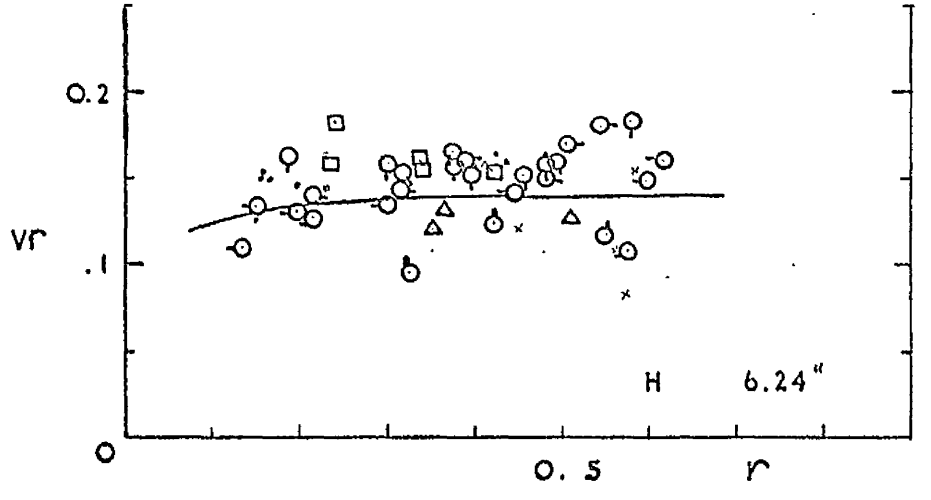
0.2
Vr
.1
H 6.24"
0
0.5
r

FIGURE 4.2.1
SURFACE AND FLOOR
FLOW PATTERNS
SERIES I D=6".

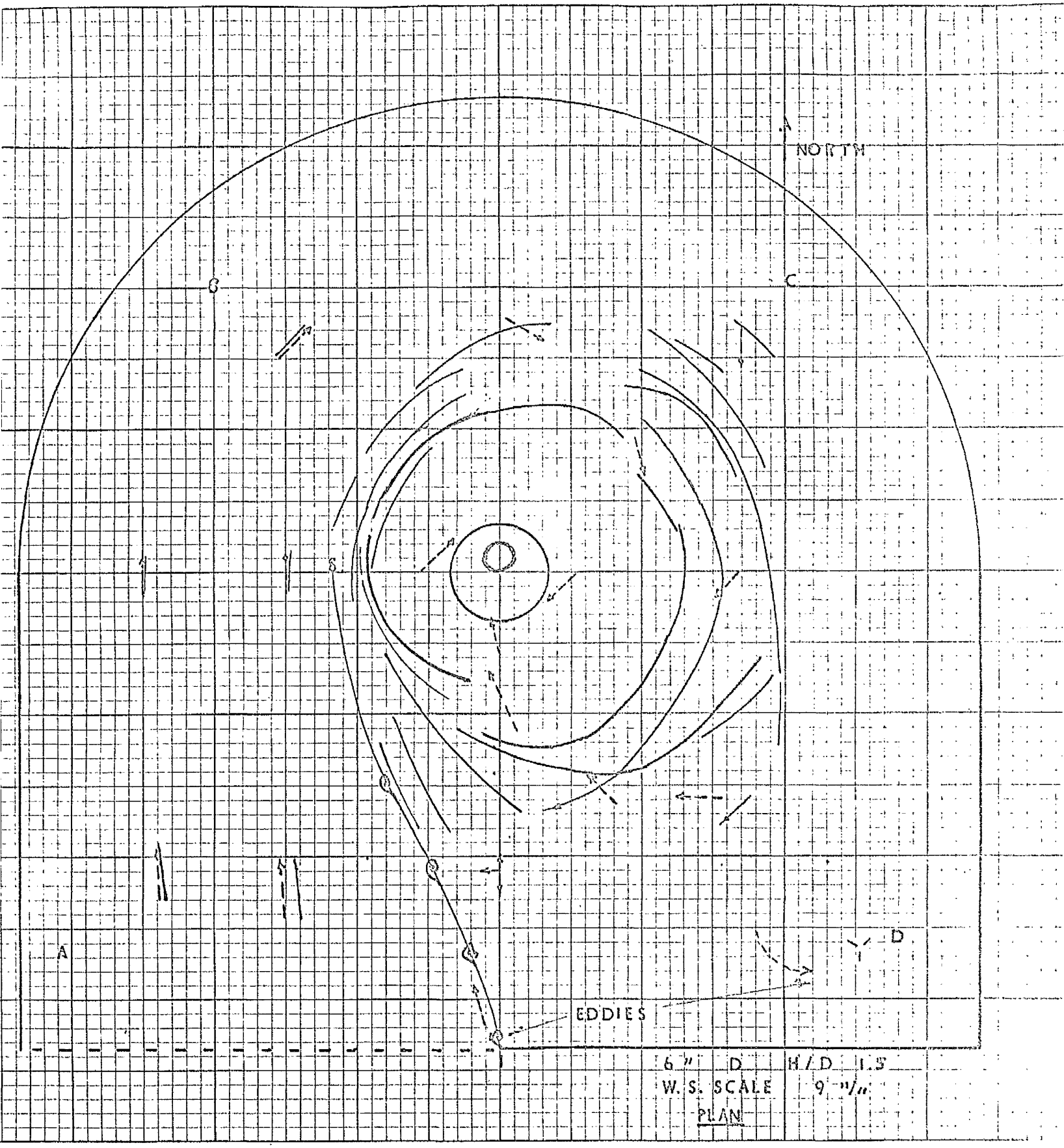

FIGURE 4.2.2
SURFACE AND FLOOR
FLOW PATTERNS
SERIES I D=4".

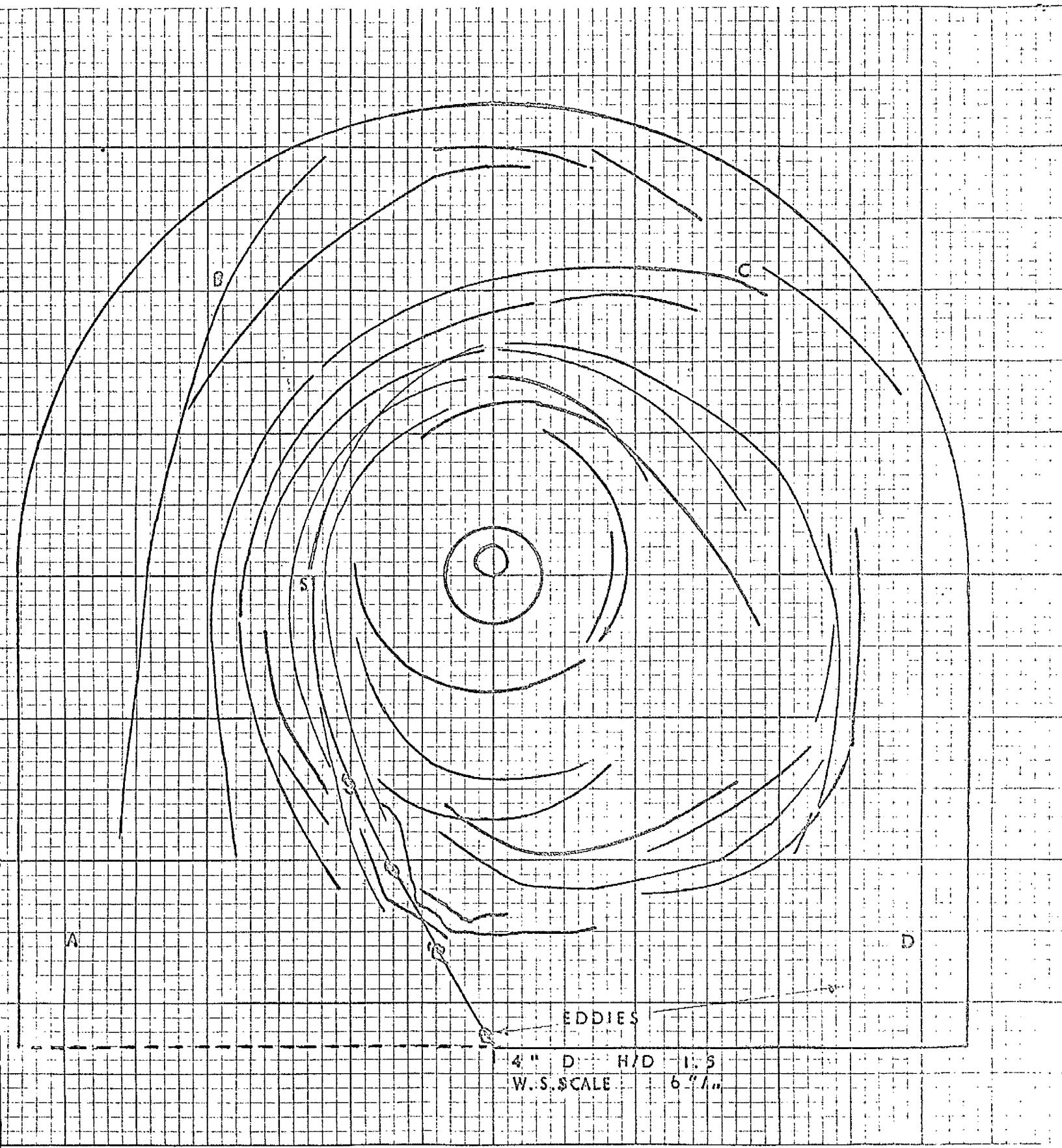

FIGURE 4.2.3
SURFACE AND FLOOR
FLOW PATTERNS
SERIES I D=2".

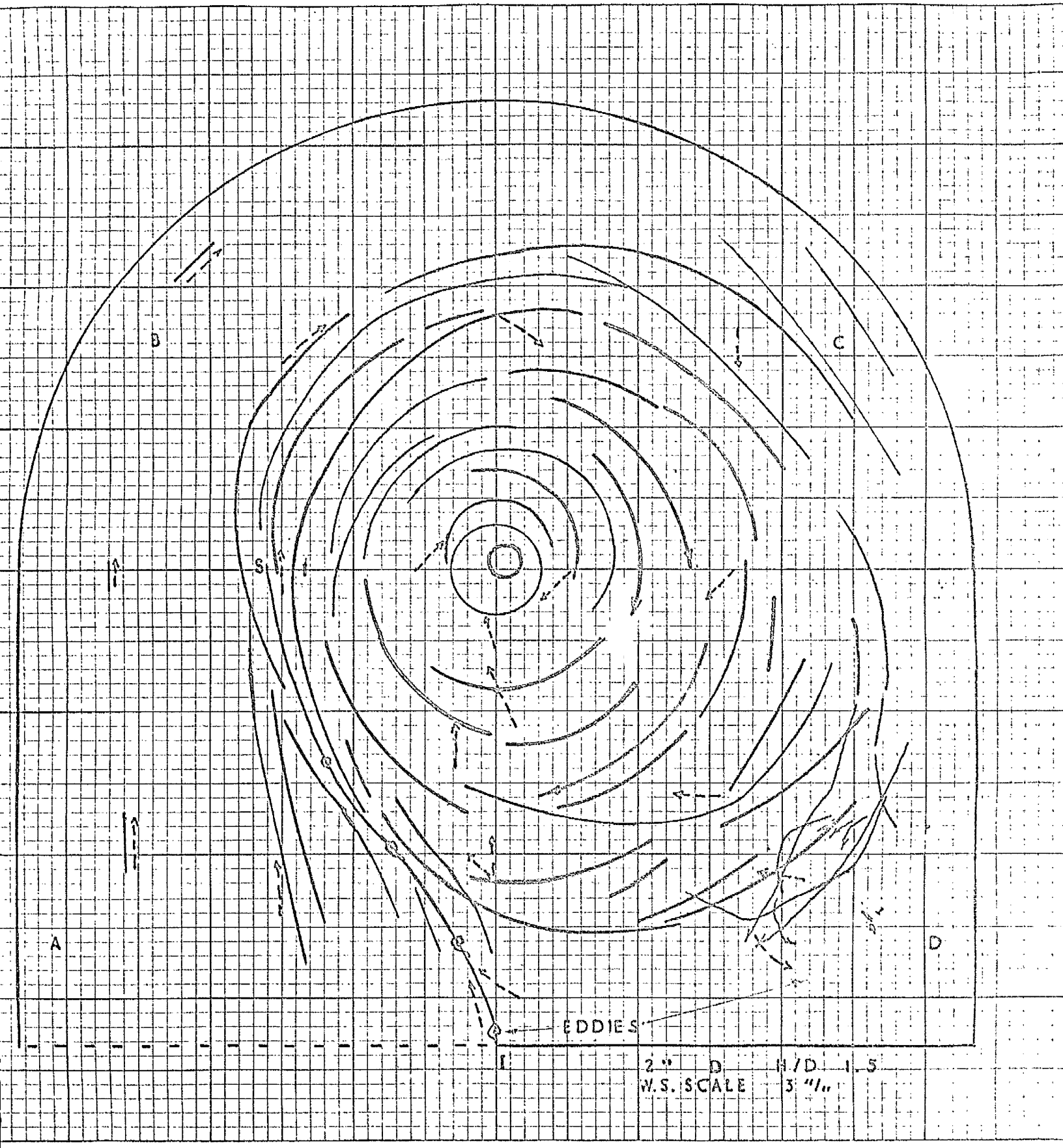

FIGURE 4.2.4

IRROTATIONAL FLOW PATTERN

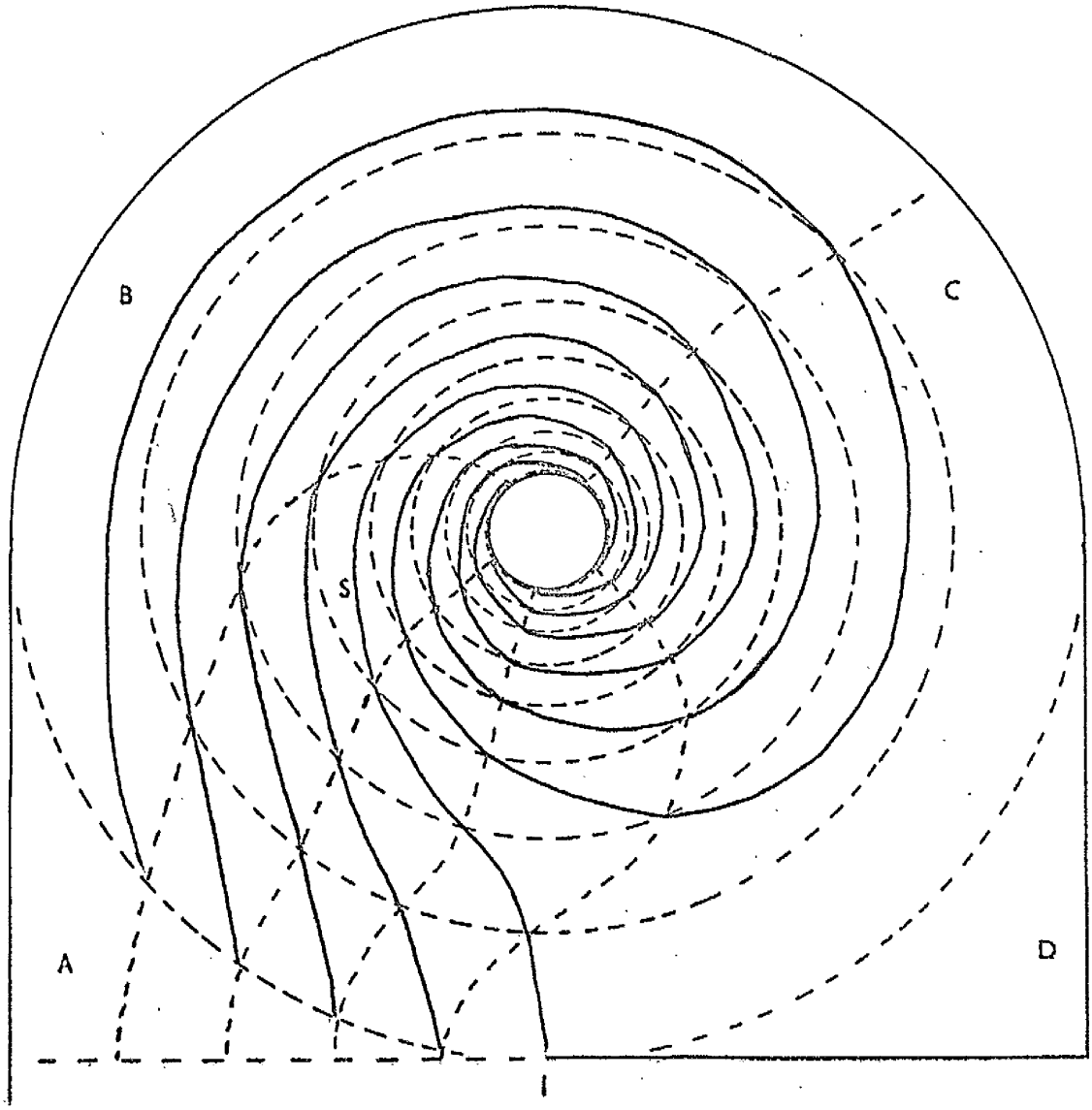

PLAN SCALE 1"=1'

c=0.60 FT^2/SEC.

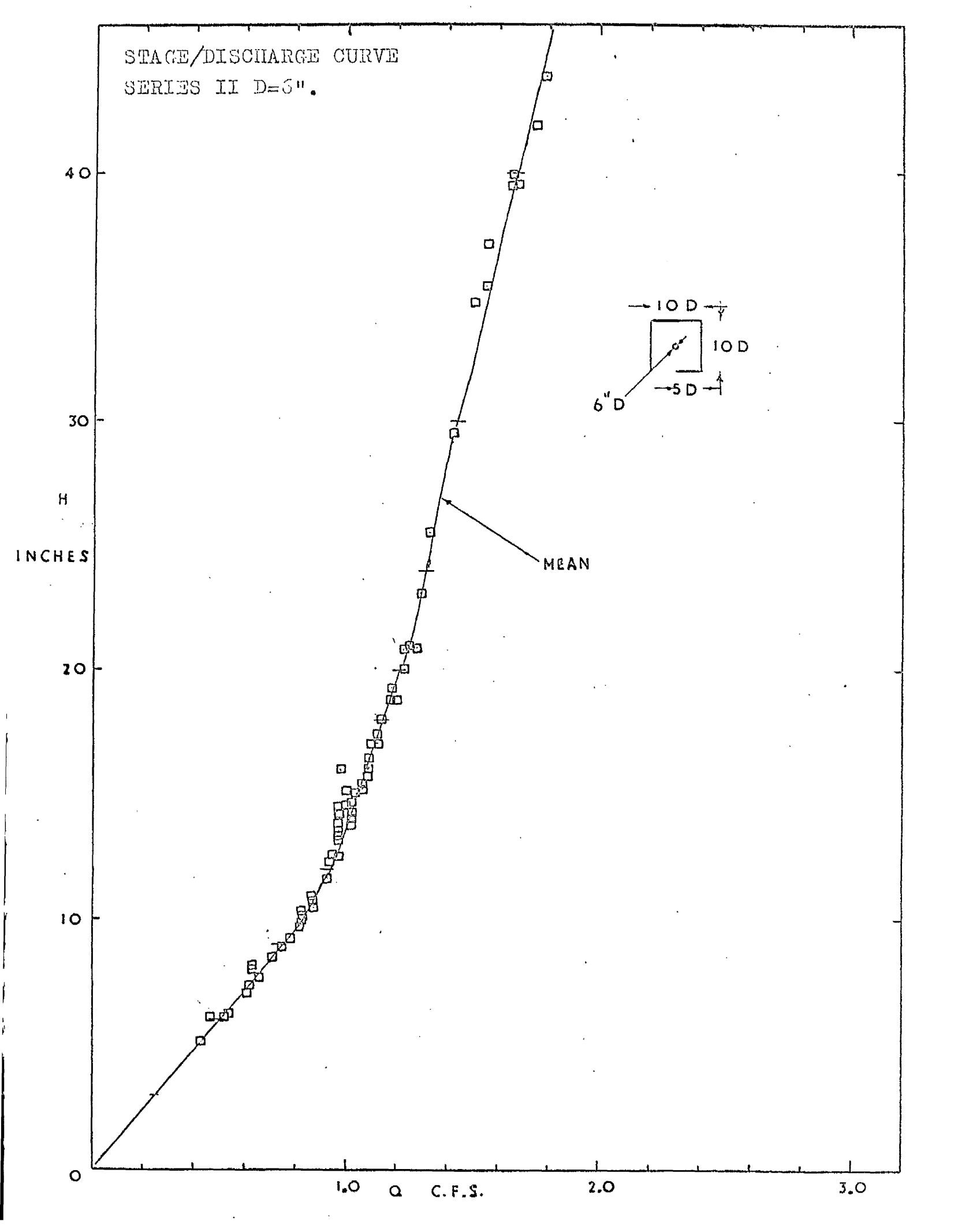
STAGE/DISCHARGE CURVE
SERIES II D=6".
40
30
20
10
0
H
INCHES
MEAN
10 D
10 D
5 D
6"D
1.0
Q C.F.S.
2.0
3.0

STAGE/DISCHARGE CURVE
SERIES II D=4".

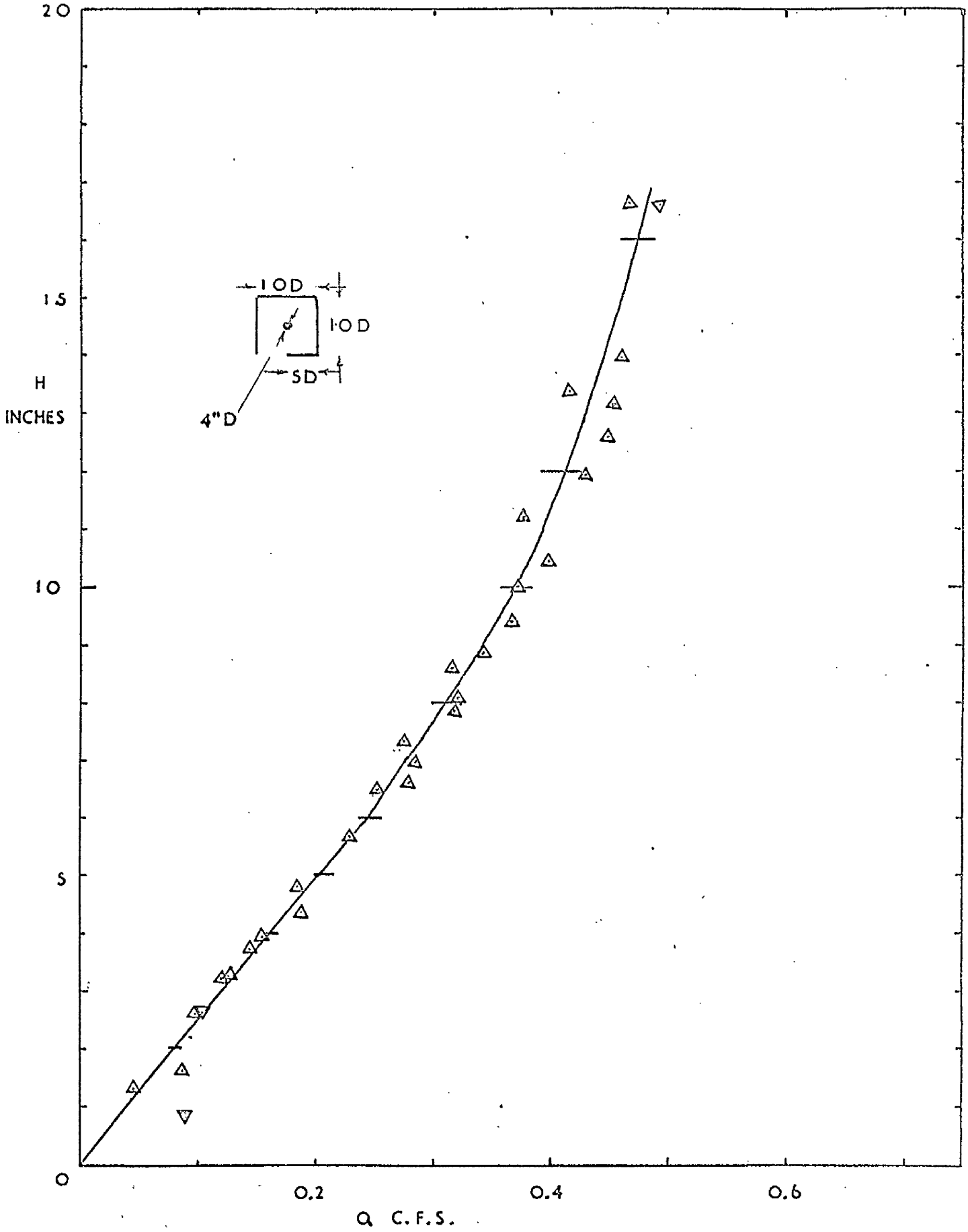

FIGURE 4.3.1 (c)

STAGE/DISCHARGE CURVE

SERIES II D=2".

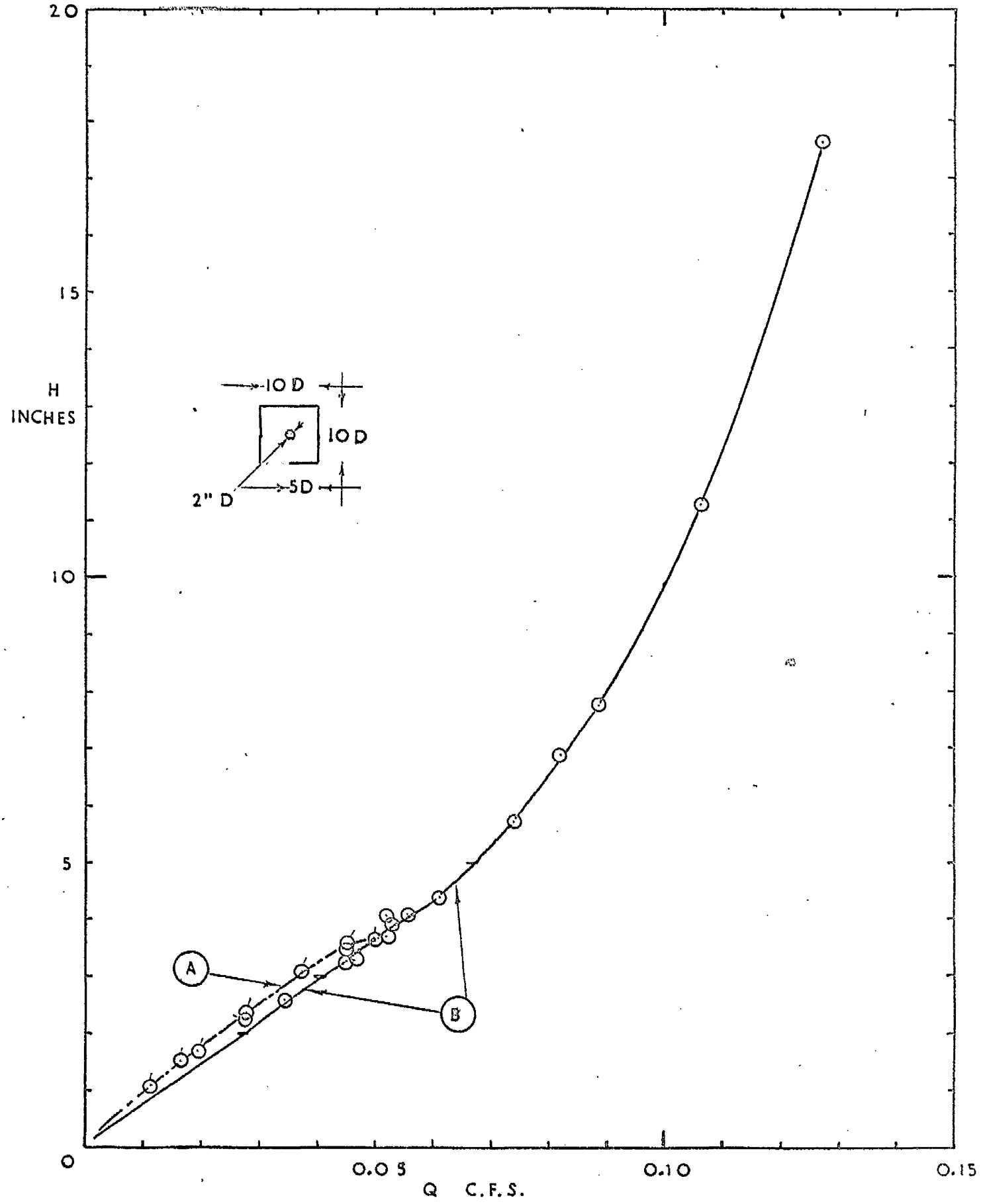

FIGURE 4.3.2 (a)
STAGE/DISCHARGE CURVE
SERIES III D=8".

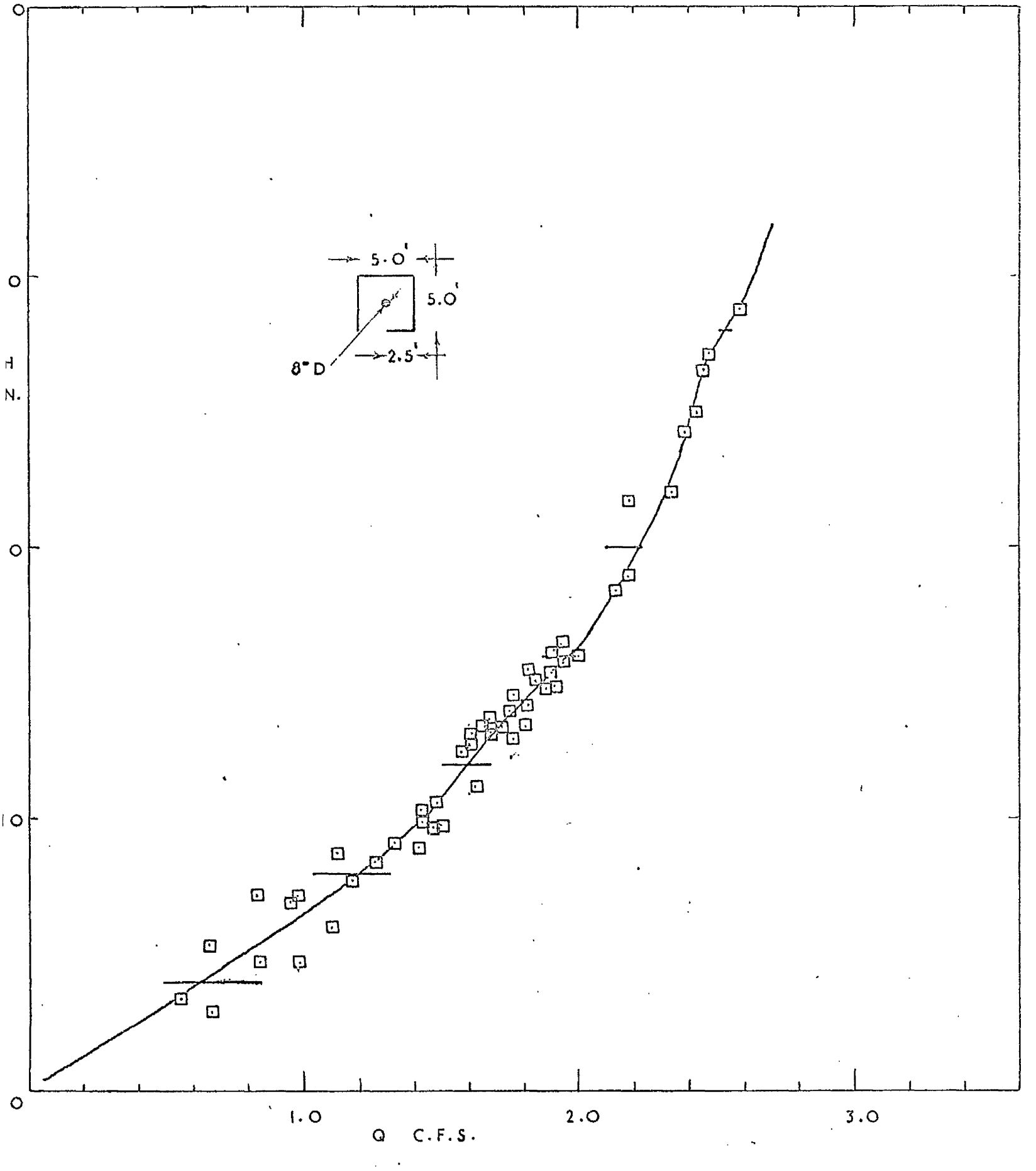

FIGURE 4.3.2 (c)

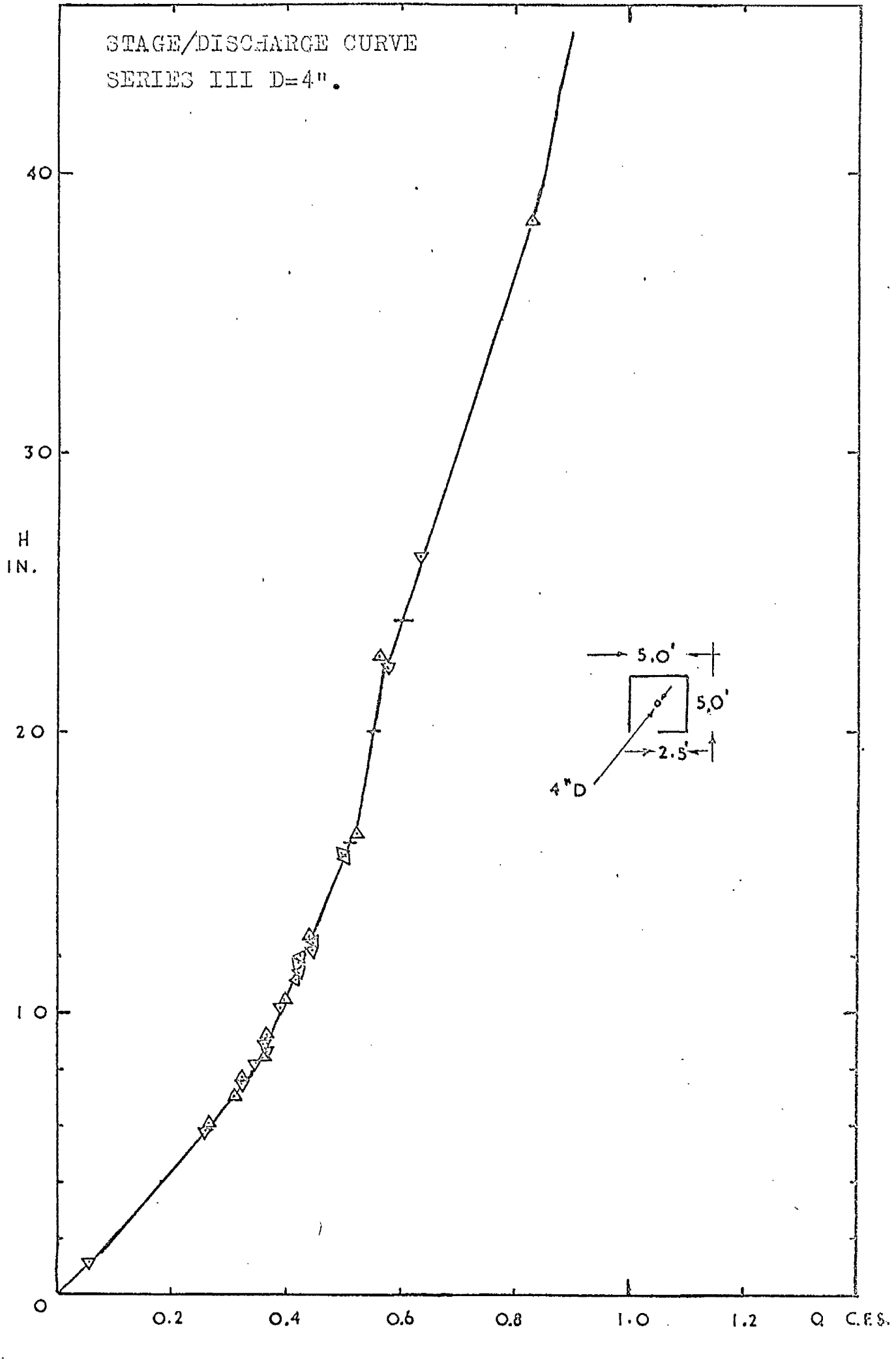
STAGE/DISCHARGE CURVE
SERIES III D=4".
40
30
20
10
0
H
IN.
0.2
0.4
0.6
0.8
1.0
1.2
Q C.F.S.
5.0'
5.0'
2.5'
4"D

FIGURE 4.3.2 (d)
STAGE/DISCHARGE CURVE
SERIES III D=2".

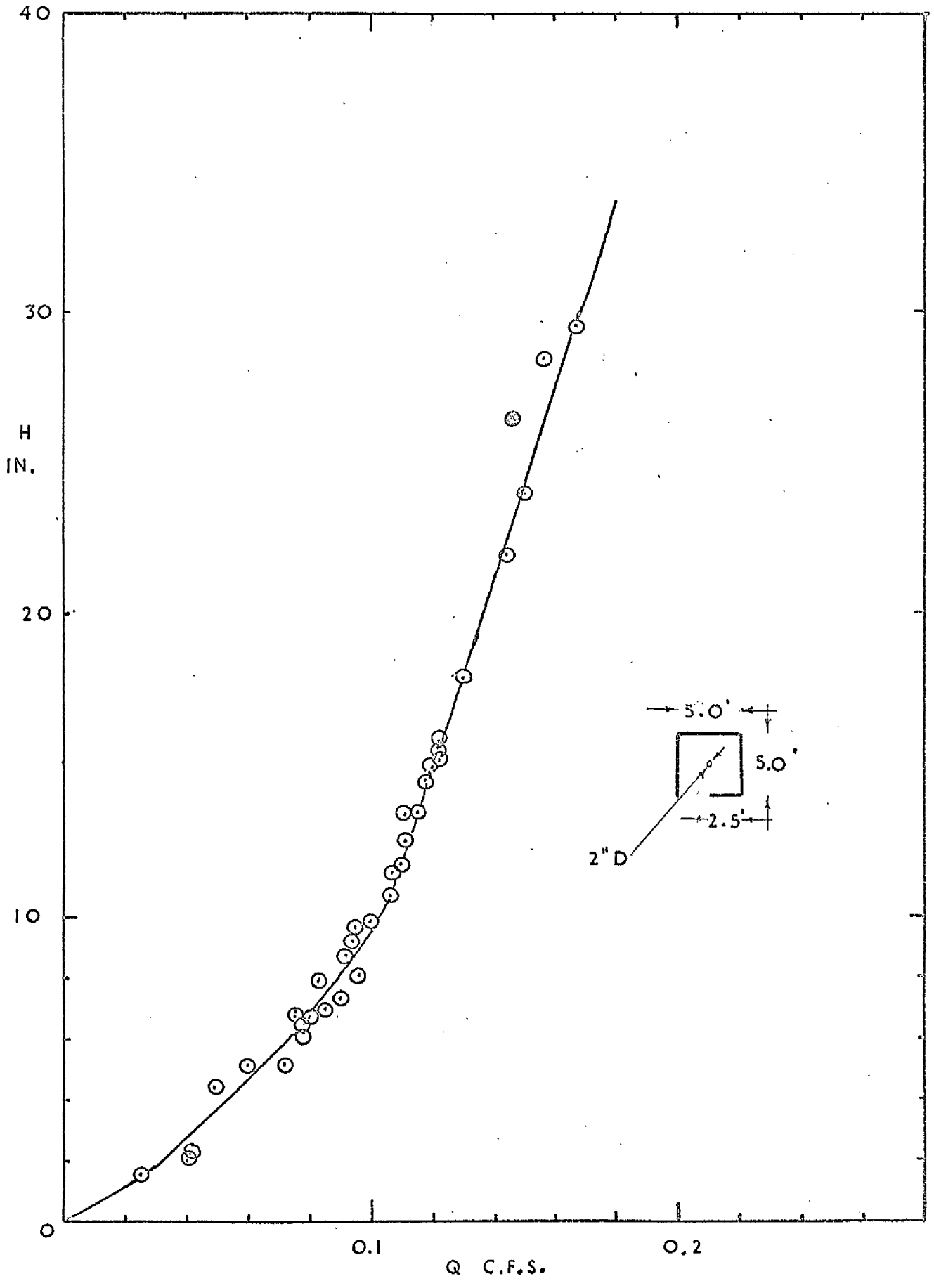

FIGURE 4.3.3 (a)

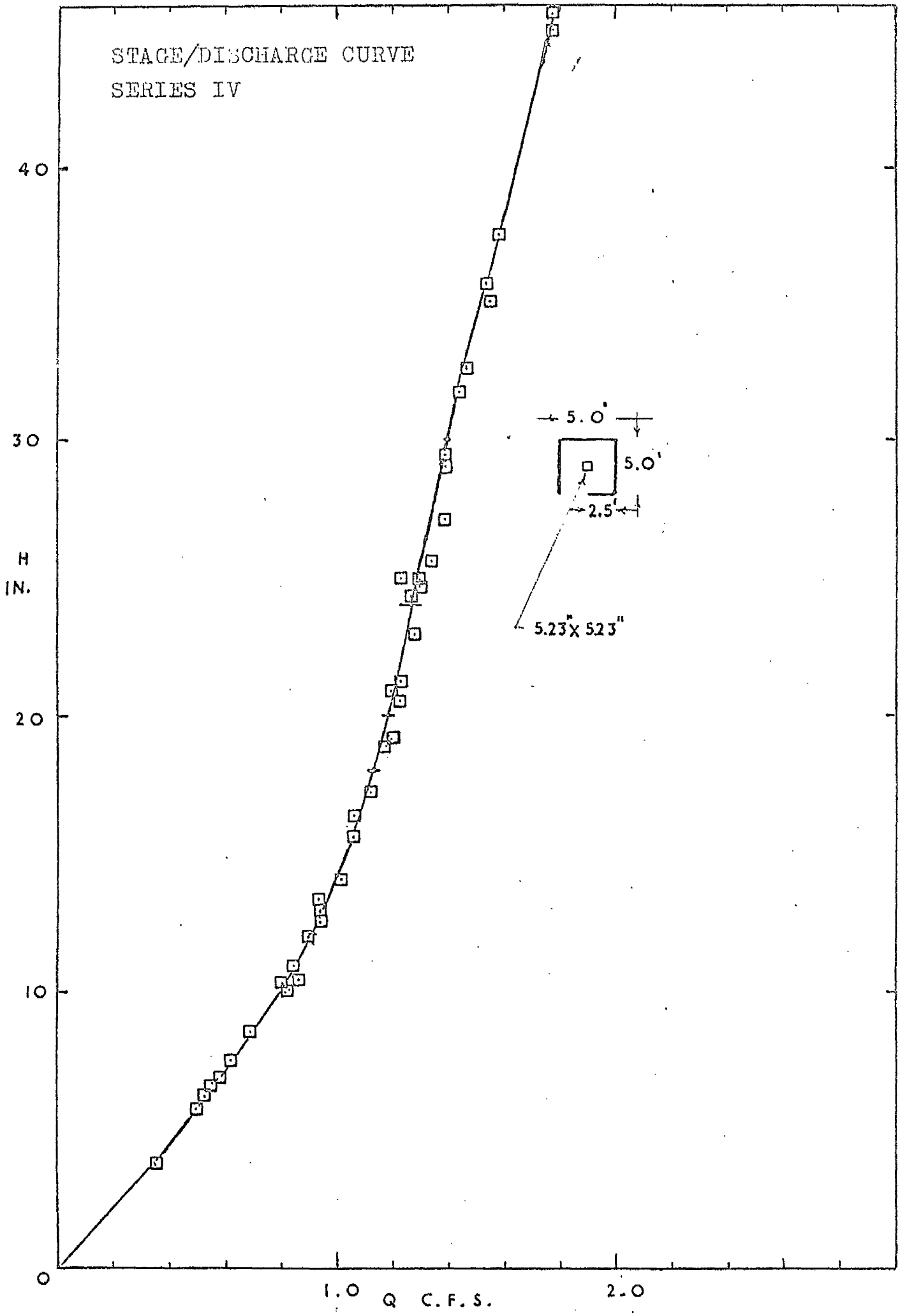
STAGE/DISCHARGE CURVE
SERIES IV
40
30
20
10
0
H
IN.
5.0"
5.0'
2.5'
5.23" X 5.23"
1.0
Q C.F.S.
2.0

FIGURE 4.3.3 (b)

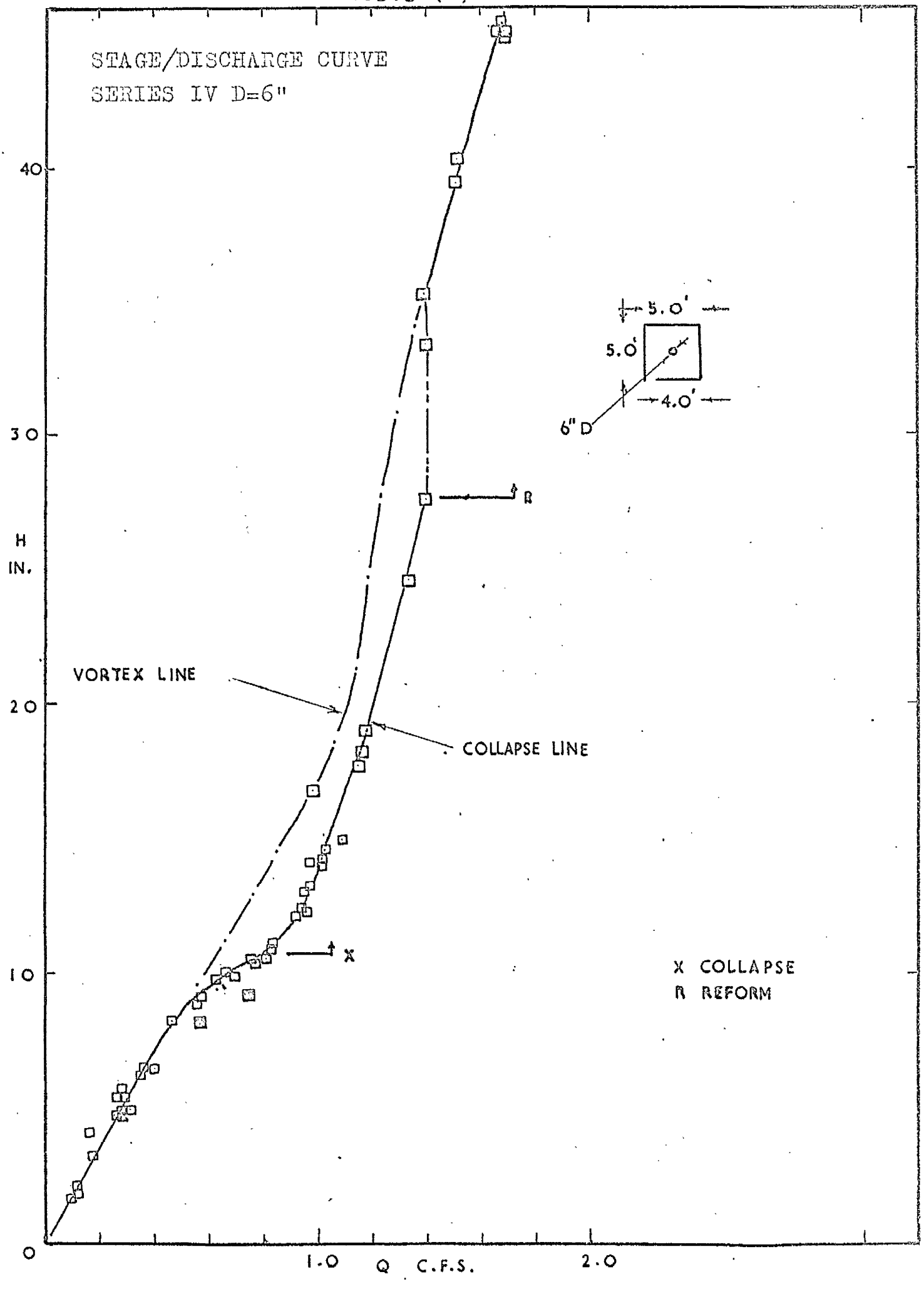
STAGE/DISCHARGE CURVE
SERIES IV D=6"
5.0'
5.0'
4.0'
6" D
R
X
VORTEX LINE
COLLAPSE LINE
X COLLAPSE
R REFORM
H IN.
40
30
20
10
0
1.0
Q C.F.S.
2.0

FIGURE 5.1.1

DISCHARGE COEFFICIENTS

SERIES I.

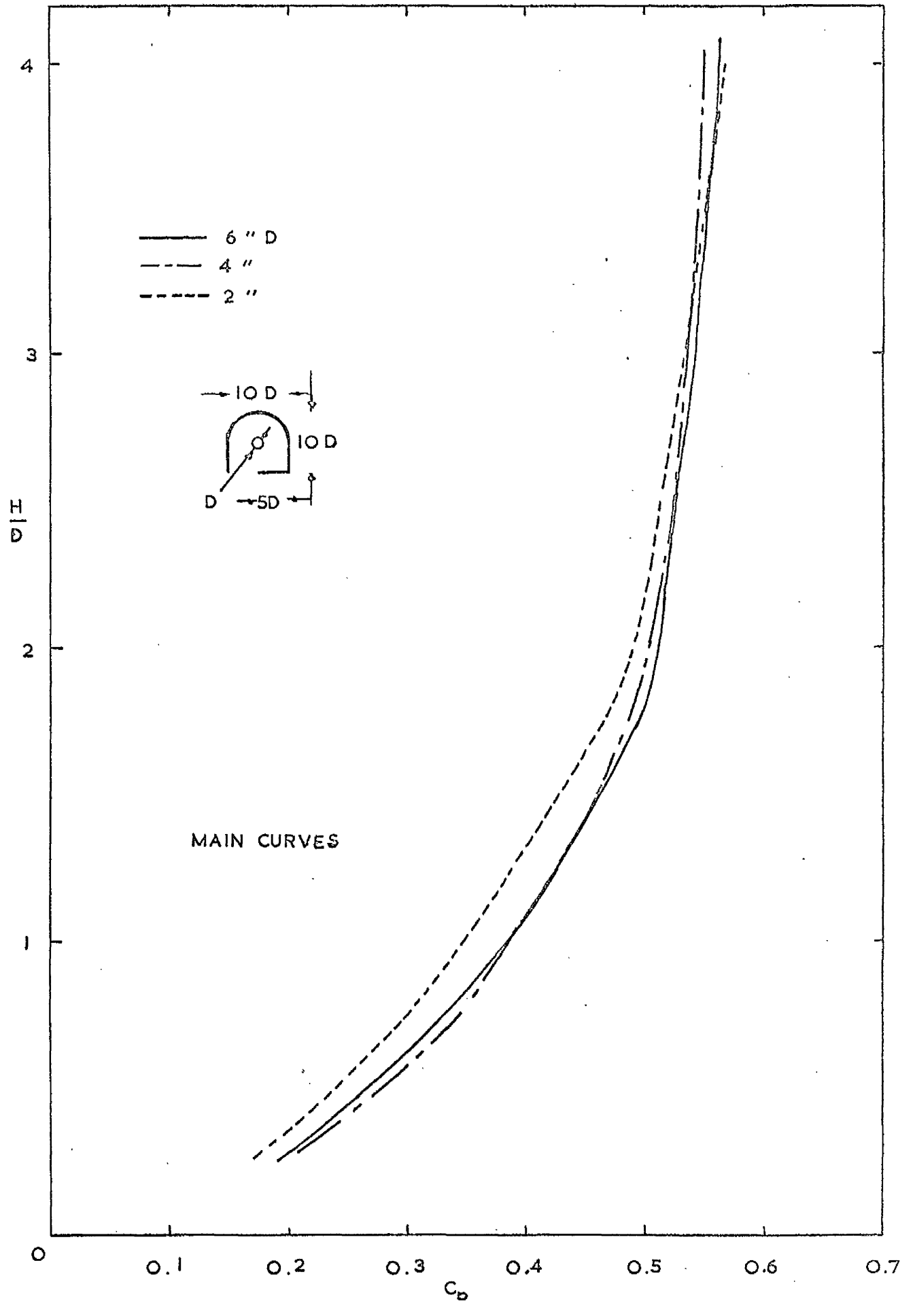

FIGURE 5.1.2

DISCHARGE COEFFICIENTS

SERIES II.

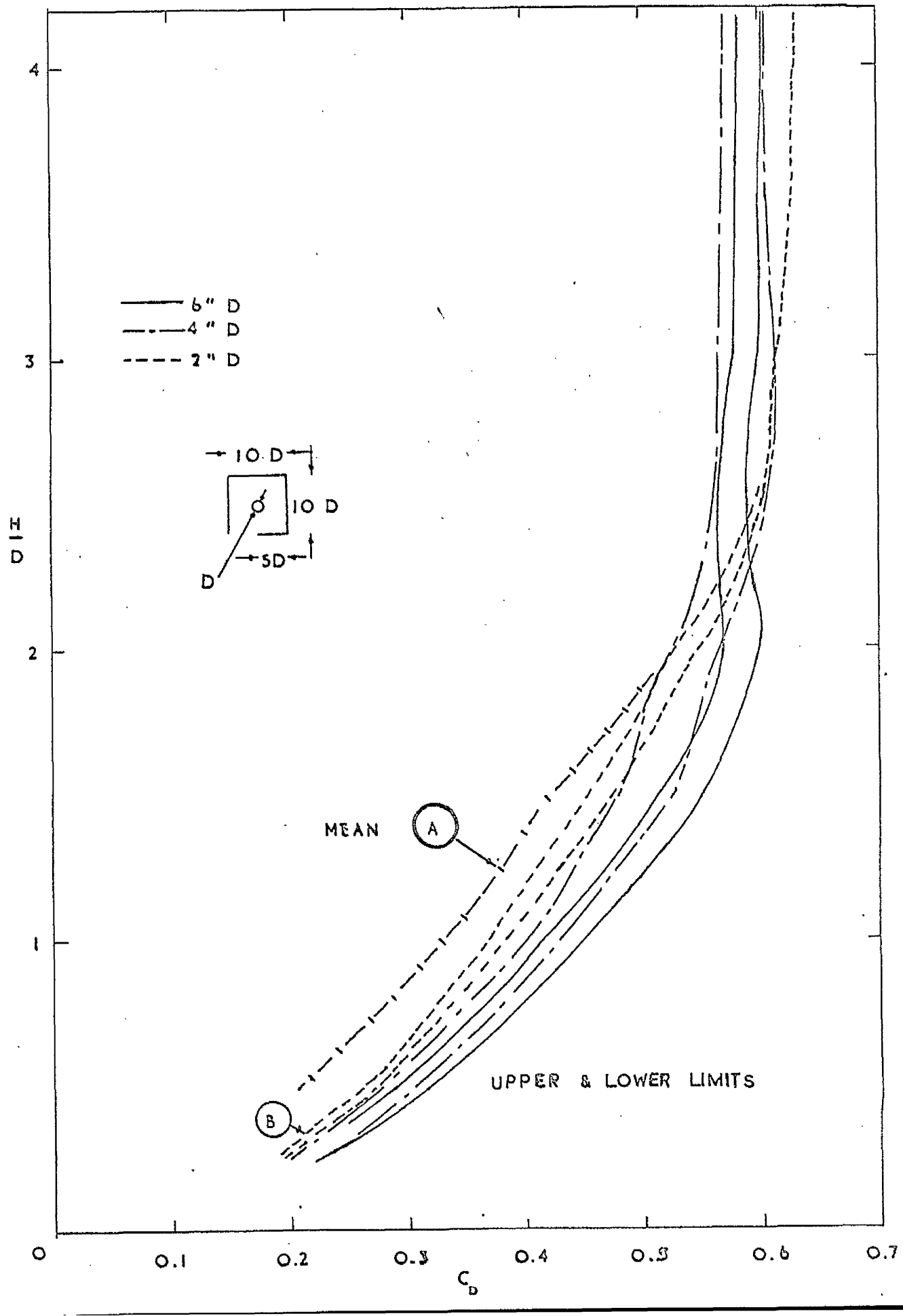

FIGURE 5.1.3
DISCHARGE COEFFICIENTS
SERIES III.

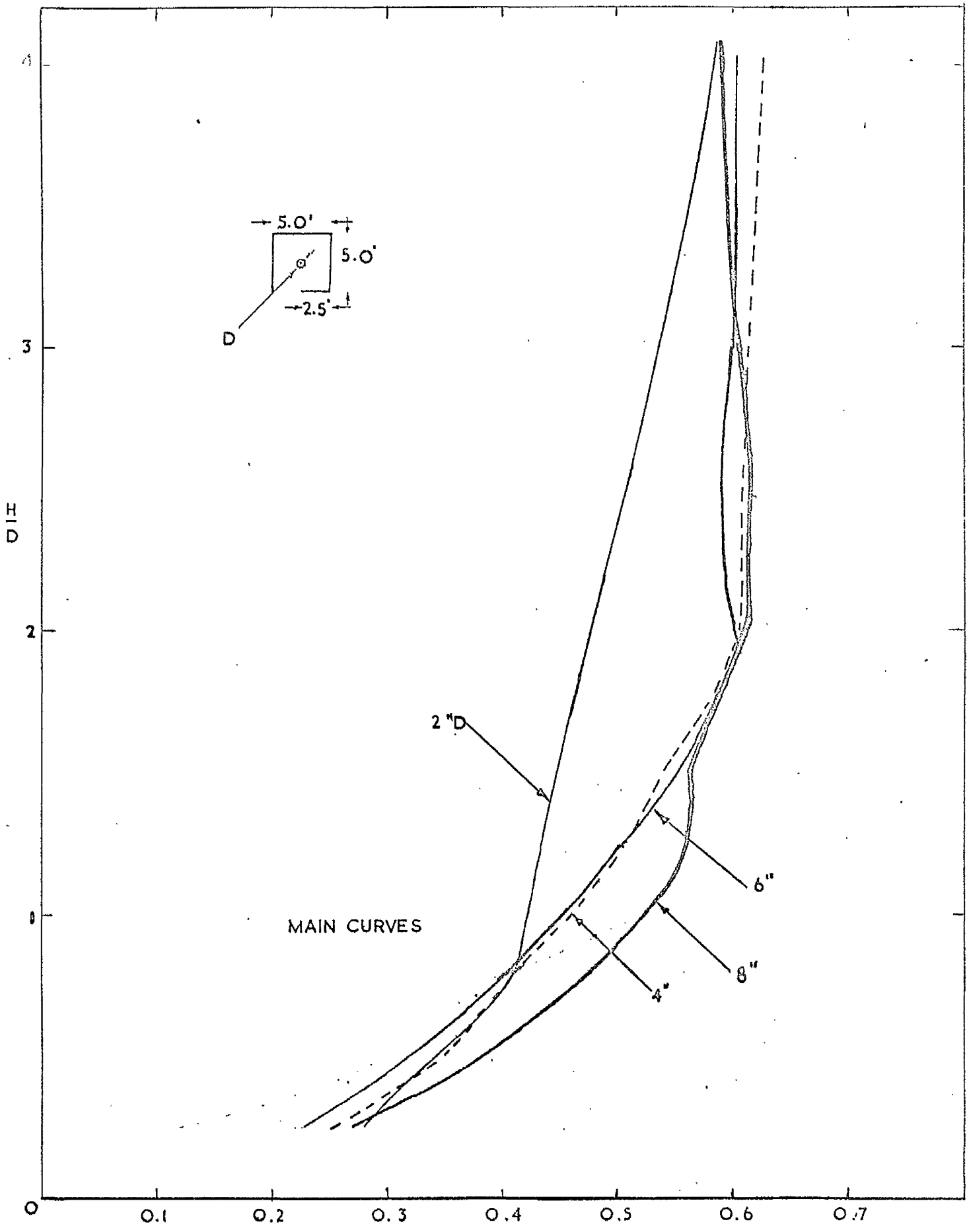

FIGURE 5.1.4 (a)
DISCHARGE COEFFICIENTS
SERIES IVa.

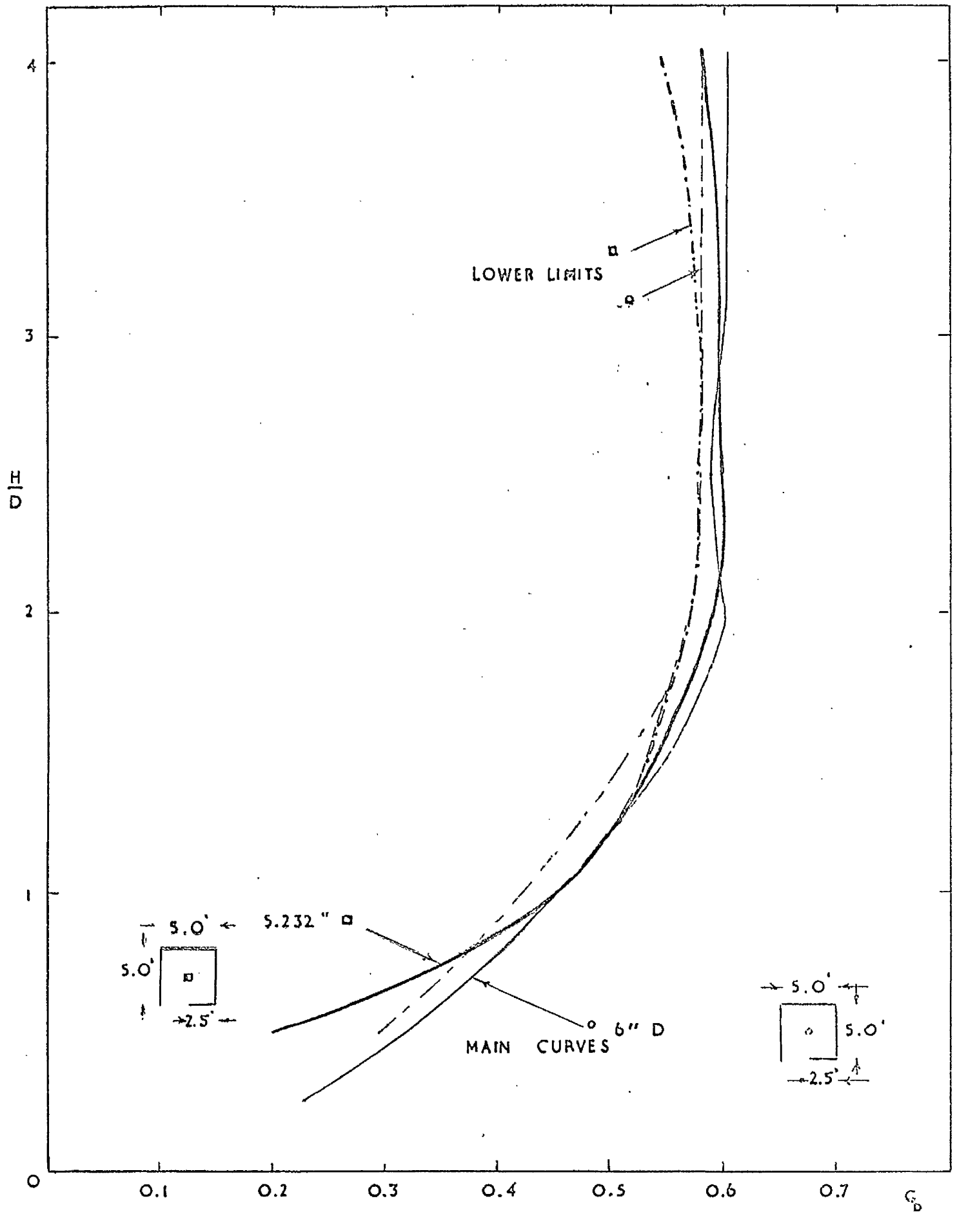

FIGURE 5.1.4 (b)
DISCHARGE COEFFICIENTS
SERIES IVb.

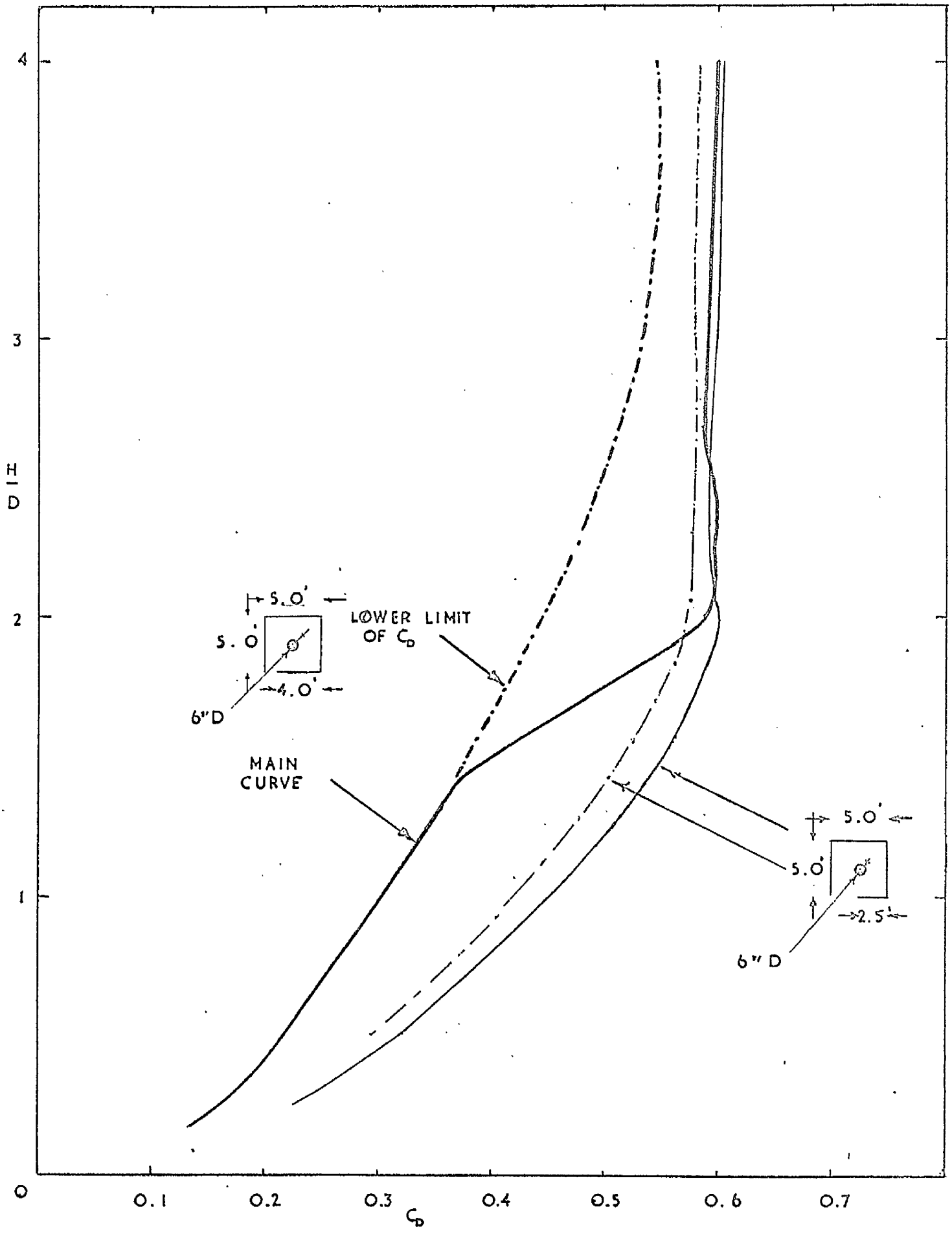

FIGURE 5.2.1
VARIATION OF SURFACE SWIRL
WITH θ (APPROXIMATE)
SERIES I.

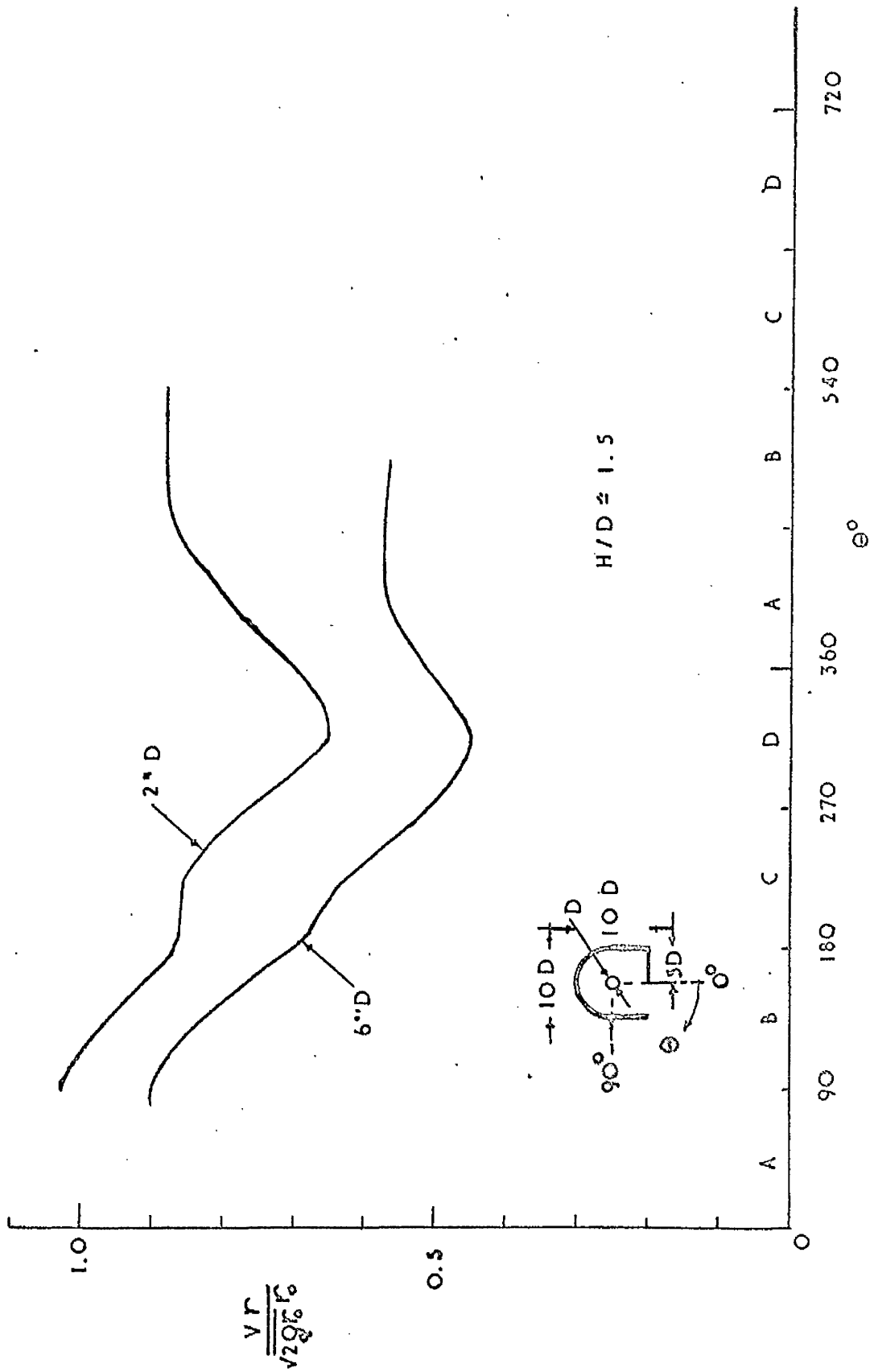

FIGURE 5.2.2

COMPARISON OF SURFACE SWIRLS

SERIES I.

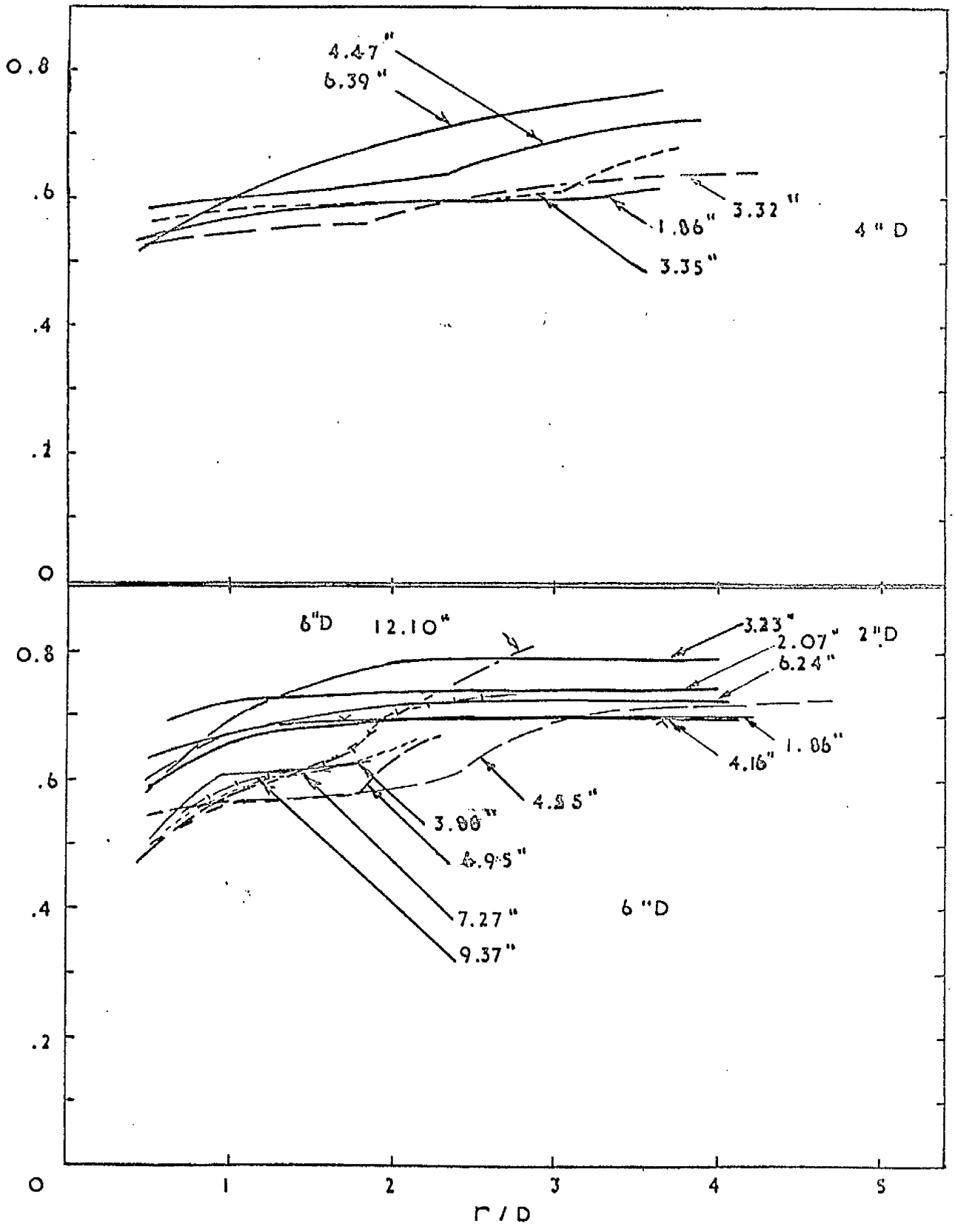

FIGURE 5.5.1

COMPARISON OF AVERAGE SWIRLS
IN THE DISCHARGE --SERIES I

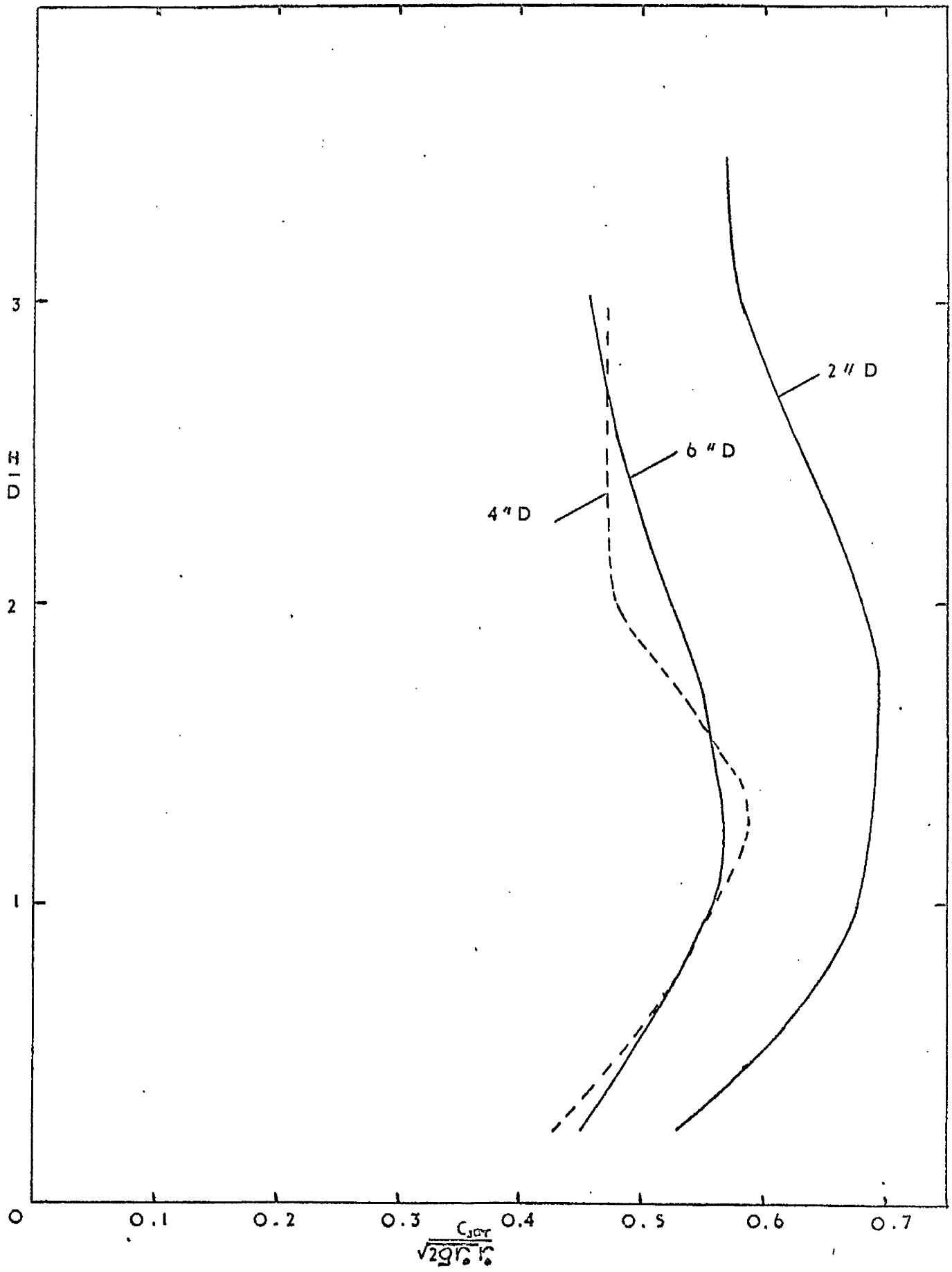

FIGURE 5.3.2
COMPARISON OF ANNULAR JET AND SURFACE FLOAT SWIRL MEASUREMENTS SERIES I.

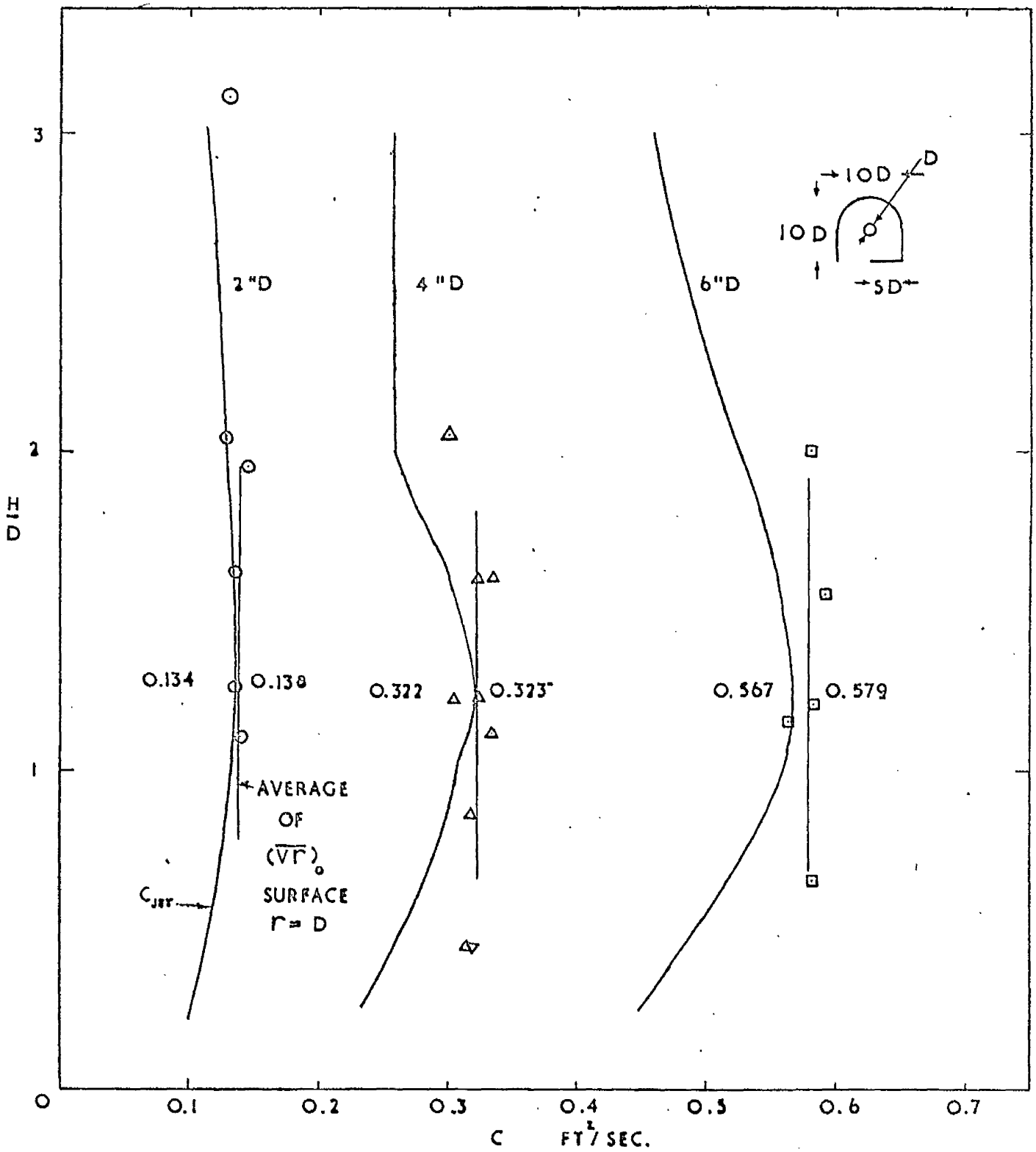

VENA CONTRACTA SWIRL NUMBERS
SERIES I.

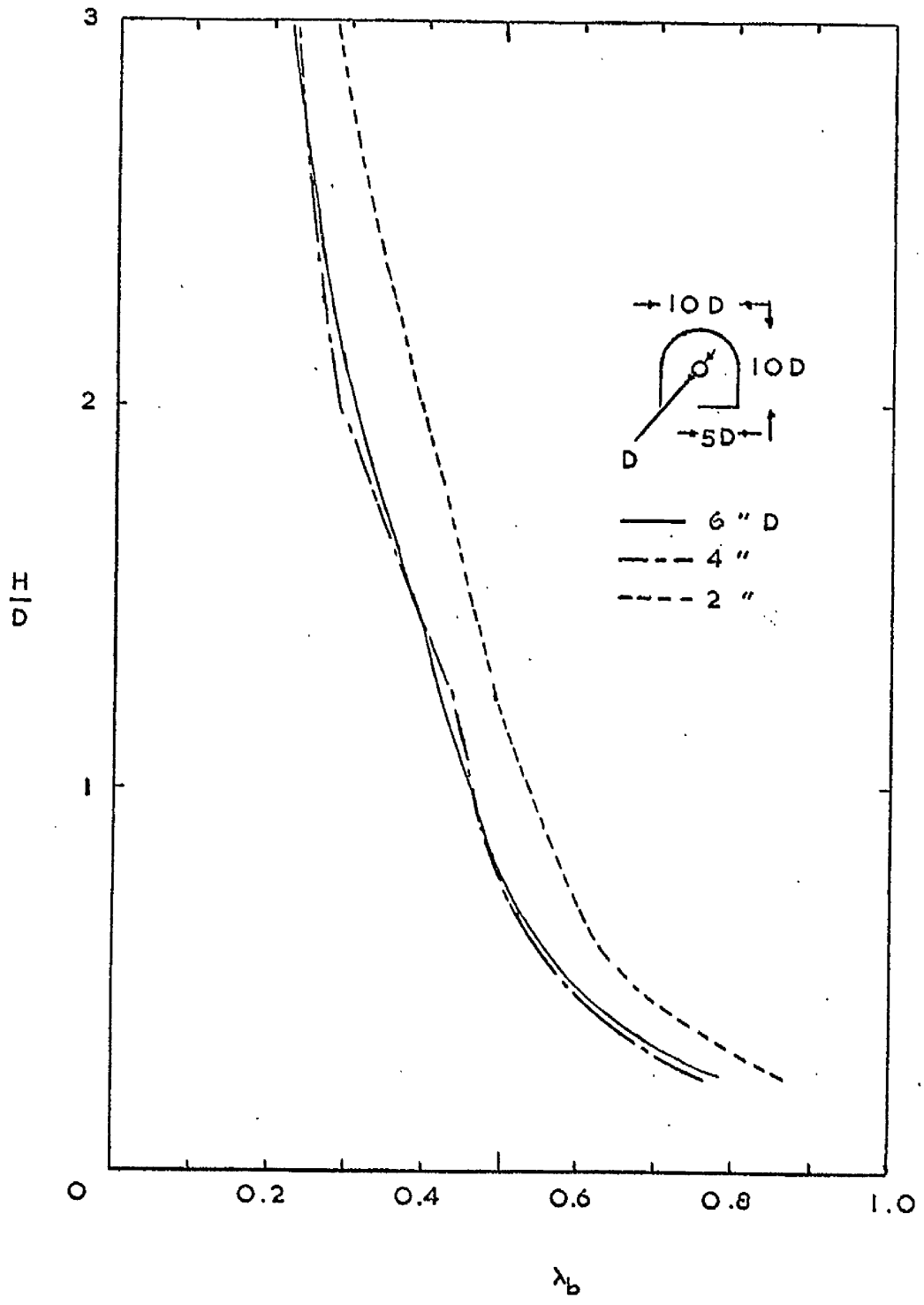

FIGURE 5.5.2

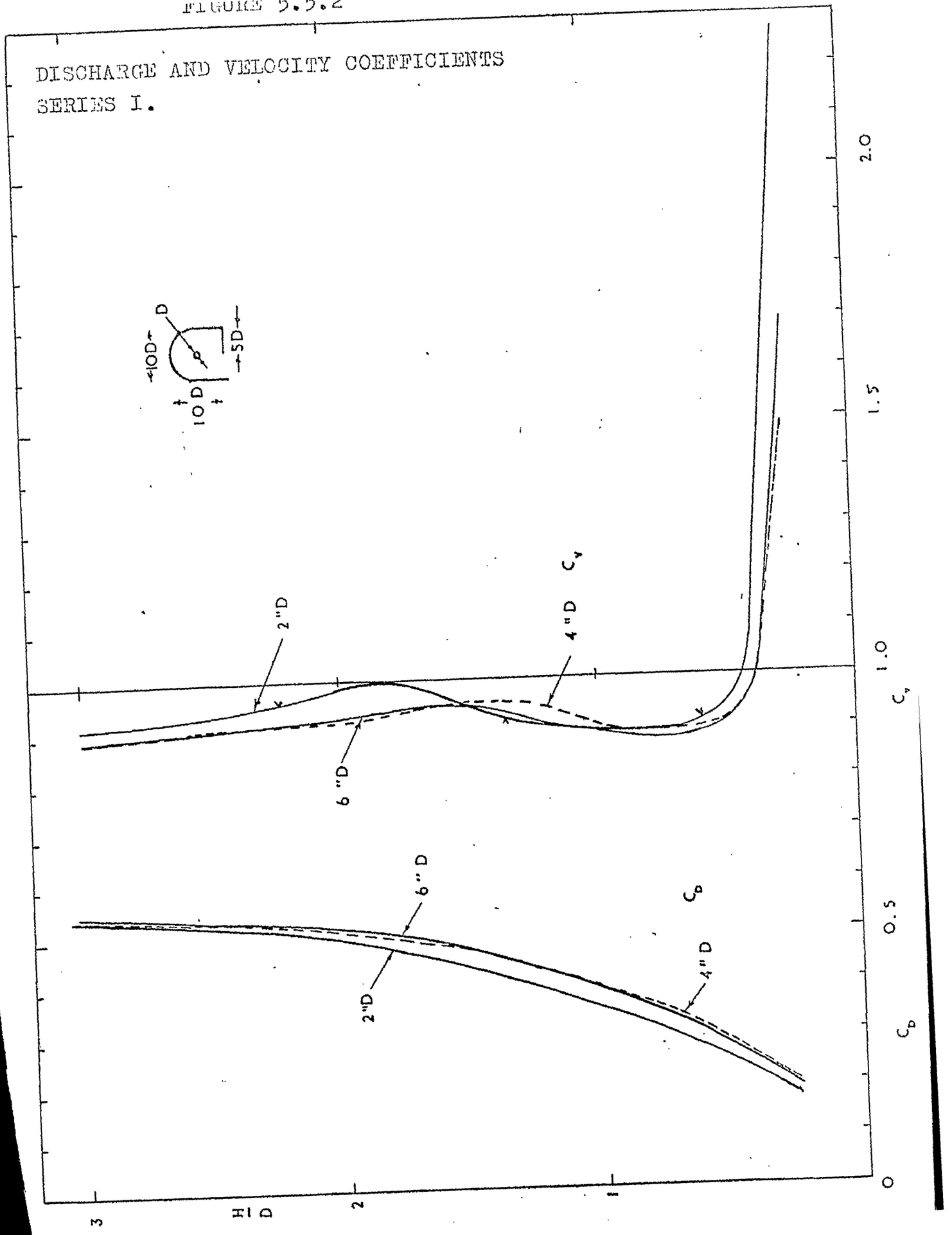
DISCHARGE AND VELOCITY COEFFICIENTS
SERIES I.
10D
D
5D
10 D
2.0
1.5
1.0
0.5
0
C_v
C_d
C_v
2"D
4"D
6"D
C_d
6"D
4"D
2"D
3
2
1
H/D

FIGURE 5.6.1
A COMPARISON OF THE OBSERVED
AND THEORETICAL AIR CORE RADII
SERIES I

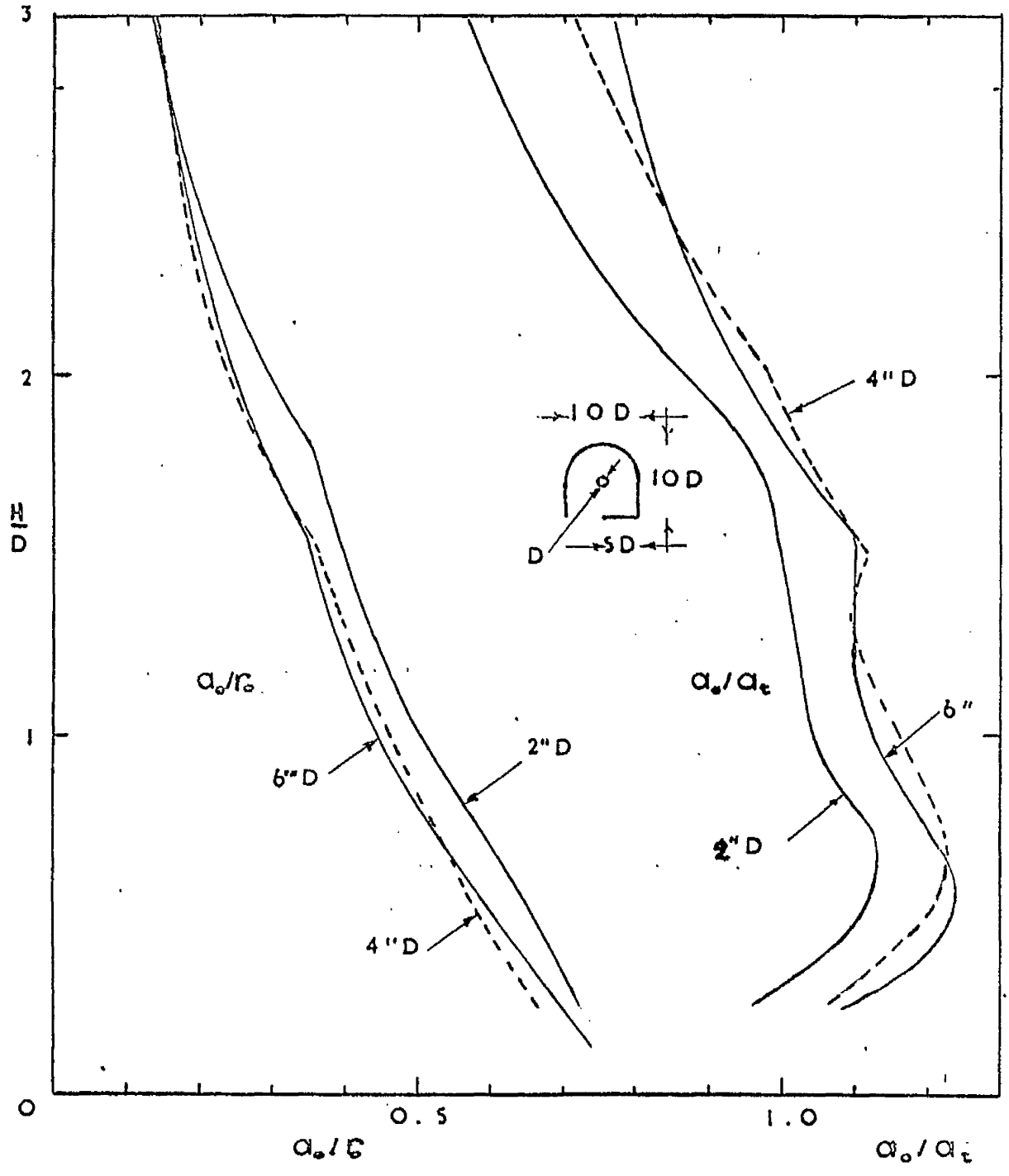

A COMPARISON OF THE DISCHARGE COEFFICIENTS OF THE RECTANGULAR AND 'HORSESHOE' MODELS

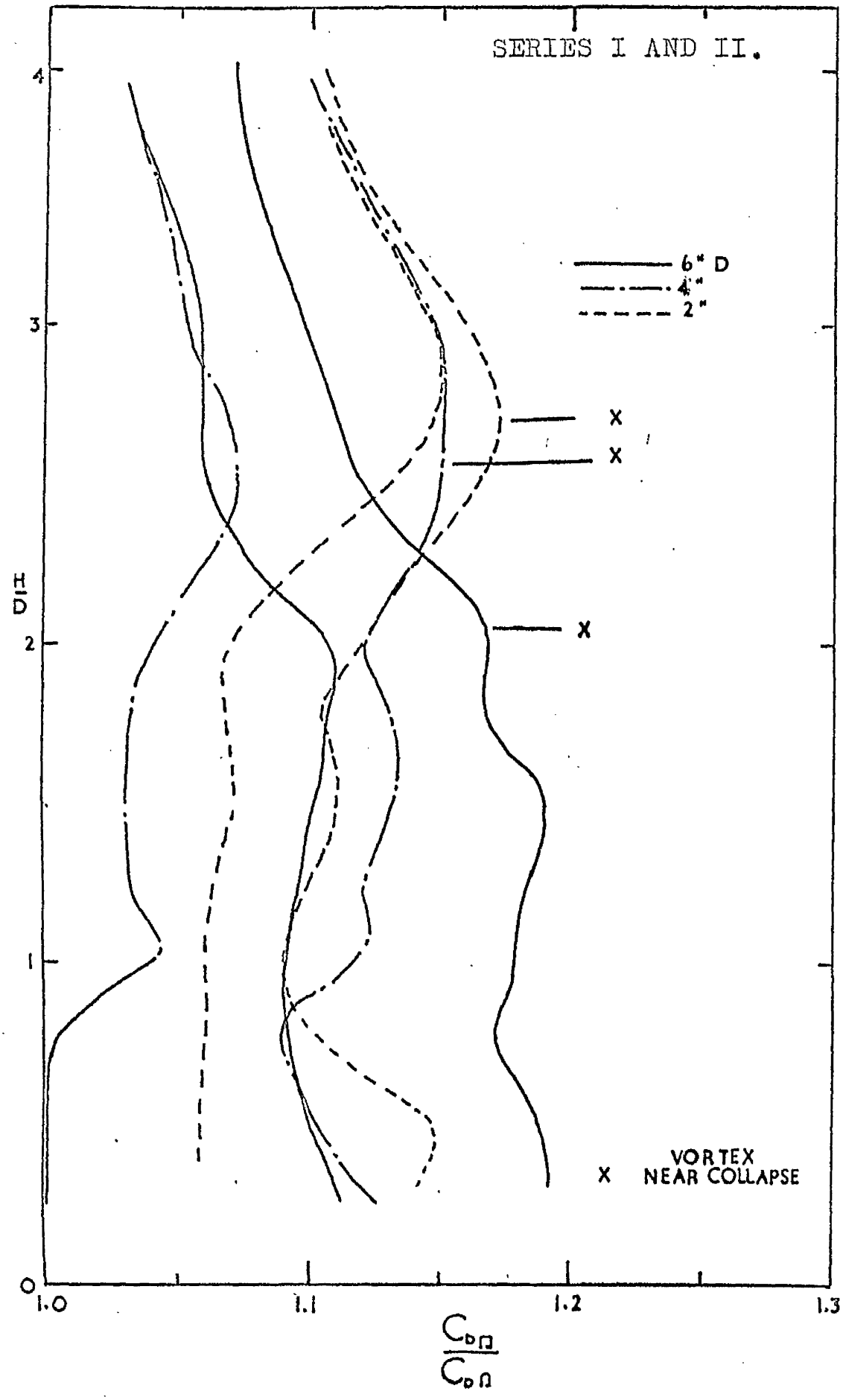

FIGURE 7.2.1

VORTEX FORMATION DURING RESERVIOR DRAINAGE

SERIES V D=4", H_o=12", (as per Table 7.1.)

PHOTO NO.

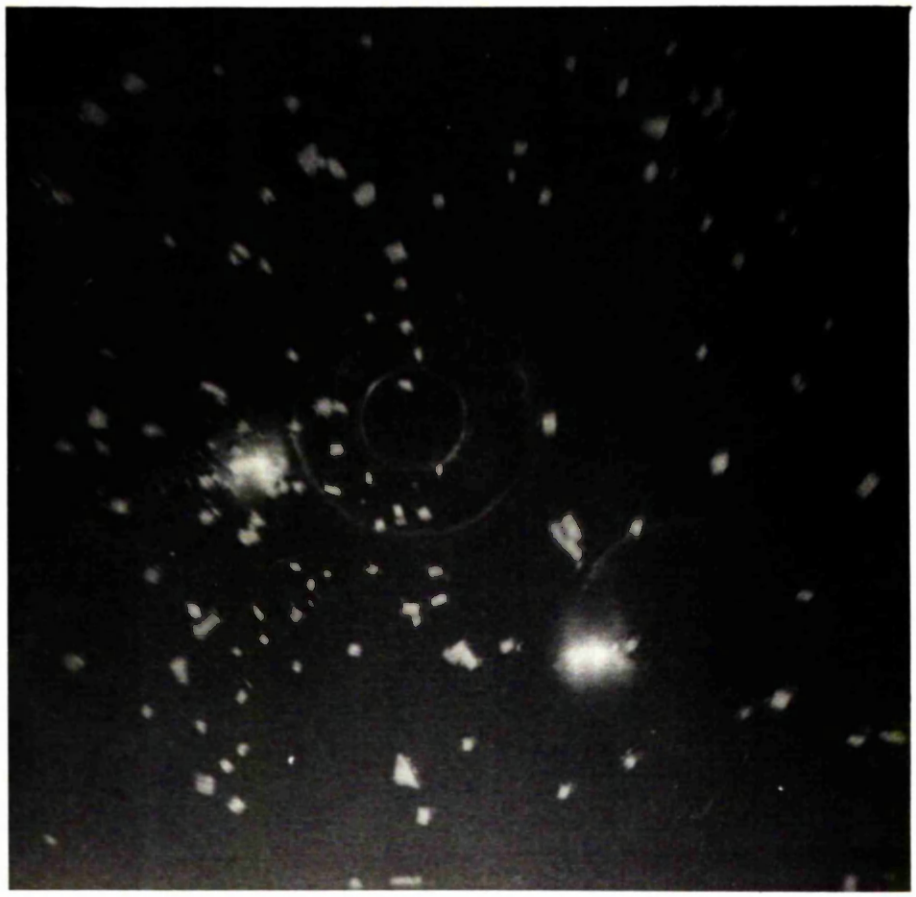

1

2

FIGURE 7.2.1 (continued)

PHOTO NO.

3

4

FIGURE 7.2.1 (continued)

PHOTO NO.

5

6

PHOTO NO.

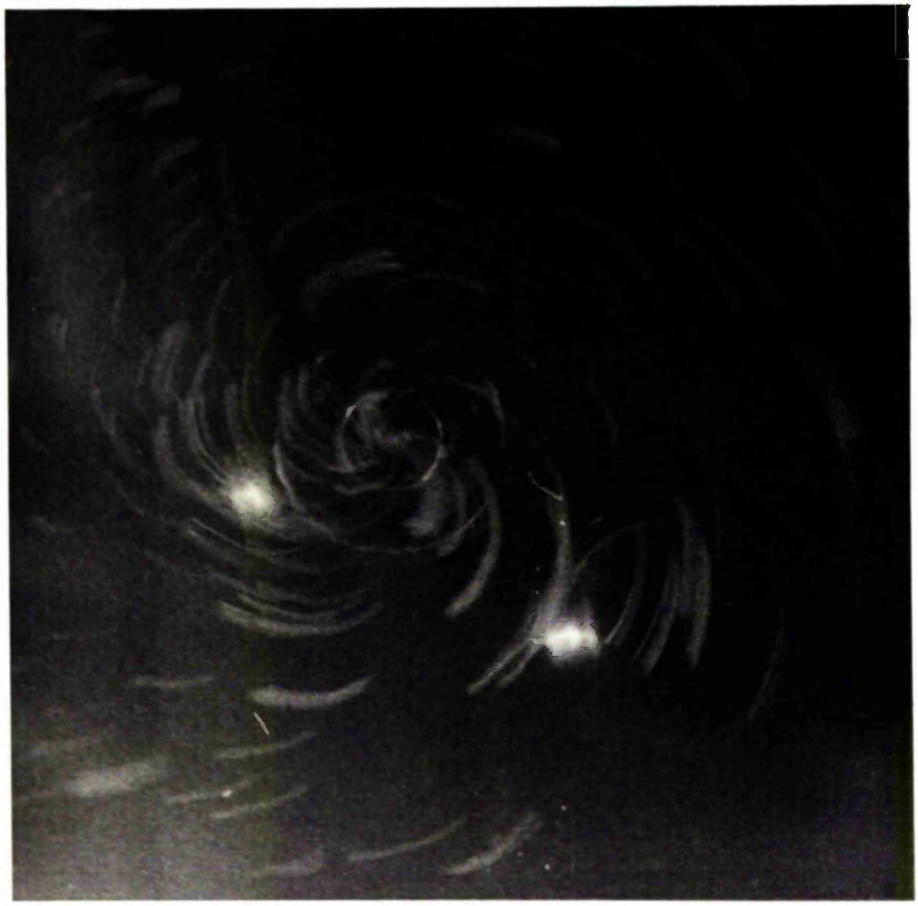

7

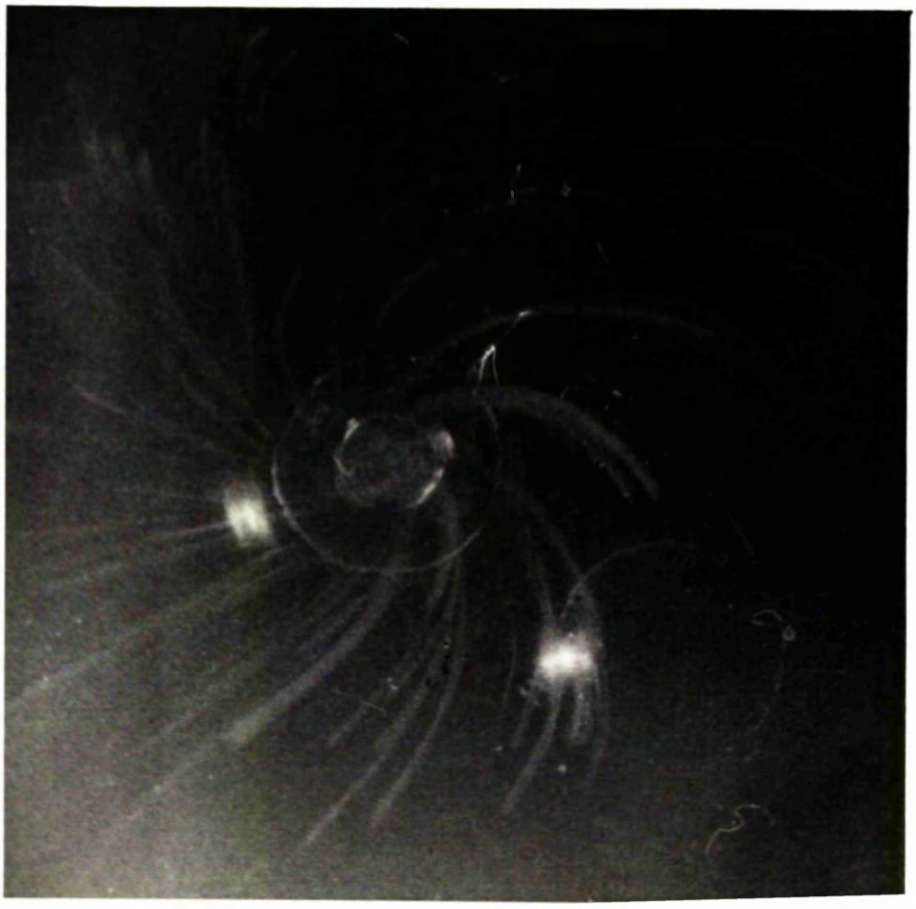

8

FIGURE 7.2.2

DEVELOPMENT OF A DRAINED VORTEX

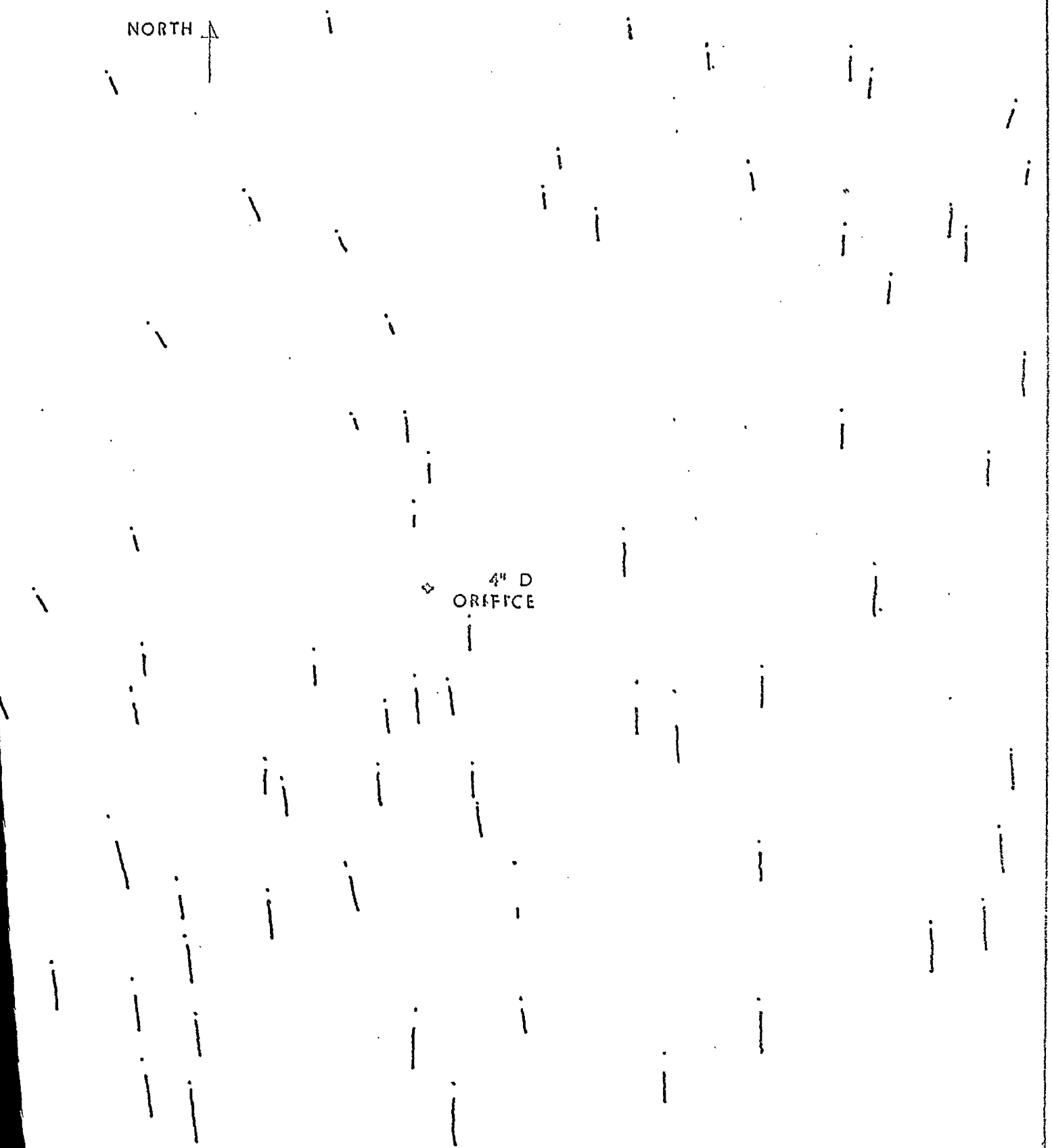


INFLOW
H 0.236 TO 0.165'
T 15 SEC.
SCALE .327 '/" OR .022 FT/SEC/"

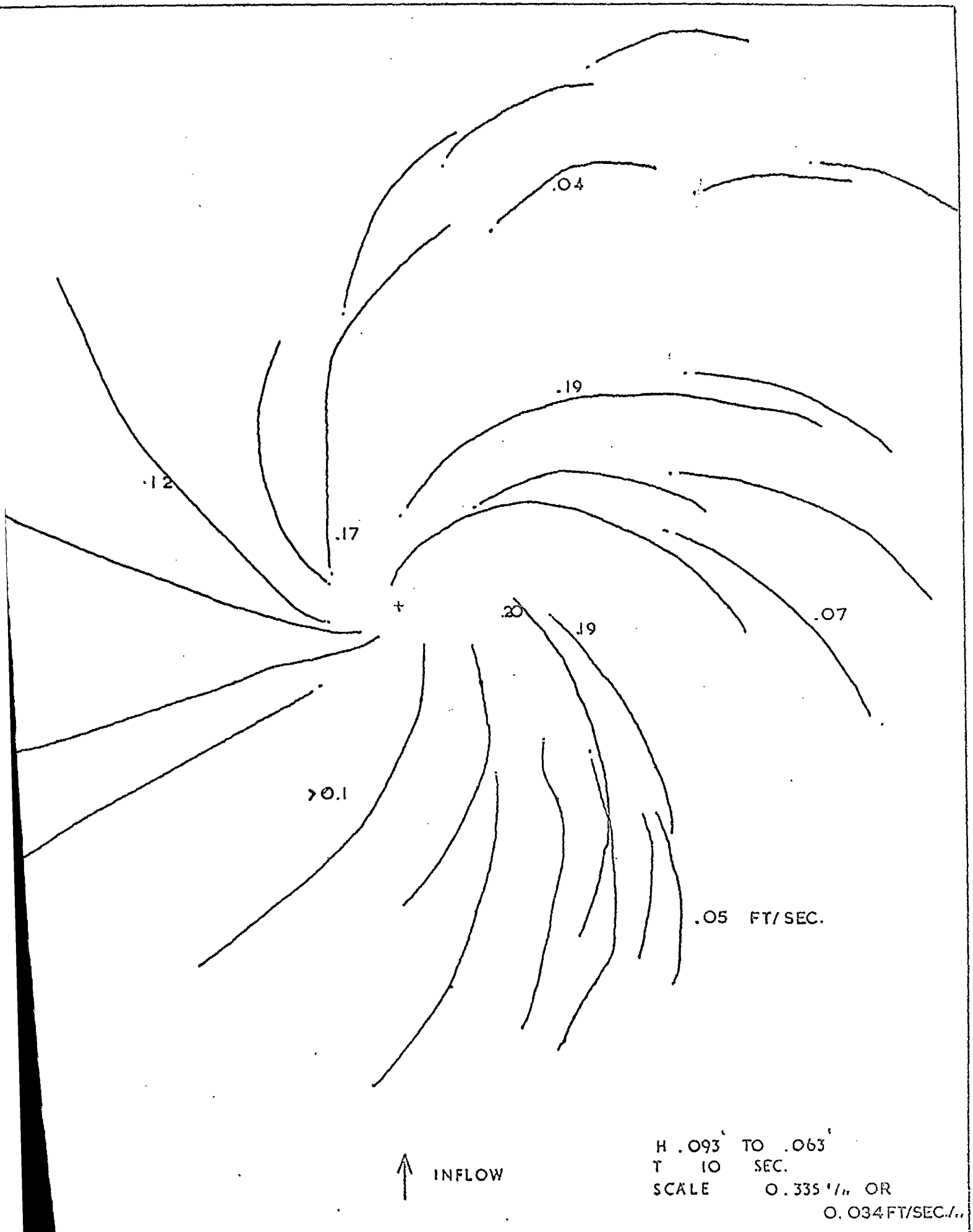
.04
.19
.12
.17
.20
.19
.07
>0.1
.05 FT/SEC.
INFLOW
H .093' TO .063'
T 10 SEC.
SCALE 0.335 "/" OR
0.034 FT/SEC./"

DRAWING NUMBER 1

DO NOT SCALE DRAWING
IF IN DOUBT—ASK.

WELDED STEEL TANK

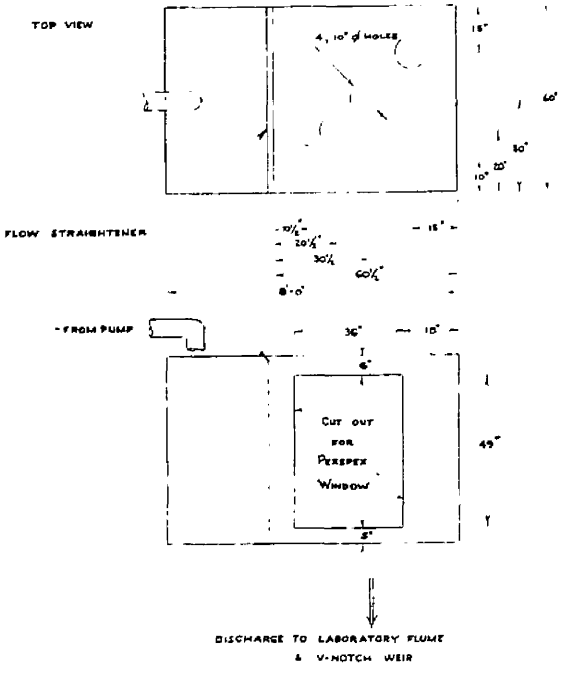

FLOW STRAIGHTENER

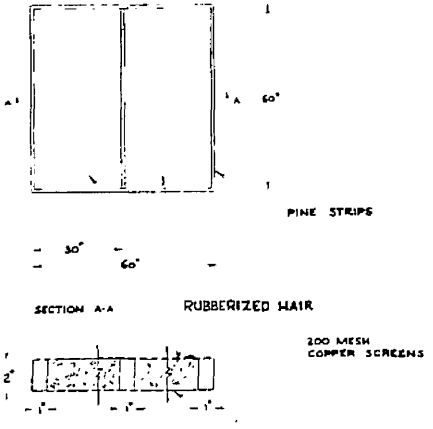

NOTES :

1) INSIDE DIMENSIONS ARE SHOWN FOR THE TEST TANK
2) TANK TO BE WELDED FROM ¼" ST ℞
3) TANK REINFORCING IS SHOWN ON DRWG Nº 6

ITEM	No. OFF	DESCRIPTION	MATL	REMARKS

UNIVERSITY GLASGOW
ENGINEERING LABORATORIES

TITLE OF DRAWING :— LAYOUT OF TEST TANK
TITLE OF PROJECT :— DRAINED VORTICES
DEPARTMENT :- FLUID MECHANICS

PROJECT No.	COST No.	WHEN QUOTING DRGS PLEASE QUOTE LETTER OF ISSUE
		SCALE: 1" = 10"
DRAWN BY	LIMPERSQUODALE	Nº 1
TRACED BY	J M	
CHECKED BY		
APPROVED BY		
DATE DRAWN	15 · 63	No OF SHEETS 2 SHEET No 1

NOTE: THIS DRAWING IS A PRIVATE AND CONFIDENTIAL COMMUNICATION AND THE PROPERTY OF THE UNIVERSITY OF GLASGOW IT MUST NOT BE COPIED OR LOANED WITHOUT THE WRITTEN CONSENT OF THE UNIVERSITY AND MUST BE RETURNED IMMEDIATELY ON COMPLETION OF TENDER OR CONTRACT.

ORIGL LETTER OF ISSUE: A

DIMENSIONS MUST NOT BE TAKEN OFF THIS DRAWING BUT FIGURED DIMENSIONS ONLY TO BE WORKED TO FINISHED DIMENSION GIVEN IN ALL CASES
MACHINE SYMBOLS MARKED THUS
1 MACHINE · SMOOTH MACHINE
2 ROUGH MACHINE ~ GROUND FINISH

ALL UNTOLERANCED DIMENSIONS IN DECIMALS TO BE WITHIN THE FOLLOWING LIMITS —
HOLES AND INTERNAL SURFACES + 010"
SHAFTS AND EXTERNAL SURFACES - 010"
CENTRES OF HOLES AND CENTRES TO FACES + 005"
FRACTIONAL DIMENSIONS · 1/64"

1 2 3 4 5 6 7 8 9 10 11 12 13 14

DRAWING NUMBER 2

DO NOT SCALE DRAWING
IF IN DOUBT—ASK.

ORIFICE - HOLDER

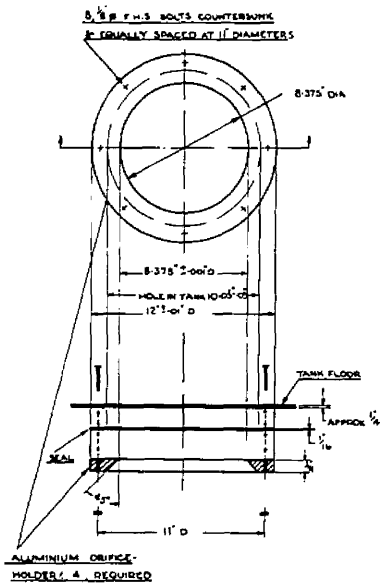

ORIFICES

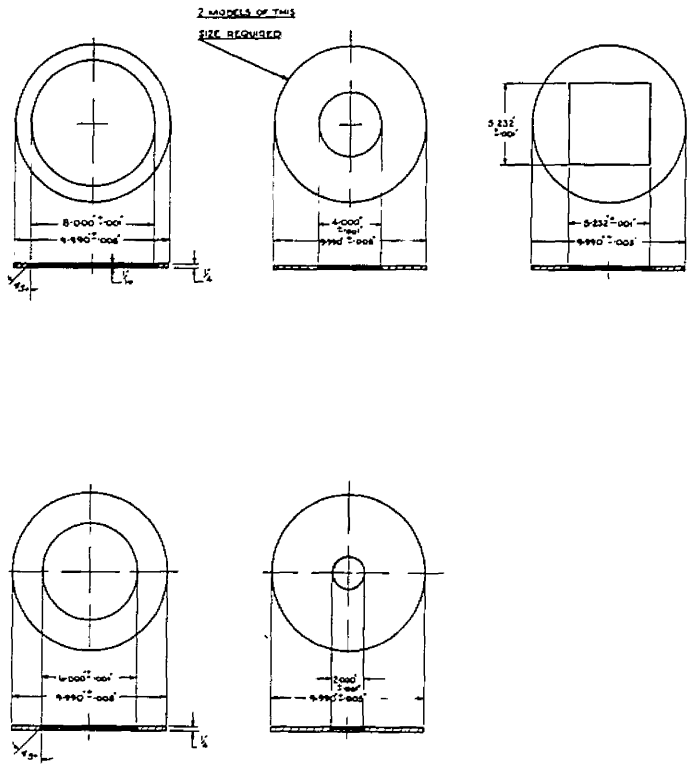

GENERAL NOTES.

① 4 ORIFICES TO BE MADE FROM ¼" BRONZE PLATE
② ALL ORIFICE LIPS TO BE 1/16"
③ ALL CHAMFERS TO BE 45°
④ IN ADDITION TO THE ORIFICES SHOWN, 3, 9·990" ±·005" D, ¾" THICK BRONZE DISCS WILL BE REQUIRED AS STOPPERS
⑤ 32 FLAT-HEADED ⅜ Ø STEEL BOLTS WITH NUTS WILL BE REQUIRED TO FASTEN THE 4 ORIFICE-HOLDERS TO FLOOR OF TANK.
⑥ 4 ORIFICE-HOLDERS TO BE MADE FROM ALUMINIUM.

ITEM	No. OFF	DESCRIPTION	MATL	REMARKS

UNIVERSITY GLASGOW
ENGINEERING LABORATORIES

TITLE OF DRAWING:— ORIFICES & HOLDERS
TITLE OF PROJECT:— A STUDY OF DRAINED VORTICES
DEPARTMENT:— FLUID MECHANICS

PROJECT No.	COST No.	WHEN ORDERING BOOKS, PLEASE QUOTE LETTER OF ISSUE
		SCALE: 1" = 4"
DRAWN BY	[illegible]	
TRACED BY	[illegible]	No 2
CHECKED BY	[illegible]	
APPROVED BY		
DATE DRAWN	15 · 1 · 63	No. OF SHEETS 2 / SHEET No. 2

NOTE: THIS DRAWING IS A PRIVATE AND CONFIDENTIAL COMMUNICATION AND THE PROPERTY OF THE UNIVERSITY OF GLASGOW IT MUST NOT BE COPIED OR LOANED WITHOUT THE WRITTEN CONSENT OF THE UNIVERSITY AND MUST BE RETURNED IMMEDIATELY ON COMPLETION OF TENDER OR CONTRACT.

A ORIG. LETTER OF ISSUE

DIMENSIONS MUST NOT BE TAKEN OFF THIS DRAWING BUT FIGURED DIMENSIONS ONLY TO BE WORKED TO FINISHED DIMENSION GIVEN IN ALL CASES
MACHINE SYMBOLS MARKED THUS :—
/ MACHINE : SMOOTH MACHINE
▽ ROUGH MACHINE ▽ GROUND FINISH

ALL UNTOLERANCED DIMENSIONS IN DECIMALS TO BE WITHIN THE FOLLOWING LIMITS :—
HOLES AND INTERNAL SURFACES + ·010"
SHAFTS AND EXTERNAL SURFACES − ·010"
CENTRES OF HOLES AND CENTRES TO FACES + ·005"
FRACTIONAL DIMENSIONS ± 1/64"

1 2 3 4 5 6 7 8 9 10 11 12 13 14